

UC Davis

UC Davis Electronic Theses and Dissertations

Title

Role of SYCP3 in Homologous Recombination

Permalink

<https://escholarship.org/uc/item/5tr3x4rc>

Author

Jay, Ash

Publication Date

2021

Peer reviewed|Thesis/dissertation

Role of SYCP3 in Homologous Recombination

By

Ash Jay

DISSERTATION

Submitted in partial satisfaction of the requirements for the degree of

DOCTOR OF PHILOSOPHY

in

Integrative Pathobiology

in the

OFFICE OF GRADUATE STUDIES

of the

UNIVERSITY OF CALIFORNIA

DAVIS

Approved:

Wolf-Dietrich Heyer, Chair

Neil Hunter

Xinbin Chen

Committee in Charge

2021

Copyright by
Ash Jay and Wolf-Dietrich Heyer
© 2021

Table of Contents

List of Figures	3
List of Table	6
Abstract	7
Acknowledgement	9
Chapter 1: Introduction	10
References	18
Chapter 2: Cancer testis antigens and genomic instability: More than immunology	22
2.1 Abstract	23
2.2 Introduction	23
2.3 A Repertoire of Cancer Testis Genes and Antigens	26
2.4 Homologous Recombination and its Functions in Somatic and Meiotic Cells	27
2.5 Mis-expressed proteins involved in meiotic chromosome metabolism and their role in carcinogenesis	31
2.6 Conclusions and Future Studies	37
2.7 References	62
Chapter 3: SYCP3 as a Potential Biomarker for HR Deficiency in Human Breast Cancers	
74	
3.1 Abstract	73

3.2 Introduction	73
3.3 Materials and Methods	77
3.4 Results	80
3.5 Conclusions	90
3.6 References	93
Chapter 4: Biochemical Analysis of SYCP3 and its Potential Role in Homologous Recombination	98
4.1 Abstract	99
4.2 Introduction	99
4.3 Experimental Procedures	102
4.4 Results	108
4.5 Conclusions	138
4.6 Future Work	141
4.7 Appendix	144
4.8 References	156

List of Figures

Figure 1.1: DSB Repair by HR	11
Figure 1.2: Specific function of BRCA2 during HR	12
Figure 1.3: SYCP3 organization in synaptonemal complex	13
Figure 1.4: SYCP3: interaction with BRCA2/RAD51	15
Figure 2.1: Somatic and meiotic homologous recombination pathways	49
Figure 2.2: Replication-dependent formation and recovery of one-sided DNA double-stranded breaks during S-phase	51
Figure 2.3: Correlation of cancer-testis antigen (CTA) expression across cancer cell lines and tumors	52
Figure 2.4: Cancer-testis antigen expression in testicular cancers compared to other tumor types and corresponding normal tissues	53
Figure 2.5: Expression of cancer-testis antigens (CTA) and somatic HR proteins in tumors and normal somatic tissues	54
Figure 2.6: Correlation of gene expression with methylation	56
Figure 2.7: Correlation of gene expression with copy number	58
Figure 2.8: Cancer testis antigen (CTA) overexpression <i>versus</i> BRCA1 or BRCA2 modifications	60
Figure 2.9: Possible mechanisms by which cancer testis antigens with a function in meiotic chromosome metabolism may affect genome stability	61
Figure 3.1: SYCP3 antibody validation on human testis sections	81

Figure 3.2: Immunoblot and IHC analysis of transient SYCP3 over-expression in HEK293 cells	82
Figure 3.3: SYCP3 expression in normal breast tissue	84
Figure 3.4: SYCP3 IHC analysis in normal breast tissue sections, breast cancer cell lines, and breast cancer (BC) tissue sections from YALE TMA	85
Figure 3.5: Semiquantitative analysis of SYCP3 protein levels by IHC	87
Figure 3.6: Kaplan-Meier survival curves of patients considering censored data separated by high vs. low nuclear SYCP3 expression	90
Figure 4.1: BRC repeat constructs used in this study compared with the different BRC repeat constructs studied in the past	99
Figure 4.2: Purification of BRC repeat fragments	110
Figure 4.3: SYCP3 purified with Chitin, Heparin and Mono Q columns has ATPase contamination	111
Figure 4.4: SYCP3 purified with Chitin, Heparin, Mono Q and Mono S columns has much lower ATPase contamination but lacks DNA binding	113
Figure 4.5: Inhibition of RAD51 strand exchange activity by SYCP3 is suppressed by the presence of RAD54	117
Figure 4.6: SYCP3 does not have a significant effect on the ATPase activity of RAD51	120
Figure 4.7: SYCP3 does not have significant effect on ATPase activity of DMC1	122
Figure 4.8: Optimization for RAD51 and DMC1 filament formation	125
Figure 4.9: SYCP3 increases RAD51 filament instability	126

Figure 4.10: SYCP3 increases RAD51 filament instability at lower concentration of proteins and DNA	128
Figure 4.11: FAR Western Immunoblot Analysis (IB) of EMSA does not provide insight on the mechanism by which SYCP3 leads to RAD51 filament dissociation	129
Figure 4.12: With Crosslinking no dissociation of RAD51 filaments by SYCP3	130
Figure 4.13: SYCP3 does not affect DMC1 filament stability	131
Figure 4.14: SYCP3 does not affect DMC1 filament stability when DMC1 filaments are more saturated	132
Figure 4.15: SYCP3-RAD51 binding inhibits RAD51 filament formation on ssDNA	134
Figure 4.16: SYCP3 titration leads to lesser disruption of RAD51 Filaments under non-turnover conditions with calcium in reaction buffer	136
Figure 4.17: SYCP3 does not disrupt RAD51 Filaments under non-turnover conditions with AMP-PNP in reaction buffer	137
Figure 4.18: Proposed model for inhibition of RAD51 activity in HR by SYCP3	140
Figure 4.19: SYCP3 has higher affinity to BRC5 than BRC3	146
Figure 4.20: SYCP3-cc purified	148
Figure 4.21: SYCP3 interacts with BRC5 through its coiled-coil region	149
Figure 4.22: D-Loop assay when BRC4 is titrated with excess RAD51	152
Figure 4.23: No effect on the stimulation of D-Loop reaction when both BRC4 and SYCP3 were present together in the reaction with excess RAD51	154

List of Tables

Table 2.1: Selected cancer-testis antigens and their established functions in meiotic chromosome metabolism and homologous recombination with their proposed roles in carcinogenesis	42
Table 2.2: Tumor-type specific correlation of gene expression with promotor methylation	
43	
Table 2.3: Tumor-type specific correlation of gene expression with copy number	45
Table 2.4: Cell line dependency on cancer-testis antigens from Table 1.1	47
Table 3.1: Tumor SYCP3 expression (h-score) in nucleus & cytoplasm grouped by patient clinical and pathological features	88

Abstract

Genome instability increases the risk for cancer. Among the diverse types of DNA damage, DNA double stranded breaks (**DSBs**) can drive genomic instability by their potential to induce genome rearrangements. Homologous recombination (**HR**) functions to accurately repair DSBs and help maintain genomic integrity. BRCA2 is a central HR protein and recruits other proteins such as RAD51 in somatic cells and RAD51 and DMC1 in germline cells to participate in the two signature steps of HR: 1) Homology search and 2) DNA strand invasion. Loss of BRCA2 and RAD51 function is associated with increased risk of breast, ovarian and other cancers.

SYCP3 is an essential structural component of the meiosis-specific synaptonemal complex and is typically expressed only in germline cells (*e.g.*, in testis, ovary) but not in somatic cells. Emerging evidence indicates that SYCP3 is mis-expressed in certain cancer cells and primary tumors, and hence SYCP3 has been termed a cancer/testis antigen (**CTA**). SYCP3 mis-expression in somatic cells has been shown to cause a DNA repair defect. Recently, it was reported that SYCP3 interacts with BRCA2 and RAD51 and impairs their function in HR involving mechanisms that remain to be defined.

In this work, we perform a review of CTAs including SYCP3 that function in meiotic chromosome metabolism and have been suggested to be involved in carcinogenesis. We analyze cancer databases with tumor and cancer cell line data to understand CTA expression patterns and gain insight into mechanisms by which they lead to tumor formation.

SYCP3 mis-expression leads to functional BRCA2 deficiency which is a key factor associated with many breast cancers. The published studies that evaluate SCYP3 mis-expression in cancers are based on RNA transcript analysis which may not be indicative of SYCP3 protein levels. Our study is the first to analyze SYCP3 protein expression in breast cancers using immunohistochemistry (**IHC**) and our results show that about 33 % of breast cancers have SYCP3 misexpression.

In the **final chapter**, we establish a biochemical mechanism by which SYCP3 leads to functional loss of HR in somatic cells by *in vitro* assays using purified proteins. Our findings show that SYCP3 inhibits RAD51 activity in HR by binding to free RAD51 and disrupting RAD51 filament formation. Another critical recombination protein RAD54 overcomes the SYCP3-mediated inhibition of RAD51 function likely by competing with SYCP3 in the interaction with RAD51.

The findings from this project help determine the mechanism by which SYCP3 mis-expression in somatic cells leads to HR deficiency and establish SYCP3 expression in tumors as a potential biomarker for HR deficiency, which may also qualify patients for cancer therapeutics like Poly (ADP-ribose) polymerase inhibitors.

Acknowledgement

The completion of my PhD and this dissertation would not have been possible without the continuous support and guidance of my advisor Dr. Wolf-Dietrich Heyer. My dissertation committee mentors Dr. Xinbin Chen and Dr. Neil Hunter have provided valuable feedback to help me progress with my research and complete this dissertation. I am also thankful to the VSTP (DVM-PhD) director Dr. Xinbin Chen for his support and encouragement throughout my graduate program. My academic advisor Dr. Lark Coffey, graduate program coordinator Dr. Erin Kent and MCB T32 academic coordinator Dr. Gaya Gomes have all been available to help me navigate the difficulties I faced during my research. I am also very thankful to my colleagues from the Heyer laboratory, Dr. Theeta Pavankumar and Dr. Naofumi Handa from the Kowalczykowski laboratory and Dr. Sumit Sandu and Dr. Dhananjaya Kulkarni from the Hunter laboratory for being available for discussions and to guide me with my research.

I am very thankful to my husband Jay Shah for all his love and support, which enabled me to pursue this career path, face numerous personal and professional challenges and successfully complete this dissertation. Without him, none of this would have even been remotely possible. I am also grateful for the continuous help and support of my parents during this long journey. Finally, I want to thank all my animals for their unconditional love. They are my motivation in this pursuit of a career to improve animal health.

Chapter 1: Introduction

Our genome is subject to several thousands of insults every day from both endogenous (*e.g.*: metabolism) and exogenous sources (*e.g.*: ionizing radiation, xenobiotic chemicals) that threaten our genomic integrity. Loss of genomic integrity predisposes to cancer and is a hallmark of most if not all cancers. To cope with these insults and protect our genome, robust DNA repair and genome maintenance pathways have evolved. Among the various kinds of DNA damages, DNA double stranded breaks (**DSBs**) and interstrand-crosslinks (**ICLs**) are more complex to repair and pose a serious risk to genomic stability. The two major DSB repair pathways are non-homologous end joining (**NHEJ**) and homologous recombination (**HR**), while only HR but not NHEJ functions in ICL repair (**Fig. 1.1**). NHEJ is a template independent pathway with variable fidelity that modifies and ligates the broken DNA ends, often resulting in small deletions or insertions. In contrast, HR is a template-dependent high-fidelity pathway that functions to accurately repair the DNA damage. Hence, HR is critical to maintain genomic stability and suppress tumor formation.

The HR pathway initiates by processing the DSBs through resection of the 5' ends of DNA leaving 3' single strand DNA (**ssDNA**) overhangs (**Fig. 1.1**). The ssDNA binding protein, RPA, binds to the ssDNA overhangs, protecting them from nucleolytic degradation and melting potential secondary structures. BRCA2, a breast cancer susceptibility protein, plays a central role in HR. BRCA2 recruits RAD51 in somatic cells and DMC1 and RAD51 in germline cells (**Fig. 1.2**) to nucleate a filament on ssDNA displacing RPA. These nucleoprotein filaments perform the two signature steps of HR: (1) Homology search for a DNA template; and (2) DNA strand invasion to position the 3'-OH end of the DSB on a homologous template for repair DNA synthesis. These processes result in displacement loops (**D-loop**), which can be processed by one of the two

pathways: (1) synthesis-dependent strand annealing (**SDSA**); and (2) the double Holiday Junction (**dHJ**) pathway. In SDSA, the extended D-loop is reversed and annealed with the other resected strand of DSB leading to non-crossover recombination products. On the other hand, dHJs involves a second independent strand invasion or capture of the other end of DSB followed by a second DNA synthesis step. It can yield either crossover or non-crossover recombination products (**Fig. 1.1**). In somatic cells, non-crossover recombination between sister chromatids is favored as opposed to germline cells where HR functions to establish crossovers between homologous chromosomes [1, 2].

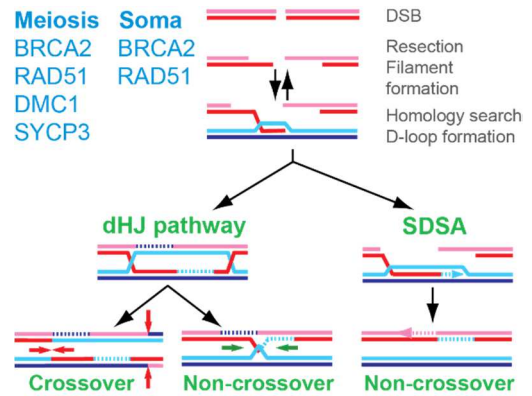


Figure 1.1: DSB repair by HR. HR can proceed via double Holiday Junction pathway (dHJ) or synthesis dependent strand annealing (SDSA). dHJ pathway can result in either crossover or non-crossover outcomes while SDSA results in non-crossover outcomes.

Loss of BRCA2 function in HR leads to accumulation of unrepaired DNA damage which increases the risk for cancer over time. Breast cancer is a commonly diagnosed cancer in women, and it is a leading cause of cancer associated deaths [3, 4]. BRCA2 is recognized as one of the main susceptibility proteins for breast and ovarian cancer [5-7]. BRCA2 is also associated with increased risk for other malignancies such as prostate and pancreatic cancer [8, 9]. Although common hereditary inactivating mutations of BRCA2 are well documented, other mechanisms leading to loss of BRCA2 function also need to be considered as they constitute additional potential risk factors [10, 11].

BRCA-deficient tumors are deficient in HR and are sensitive to Poly (ADP-ribose) polymerase inhibitors (**PARPi**) [12-15]. PARP functions in the repair of ssDNA breaks. PARPi stabilizes PARP at the site of DNA damage and blocks the repair of ssDNA breaks, causing them to convert into DSBs during DNA replication. This leads to the selective death of cells deficient in the HR repair pathway. Genetic conditions that lead to loss of BRCA2 function could enable patients to be eligible for PARP inhibitor therapeutics.

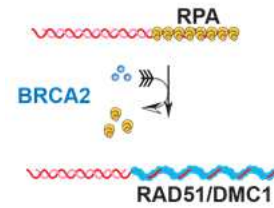


Figure 1.2: Specific function of BRCA2 during HR. BRCA2 recruits RAD51 in somatic cells and DMC1 and RAD51 in germline cells to displace RPA and form filaments on ssDNA.

Like BRCA2, RAD51 mutants lead to DNA repair defects [1, 2, 17]. RAD51 has recently been recognized as a Fanconi anemia gene (**FA-R**) where a dominant negative mutation in RAD51 causes loss of interstrand crosslink repair [18, 19]. RAD51 is required for HR in both somatic and germline cells [20, 21]. While in somatic cells, RAD51 filaments perform homology search and DNA strand invasion, in germline cells RAD51 is believed to act as an accessory factor that promotes DMC1 strand exchange activity [22].

Another protein that has recently been shown to interact with BRCA2 is SYCP3 [23]. SYCP3 is a structural component of the synaptonemal complex (**SC**) (**Fig. 1.3 A**) [24]. The SC is important for chromosome organization, efficient synapsis of homologous chromosomes, normal levels of crossing over and accurate chromosome segregation during meiosis [25]. The SC is comprised of two parallel lateral elements or homolog axes that are connected via a central region to transverse filaments. SYCP3 is an essential part of the lateral elements of the SC [16]. It is a

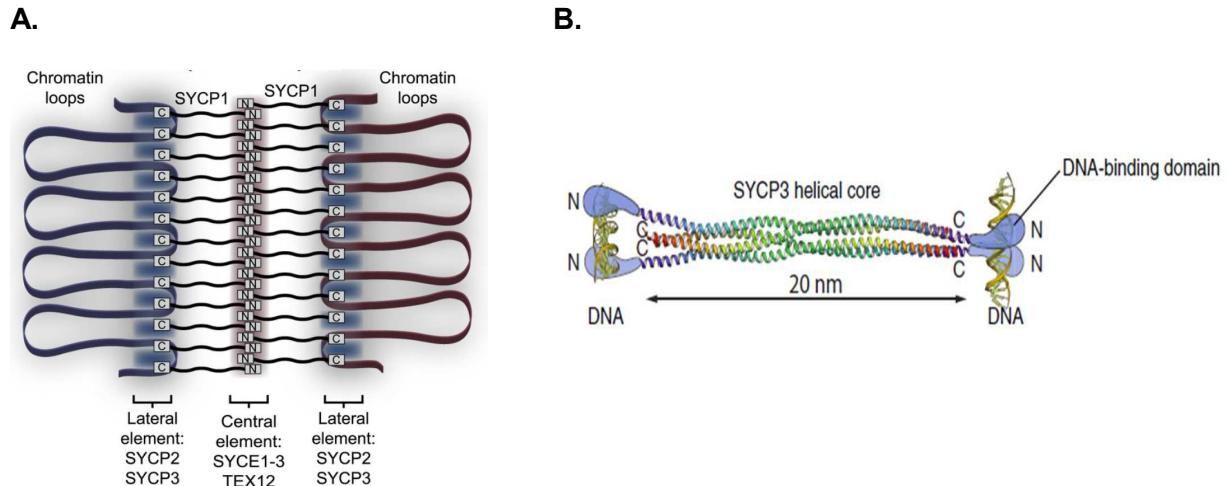


Figure 1.3: SYCP3 organization in synaptonemal complex. A. Model for assembly of the SC. SYCE1, SYCE2, SYCE3 and TEX12 form the central elements. SYCP1 forms the transverse filaments that link the central and lateral elements of the SC. The lateral elements are comprised of SYCP2 and SYCP3; **B.** SYCP3 self-assembles into elongated helical tetramers. The helical chains are arranged in alternating anti-parallel fashion with each end of the tetramer comprising of 2 N terminals and 2 C terminals. SYCP3 binds DNA *via* the N terminal regions [16].

small protein with a central coiled coil region that mediates its self-assembly into tetramers (**Fig. 1.3 B**) [16]. Through DNA binding at its N-termini, SYCP3 is thought to function as a strut connecting the bases of chromatin loops and bridging distant sites of DNA [26]. In both mice and humans, mutations in SYCP3 are associated with azoospermia in males and increased fetal deaths in females [27-30]. In addition, SYCP3 knockout female mice show inefficient DSB repair in oocytes indicating that SYCP3 might be required for HR during meiosis [31, 32].

SYCP3 is expressed only in germline cells and is silenced in somatic cells [24, 33]. However, emerging evidence documents SYCP3 misexpression in cancer cells and some primary tumors

[23, 34]. Hence, SYCP3 has been termed a cancer/testis antigen (**CTA**) which are a class of proteins whose expression is normally restricted to the adult testis and show sporadic re-expression in some human cancers [35].

Chapter two of this thesis provides a detailed review of CTAs with a function in meiotic chromosome metabolism and chromosome structure. We evaluate whether CTA expression leads to a transformation to a germ-cell state that is beneficial to tumor development and growth. We perform database analysis of tumors and cancer cell lines to gain insight into expression patterns of CTAs. Our model proposes that when cancer testis antigens are mis-expressed in somatic cells that lack an environment containing other meiotic proteins, CTAs malfunction by interacting with either DNA or other mitotic HR proteins and thereby disrupt HR leading to genome instability and increased risk for cancer.

Recent findings associate SYCP3 misexpression in somatic cells with a DNA repair defect [23]. While the structural role of SYCP3 in meiosis is well understood, not much is known about potential effects of SYCP3 misexpression in somatic cells. Co-immunoprecipitation (Co-IP) experiments suggest that SYCP3 interacts with BRCA2 and partially inhibits its interaction with RAD51 [23]. However, it was unclear whether the interaction between BRCA2 and SYCP3 is direct or indirect. Preliminary results by Dr. Jie Liu in the Heyer laboratory using purified proteins demonstrated the direct interaction between SYCP3 and BRCA2 and that SYCP3 impairs the BRCA2-RAD51 interaction (**Fig. 1.4**). This constitutes a novel mechanism of regulating BRCA2 function by aberrant expression of the germline specific protein SYCP3.

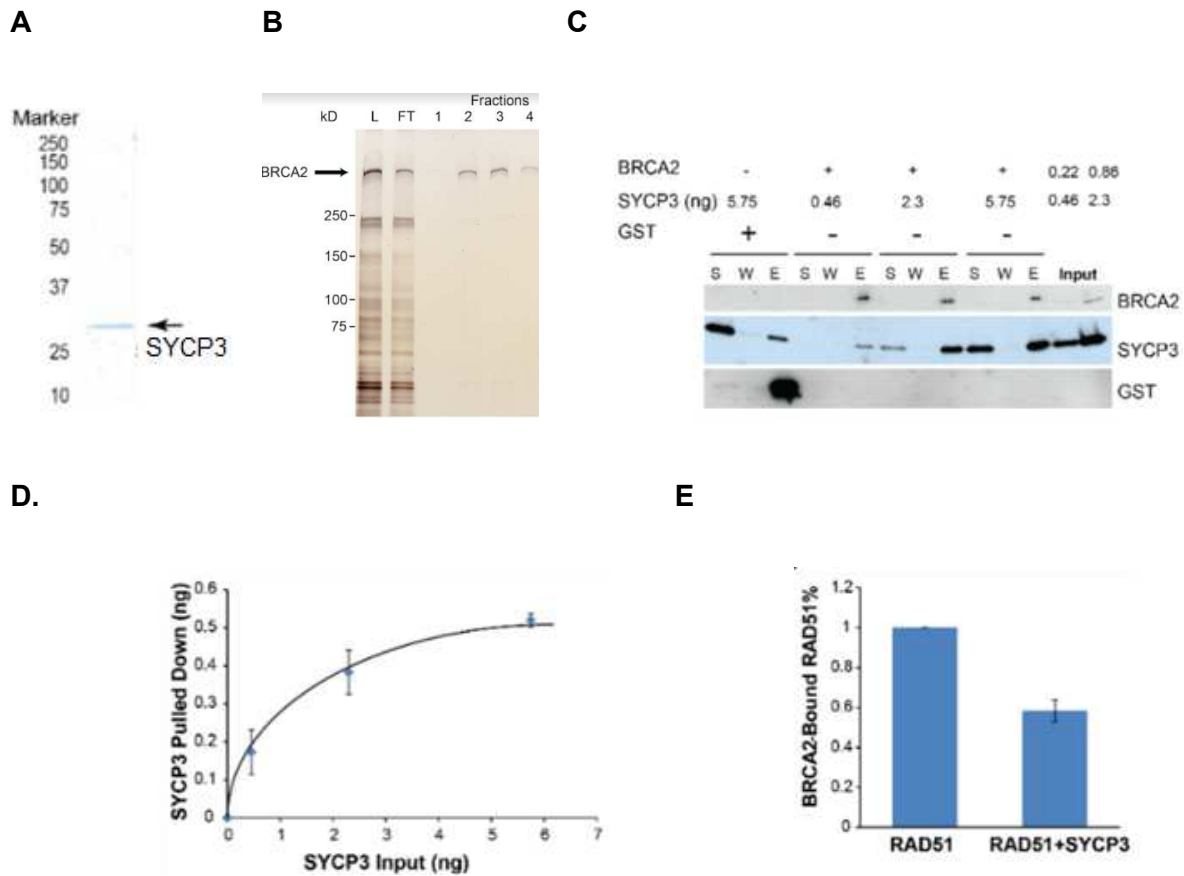


Figure 1.4: SYCP3: interaction with BRCA2/RAD51. **A.** Purified native SYCP3 stained with Coomassie; **B.** Silver-stained purified GST-BRCA2 fractions. **C-D.** SYCP3-BRCA2 direct interaction from GST pull down assay. Non-specific SYCP3 interaction was corrected for in the quantitation; **E.** SYCP3 titration reduces the BRCA2-RAD51 interaction in GST pull down assay. Shown are mean \pm sd, n=3. (unpublished data, Dr. Jie Liu, Heyer laboratory). Abbreviations: S, solution; W, wash; E, eluant.)

SYCP3 has also been shown to interact with both RAD51 and DMC1 though the interaction with RAD51 is relatively much weaker [36, 37]. SYCP3 suppresses RAD51 D-Loop stimulation by HOP2-MND1 but not that of DMC1 (**Fig. 1.5**) [36]. One of the possible mechanisms by which

SYCP3 could affect RAD51 activity could be by binding to dsDNA and blocking RAD51 strand invasion. But this was shown to not be the case because when SYCP3 was preincubated with dsDNA it did not affect RAD51 D-Loop formation [36]. This shows that SYCP3 binding to dsDNA does not block strand invasion by RAD51 filaments. In germline cells, SYCP3, BRCA2, RAD51 and DMC1 are present, and they function together for normal HR-mediated repair of meiotic DSBs, but SYCP3 expression in somatic cells that lack DMC1 results in a DNA repair defect. My working model is that when SYCP3 is expressed in somatic cells that lack other meiotic proteins, SYCP3 interacts with BRCA2 and/or RAD51 and inhibits them from functioning normally in HR.

Though there have been studies evaluating SYCP3 expression in a few types of cancers, there has not been a systematic study of SYCP3 protein expression in breast cancer. The published studies that evaluated SCYP3 misexpression in breast cancer are based on RNA transcript analysis. RNA transcript levels may or may not correlate with protein expression, especially as the transcripts of meiotic genes are known to be subject to regulation during translation [38-40].

In the **third chapter**, we study SYCP3 protein expression in breast cancer since SYCP3 misexpression disrupts BRCA2 mediated HR and loss of BRCA2 function is a key factor associated with many breast cancers. We perform immunohistochemistry (**IHC**) to evaluate SYCP3 protein expression in breast cancers. Our findings indicate that 33% of breast cancers have misexpression of SYCP3.

In the **fourth chapter**, we aim to establish the biochemical mechanism by which SYCP3 leads to functional loss of BRCA2 and HR in somatic cells by *in vitro* assays using purified proteins. Our findings indicate that SYCP3 directly disrupts RAD51 mediated strand invasion. This disruption is

not due an effect on the ATPase activity of RAD51 by SYCP3. Instead, SYCP3 affects RAD51 activity via direct interaction which inhibits DNA binding by RAD51 and dissociates preformed RAD51 filaments. Another critical recombination protein, RAD54, can overcome SYCP3-mediated inhibition of RAD51 function, likely by out-competing SYCP3 for interaction with RAD51. Function of RAD51 in HR is regulated by its intrinsic activity of ATP binding and hydrolysis [41]. Since we use purified SYCP3 protein with RAD51 in functional *in vitro* HR assays, our first step was to perform quality control to monitor for potential ATPase contamination in the SYCP3 protein preparation. After purifying SYCP3 protein without ATPase contamination, we verified its ability to inhibit RAD51 mediated D-Loop formation which builds on results published earlier [36]. We later discovered that the purified SYCP3 protein used in these assays was deficient in DNA interaction. So, these assays will have to repeated with another preparation of SYCP3 protein that displays the expected DNA binding activity.

The findings from this research will help determine the mechanism by which SYCP3 expression in somatic cells may contribute to cancer development. This will have implications for the utility of SYCP3 as a biomarker that may influence the choice of cancer therapeutics.

References

1. Li, X. and W.D. Heyer, *Homologous recombination in DNA repair and DNA damage tolerance*. Cell Res, 2008. **18**(1): p. 99-113.
2. Heyer, W.D., K.T. Ehmsen, and J. Liu, *Regulation of homologous recombination in eukaryotes*. Annu Rev Genet, 2010. **44**: p. 113-39.
3. DeSantis, C., et al., *Breast cancer statistics, 2013*. CA Cancer J Clin, 2014. **64**(1): p. 52-62.
4. Donepudi, M.S., et al., *Breast cancer statistics and markers*. J Cancer Res Ther, 2014. **10**(3): p. 506-11.
5. Wooster, R., et al., *Identification of the breast cancer susceptibility gene BRCA2*. Nature, 1995. **378**(6559): p. 789-92.
6. Levy-Lahad, E. and E. Friedman, *Cancer risks among BRCA1 and BRCA2 mutation carriers*. British Journal of Cancer, 2007. **96**(1): p. 11-15.
7. Lancaster, J.M., et al., *BRCA2 mutations in primary breast and ovarian cancers*. Nat Genet, 1996. **13**(2): p. 238-40.
8. Taylor, R.A., et al., *Germline BRCA2 mutations drive prostate cancers with distinct evolutionary trajectories*. Nat Commun, 2017. **8**: p. 13671.
9. Iqbal, J., et al., *The incidence of pancreatic cancer in BRCA1 and BRCA2 mutation carriers*. Br J Cancer, 2012. **107**(12): p. 2005-9.
10. Apostolou, P. and F. Fostira, *Hereditary breast cancer: the era of new susceptibility genes*. Biomed Res Int, 2013. **2013**: p. 747318.
11. Mutter, R.W., et al., *Bi-allelic alterations in DNA repair genes underpin homologous recombination DNA repair defects in breast cancer*. Journal of Pathology, 2017. **242**(2): p. 165-177.

12. Bryant, H.E., et al., *Specific killing of BRCA2-deficient tumours with inhibitors of poly(ADP-ribose) polymerase*. Nature, 2005. **434**(7035): p. 913-7.
13. Farmer, H., et al., *Targeting the DNA repair defect in BRCA mutant cells as a therapeutic strategy*. Nature, 2005. **434**(7035): p. 917-921.
14. Lord, C.J. and A. Ashworth, *PARP inhibitors: Synthetic lethality in the clinic*. Science, 2017. **355**(6330): p. 1152-1158.
15. Fong, P.C., et al., *Inhibition of poly(ADP-ribose) polymerase in tumors from BRCA mutation carriers*. N Engl J Med, 2009. **361**(2): p. 123-34.
16. Syrjanen, J.L., L. Pellegrini, and O.R. Davies, *A molecular model for the role of SYCP3 in meiotic chromosome organisation*. Elife, 2014. **3**.
17. Godin, S.K., M.R. Sullivan, and K.A. Bernstein, *Novel insights into RAD51 activity and regulation during homologous recombination and DNA replication*. Biochemistry and Cell Biology, 2016. **94**(5): p. 407-418.
18. Wang, A.T., et al., *A Dominant Mutation in Human RAD51 Reveals Its Function in DNA Interstrand Crosslink Repair Independent of Homologous Recombination*. Molecular Cell, 2015. **59**(3): p. 478-490.
19. Ameziane, N., et al., *A novel Fanconi anaemia subtype associated with a dominant-negative mutation in RAD51*. Nat Commun, 2015. **6**: p. 8829.
20. Krejci, L., et al., *Homologous recombination and its regulation*. Nucleic Acids Res, 2012. **40**(13): p. 5795-818.
21. Dai, J., et al., *Meiotic Knockdown and Complementation Reveals Essential Role of RAD51 in Mouse Spermatogenesis*. Cell Rep, 2017. **18**(6): p. 1383-1394.
22. Cloud, V., et al., *Dmc1 catalyzes interhomolog joint molecule formation in meiosis with Rad51 and Mei5-Sae3 as accessory factors*. Science, 2012. **337**(6099): p. 1222-5.
23. Hosoya, N., et al., *Synaptonemal complex protein SYCP3 impairs mitotic recombination by interfering with BRCA2*. EMBO Rep, 2011. **13**(1): p. 44-51.

24. Botelho, R.J., et al., *The genomic structure of SYCP3, a meiosis-specific gene encoding a protein of the chromosome core*. *Biochimica Et Biophysica Acta-Gene Structure and Expression*, 2001. **1518**(3): p. 294-299.
25. Heyting, C., *Synaptonemal complexes: structure and function*. *Curr Opin Cell Biol*, 1996. **8**(3): p. 389-96.
26. Syrjanen, J.L., et al., *Single-molecule observation of DNA compaction by meiotic protein SYCP3*. *Elife*, 2017. **6**.
27. Miyamoto, T., et al., *Male infertility and its causes in human*. *Adv Urol*, 2012. **2012**: p. 384520.
28. Bolor, H., et al., *Mutations of the SYCP3 Gene in Women with Recurrent Pregnancy Loss*. *American Journal of Human Genetics*, 2009. **84**(1): p. 14-20.
29. Yuan, L., et al., *The murine SCP3 gene is required for synaptonemal complex assembly, chromosome synapsis, and male fertility*. *Molecular Cell*, 2000. **5**(1): p. 73-83.
30. Yuan, L., et al., *Female germ cell aneuploidy and embryo death in mice lacking the meiosis-specific protein SCP3*. *Science*, 2002. **296**(5570): p. 1115-1118.
31. Wang, H. and C. Hoog, *Structural damage to meiotic chromosomes impairs DNA recombination and checkpoint control in mammalian oocytes*. *Journal of Cell Biology*, 2006. **173**(4): p. 485-495.
32. Li, X.C., E. Bolcun-Filas, and J.C. Schimenti, *Genetic evidence that synaptonemal complex axial elements govern recombination pathway choice in mice*. *Genetics*, 2011. **189**(1): p. 71-82.
33. Mobasher, M.B., et al., *Expression of two testis-specific genes, TSGA10 and SYCP3, in different cancers regarding to their pathological features*. *Cancer Detection and Prevention*, 2007. **31**(4): p. 296-302.

34. Mobasheri, M.B., R. Shirkoohi, and M.H. Modarressi, *Synaptonemal Complex Protein 3 Transcript Analysis in Breast Cancer*. Iranian Journal of Public Health, 2016. **45**(12): p. 1618-1624.
35. Fratta, E., et al., *The biology of cancer testis antigens: putative function, regulation and therapeutic potential*. Mol Oncol, 2011. **5**(2): p. 164-82.
36. Kobayashi, W., et al., *SYCP3 regulates strand invasion activities of RAD51 and DMC1*. Genes Cells, 2017. **22**(9): p. 799-809.
37. Tarsounas, M., et al., *RAD51 and DMC1 form mixed complexes associated with mouse meiotic chromosome cores and synaptonemal complexes*. J Cell Biol, 1999. **147**(2): p. 207-20.
38. Liu, Y., A. Beyer, and R. Aebersold, *On the Dependency of Cellular Protein Levels on mRNA Abundance*. Cell, 2016. **165**(3): p. 535-50.
39. Vogel, C. and E.M. Marcotte, *Insights into the regulation of protein abundance from proteomic and transcriptomic analyses*. Nat Rev Genet, 2012. **13**(4): p. 227-32.
40. Wang, C., et al., *Systematic identification of genes with a cancer-testis expression pattern in 19 cancer types*. Nat Commun, 2016. **7**: p. 10499.
41. Chi, P., et al., *Roles of ATP binding and ATP hydrolysis in human Rad51 recombinase function*. DNA Repair (Amst), 2006. **5**(3): p. 381-91.

Chapter 2: Cancer testis antigens and genomic instability: More than immunology!

This work has not been published yet and includes contributions from:

Ash Jay, Diedre Reitz, Satoshi H. Namekawa and Wolf-Dietrich Heyer

2.1 Abstract

Cancer testis antigens (CTA) are predominantly expressed in the adult testis while silenced in somatic tissues showing sporadic expression in many human cancers. A surprising number of CTAs are involved in meiotic chromosome metabolism and specifically in meiotic recombination. Recent discoveries with this group of CTAs established that their misexpression in somatic cells results in genomic instability by interfering with homologous recombination (HR), a DNA repair pathway for complex DNA damage such as DNA double-stranded breaks, interstrand crosslinks, and DNA gaps. HR-deficient tumors have specific vulnerabilities and show synthetic lethality with inhibition of polyADP-ribose polymerase, opening the possibility that expression of CTAs that result in an HR-defect could be used as an additional biomarker for HR status. Here we review the repertoire of CTAs focusing on a cohort of CTAs that function in meiotic chromosome metabolism interrogating relevant cancer databases and discussing recent discoveries.

2.2 Introduction

Cancer testis antigens (**CTA**) describe a group of proteins which are predominantly expressed in the adult testis while silenced in most other somatic tissues [1, 2]. CTAs are frequently misexpressed in cancers potentially by genome-wide epigenetic modifications that often accompany carcinogenesis or by misexpression of meiosis-specific factors [3, 4]. As the testis is immune privileged, the immune system does not recognize CTAs as self-proteins. Expression of CTAs outside of immune privileged sites can induce an immune response, thereby enabling a cancer-specific immune response to CTAs. These observations support the rationale that CTAs expressed in cancers constitute promising targets for immune therapy. Immune targeting of CTAs could activate a long-term response against CTA-expressing cancer cells with minimal side

effects on normal tissue. Since their characterization, there has been growing interest in developing immune therapeutics against CTAs [5]. Clinical trials targeting CTAs are ongoing despite some early setbacks [6-10]. Recently, it was recognized that apart from being immune targets, some of the CTA can be drivers in promoting carcinogenesis and their expression could be selected during tumor evolution [11].

In terms of their neoplastic potential, CTAs may engage diverse mechanisms in somatic cells [11]. One prominent class of CTAs appears to lead to genome instability by impeding DNA repair, especially the process of homologous recombination (**HR**). Factors impacted by this class of CTAs include BRCA1 and BRCA2. Defective BRCA1 or BRCA2 function is associated with increased risk of breast, ovarian, prostate, pancreatic, and other cancers [12-15]. Yet only a small fraction (~5%) of cancers are caused by inherited mutations in BRCA1 or BRCA2 [16]. A much larger number of tumors appears to exhibit a **BRCA-ness** phenotype, mimicking the HR defects of *BRCA1* or *BRCA2* mutants, but caused by alternative mechanisms [17]. Emerging evidence discussed in this review suggests that one mechanism to induce BRCA-ness is the misexpression of CTAs, which may interfere with BRCA1, BRCA2 or other HR proteins.

The BRCA-ness phenotype in tumors is commonly defined by genomic scars, classified as specific mutational signatures, at least five of which are caused by defects in BRCA1 or BRCA2 [16, 17]. While exceedingly useful as a molecular tumor classification tool, genome sequence-based approaches may not report accurately on the extant HR-status of tumor cells, as HR-deficiencies are known to revert but retain their genomic scars [18-20]. Alternatively, a cytological assay to assess HR-status measures the DNA damage-induced focus formation of RAD51, a central HR protein [21-23]. While this approach can help define functional HR status, it likely

underestimates the extent of HR-deficiency, as RAD51 focus formation only reports on the early HR steps of DSB resection and RAD51 filament formation but not the subsequent steps of homology search, DNA strand invasion, and joint molecule resolution/dissolution [24] (**Fig. 2.1**). Hence, additional biomarkers to report on HR status are needed, and protein level expression of HR inhibitors, such as certain CTAs that cause HR defects, could be an independent complementary approach to detect HR deficiency in tumors.

This chapter highlights recent research identifying CTAs, either described as cancer testis genes (**CTG**) or proteins/antigens (CTA), that normally function in meiotic chromosome biology and DNA metabolism with special emphasis on DNA repair by HR (**Table 2.1**). Tumors deficient in HR are sensitive to targeted molecular therapies such as poly (ADP-ribose) polymerase (**PARP**) inhibitors [25-28]. PARP functions in the repair of ssDNA breaks that can be caused as byproducts of DNA damage and during DNA repair. PARP inhibitors trap PARP at the site of DNA damage and block the repair of ssDNA breaks, causing them to convert to one-ended DNA double-stranded breaks (**DSBs**) during DNA replication. During S-phase, such breaks can only be productively repaired by the HR pathway, whereas end-joining may result in mutations or genomic rearrangements (**Fig. 2.2**). This provides the rationale why HR-defective cells are hypersensitive to PARPi. Thus, CTAs that lead to HR defects could serve as biomarkers to make patients eligible for treatment with PARP inhibitor therapy. We evaluate this rationale by discussing published studies and results from relevant public databases to analyze expression and co-expression patterns of CTAs/CTGs, their genetic and epigenetic regulation, the dependency of cancer cells on CTA/CTG expression, as well as their relationship to known driver mutations. Lastly, we discuss how future studies could maximize our knowledge of CTAs and their role in genomic instability.

2.3 A Repertoire of Cancer Testis Genes and Antigens

Identification of CTAs began with the discovery of an X-linked protein, Melanoma Antigen Gene Family-A1 (MAGE-A1), as a tumor-specific antigen recognized by T cells in human melanomas [29]. Following this discovery, numerous tumor antigens, including another X-linked protein NY-ESO-1 (also known as CTAG1B) [30], were found to be expressed in testes and termed cancer testis antigens [5]. Many of these early members of CTAs are X-linked multi-copy genes that are located in rapidly evolving palindromic sequences of the X chromosomes, with many of them evolving distinctly in rodents and primates, including humans [31, 32]. Expression of these CTAs is predominant in testis, but some of them are also expressed in the placenta, brain, and embryonic ovaries [33, 34]. Among these X-linked CTAs, the MAGE family proteins and NY-ESO-1 attracted particular attention as potential targets of immunotherapy.

Although initially CTAs were defined as tumor-specific antigens, later studies using genomic approaches identified an increasing number of testis-specific genes that are ectopically expressed in cancers as cancer testis genes (**CTGs** or cancer germline genes) without direct validation as tumor-specific antigens [34-36]. Based on these findings, a manually curated public database recorded 204 genes as CTGs as of 2009 and was listed in the CT database (<http://www.cta.lncc.br>) [2]. Notably, half of these CTGs are X-linked genes (termed CT-X genes), and the other half are autosomal-linked single-copy genes (non-CT-X genes). The advent of next-generation sequencing facilitated identification of additional CTGs; one studies identified 1,019 CTGs [37] and another studies identified 1,103 CTGs [38]. These genome-wide analyses increased the number of single-copy non-CT-X genes, of which many are evolutionarily conserved germline genes, but many await validation as tumor-specific antigens.

Additionally, the systematic analysis of various cancer types provided a clue about the regulation of CTGs in various cancers. Only a few CTGs (typically between 0 and 2) were highly expressed in a given tumor, indicating that wide-scale misexpression of germline proteins or activation of a germline transcriptional program is not occurring in cancers [37]. The genome-wide analysis found that demethylated promoters were often located proximally upstream of testis-specific genes [37], supporting the notion that DNA demethylation is a key process in the activation of CTGs [3]. Of note, many testis-specific non-coding RNAs were found to be associated with CTG expression in various cancers, raising the possibility that non-coding RNAs regulate CTG expression [37].

In conclusion, the genome-wide analyses significantly expanded the universe of CTA/CTG candidates providing a rich source for studies of their role in carcinogenesis and as potential therapeutic targets and biomarkers.

2.4 Homologous Recombination and its Functions in Somatic and Meiotic Cells

The mitotic and meiotic divisions give rise to daughter cells following chromosome replication, but the two pathways are mechanistically distinct from one another (**Fig. 2.1**). The mitotic program consists of a single, equational division, giving rise to two daughter cells that are genetically identical to the parent cell. This mode of cell division is typically utilized as a mechanism of proliferation. In contrast, the meiotic program is made up of two successive divisions: a reductional division (meiosis I) that segregates the maternal and paternal homologs, followed by an equational division (meiosis II) that segregates sister chromatids, similar to the mitotic program, resulting in an overall halving of ploidy. Meiosis generates the haploid gametes that are required for biparental reproduction. In addition, meiosis reassorts genetic information from the

two parents, thereby producing daughter cells that are genetically distinguishable from the parental cells [39].

A critical feature of the meiotic program is the first meiotic division. This reductional division is achieved through the pairing and disjunction of homologous chromosomes. Two important modifications of the mitotic chromosome segregation program are required for this reductional division during meiosis I. First, the kinetochores of each pair of sister chromatids must attach to spindle microtubules emanating from the same pole. This is achieved through a structural modification of sister kinetochores conferred by the monoplin protein. Additionally, the homologous chromosomes must become physically linked to one another to enable their stable biorientation on the meiosis I spindle. These links are formed via crossover recombination between homologs [39] (**Fig. 2.1**). Over the course of the mitotic and meiotic cell cycles, the sister chromatids are connected *via* ring-link protein complexes called cohesins. During mitosis and meiosis II, centromere cohesion provides an opposing force to that of the spindle, leading to stable biorientation and accurate segregation of sister chromatids. Similarly, a crossover between the homologous chromosomes in combination with sister-chromatid cohesion is required for accurate segregation during meiosis I.

Meiotic recombination is a unique and highly specialized form of HR, and we emphasize here the differences between somatic and meiotic recombination [39-41] (See **Fig. 2.1** and its legend for the mechanistic steps in the HR pathway.) Meiotic recombination utilizes many components of the somatic recombination pathway as well as meiosis-specific components in order to pair and link the homologous chromosomes by crossovers (**Fig. 2.1**). Hence, meiosis-specific

recombination proteins interact with proteins that also function during somatic HR to bias the outcome of HR to achieve interhomolog crossing over.

Meiotic recombination differs from somatic recombination in that it is initiated by programmed DSBs at predetermined sites. By comparison, somatic recombination is triggered by unscheduled DNA lesions including DSBs, ssDNA gaps, and stalled/collapsed replication forks. In addition, somatic HR competes with other somatic DNA repair pathways such as non-homologous end-joining (NHEJ), microhomology-mediated end-joining (MMEJ), and break-induced replication (BIR). By comparison, competition between the meiotic HR pathway and alternative DNA repair pathways is limited through several mechanisms, including the covalent linkage of SPO11 to the DNA following DSB formation [42]. Modification of the DNA ends by SPO11 prevents non-homologous end-joining, a major competitor with the HR pathway for repair of two-ended DSBs in somatic cells.

Another important distinction between the somatic and meiotic recombination pathways is template choice. Somatic HR typically occurs between allelic sites on sister chromatids, thereby limiting the risk of associated homozygosity or chromosome rearrangement. By contrast, meiotic HR must occur between homologs in order to link them by crossovers. In many organisms, including mammals, a meiosis-specific RAD51 homolog DMC1 defines this inter-homolog bias mechanism. Interactions between RAD51, DMC1, and numerous protein-specific accessory factors, including the RAD51 paralogs for RAD51 and HOP2-MND1 for DMC1, may act to enforce these template choice preferences. [39-41]

Lastly, there are differences in the mechanisms through which the DNA strand exchange intermediates are matured and resolved into products. During meiosis I, at least one crossover

forms between each pair of homologs, even though a majority of DSBs are repaired without crossing over. This highly regulated distribution of crossovers is achieved using meiosis-specific factors, which include HFM1, MSH4-MSH5, TEX11-SHOC1-SPO16, HEI10, PRR19, RNF212 and CNTD1 that stabilize interhomolog recombination intermediates, and promote their maturation into COs via the MutL γ endonuclease (MLH1-MLH3) (**Fig. 2.1**). While CO in somatic HR is generally considered to be a minority outcome [24], recent genetic analysis of the U2OS and Saos-2 human cell lines unexpectedly revealed that CO formation can also be a relatively common outcome of repair of two-ended DSBs by somatic HR [43].

Our understanding of meiotic recombination is continuously evolving. Many highly conserved meiosis-specific proteins, such as SPO11, DMC1 and REC8, have clearly established activities across budding yeast, plants, mice, and humans (**Fig. 2.1**). Yet the functions of other factors that are essential to meiotic recombination, like HOP2-MND1, have not been fully elucidated. Our understanding of meiotic recombination in higher eukaryotes is further complicated by continuing discovery of novel recombination factors that have no homologs in budding yeast. Recent examples of novel, meiosis-specific proteins include MEIOB, SPATA22, HSF2BP/MEILB2, and BRME1/C19orf57 [44-49] that were also identified as CTAs (**Table 2.1**). This lack of mechanistic information as to the roles of many meiotic recombination proteins limits our ability to understand how they could interfere with somatic recombination when mis-expressed in mitotically cycling cells.

In summary, meiotic recombination is a specialized type of HR that functions to physically link the homologous chromosomes to one another to promote their reductional segregation at meiosis I.

Importantly, meiosis-specific HR proteins cooperate with general HR factors that also function during DNA damage repair/tolerance in somatic cells.

2.5 Mis-expressed proteins involved in meiotic chromosome metabolism and their role in carcinogenesis

The genome-wide analyses significantly expanded the numbers of CTA/CTG candidates, but their relationships to cancer largely remain to be determined. To start closing this knowledge gap, we conducted highly focused database analyses using the CTAs listed in **Table 2.1** which have known roles in meiotic chromosome biology and HR.

There are many similarities between testicular germ cells and cancers such as CTA expression, hypoxic environments, metabolic states, reductional division which could lead to aneuploidy in cancers and chromosomal exchanges that can cause homozygosis and chromosome rearrangement [50-52]. It has been proposed that CTA expression in somatic cells could promote tumor development by leading to a germ-cell state transition that is beneficial to tumor development and growth [4, 5, 53]. The premise is that multiple germ cell antigens, especially those that function together in meiosis, are simultaneously mis-expressed in cancer cells. While genome-wide analysis has revealed that generally only a few CTAs are highly expressed in a given tumor [37], we specifically analyzed the co-expression patterns of the CTAs in tumors and cancer cell lines using the Metabolic gEne Rapid Visualizer (MERAV, <http://merav.wi.mit.edu>) portal [54] (**Table 2.1**). This platform analyzes transcriptomic data from cancers and cell lines from a variety of cancer databases and calculates the gene expression correlation. Our findings indicate that multiple CTAs, especially those that function in the same pathway in germ cells, are often not co-expressed in cancer cell lines and tumors (**Fig. 2.3**). For example: In germ cells,

MEIOB and SPATA22 form a RPA-related complex that localizes to sites of meiotic DSBs and facilitates strand exchange. However, in lung adenocarcinomas expression of MEIOB and SPATA22 is mutually exclusive [37]. Surprisingly, testicular germ cell tumors (**TGCTs**) have reduced expression of CTAs and meiotic entry regulator genes (**Fig. 2.4**) [4]. Hence, it appears unlikely that cancer cells expressing these germline antigens are undergoing a programmed transition to a germ cell state.

CTAs are classified as testis-selective (expression in testis and a few somatic tissues) or testis-restricted (expression only in testis) [55]. We analyzed gene expression patterns across tumors and normal tissues using the Gene Expression Profiling Interactive Analysis (GEPIA; <http://gepia.cancerpku.cn>) database [56]. Our analysis reveals that most CTAs are expressed in a variety of normal somatic tissues, in addition to being highly expressed in testis (**Fig. 2.5**). However, it is unclear, how well the RNA levels correlate with protein levels. There are limited CTA protein level expression data available, and they are also subject to variations in detection sensitivity and expression cutoff [37]. Protein data in somatic tissues and cell lines are available for some CTAs listed in **Table 2.1** including REC8, DMC1, SPO11, HORMAD1 and HOP2, and show that their expression is not strictly specific to the germline [57-61]. The functional significance of the expression of these germ-line proteins in normal somatic tissues is unknown. When comparing the expression levels of the CTAs from **Table 2.1** with the expression of somatic HR proteins including RAD51, RAD54, RAD51AP1, RAD21 and SMC1 α across various normal tissues and cancers (**Fig. 2.5**), we identified highly variable expression without a recognizable pattern. Surprisingly, CTA expression is lower in testicular germ cell tumors (**TGCT**) than in normal testis unlike somatic HR proteins whose levels appear to be higher in TGCT than in normal testis. We conclude that many CTAs in **Table 2.1**, such as DMC1, HELLS, HOP2, MND1, HFS2BP, REC8, STAG3, SYCP2, and SYCE1 show appreciable RNA-level expression levels in somatic

tissues, some in the range of somatic HR factors. Others, such as PRDM9, RAD21L, SPO11, SSX1, SYCP1, SYCP3, TEX12, and TEX19 show little if any RNA-level expression outside of the testis.

We next explored some of the genome changes that could lead to CTA expression focusing on the CTAs from **Table 2.1**. CTAs are hypothesized to be mis-expressed by genome-wide hypomethylation changes that occur in cancer [3]. In germ cells, CTA genes are regulated on a background of promoter hypomethylation [62]. Promoter hypomethylation is a prerequisite for gene activation, but it is not the only mechanism of gene activation. We explored if CTA expression is correlated with promoter demethylation using the Dependency Map (DepMap; <https://depmap.org/portal>) and the Broad Institute Cancer Cell Line Encyclopedia (CCLE; <https://portals.broadinstitute.org/ccle>) databases (**Fig. 2.6**) [63, 64]. The gene encoding SRY-related HMG-box genes (SOX10) was utilized as a positive control, and none of the CTAs reached that level of correlation. In cancer cell lines, some CTAs like DMC1, HOP2, MND1, HSF2BP and STAG3 seem to be predominantly hypomethylated in contrast to SYCP3 and TEX12 which are primarily hypermethylated. Both these groups of CTAs show no-correlation to gene expression indicating other mechanisms might regulate gene expression. In contrast, REC8, SYCE1 and SYCP2 expression appears to be inversely correlated with DNA methylation (*i.e.*, expressed when hypomethylated). However, tumor type-resolved analysis showed significant correlation between RNA levels and promoter demethylation for these and additional CTAs in certain tumor types (**Table 2.2**) indicating that promoter demethylation could lead to CTA expression in some cancer subtypes. The analysis by *Wang et al.* indicates that promoters for testis-specific genes and demethylation sites were often located 100 to 1 kb upstream of CTGs. In specific cancers, promoter demethylation leads to expression of some of the CTAs while other CTAs could be activated by alternate mechanisms [37]. Another factor likely influencing CTA

expression is the expression of ncRNAs. CTAs could be either activated (e.g. ncRNA LINC00577 activates CTA LIN28B expression) or inhibited (e.g. ncRNA LINC00254 inhibits CTA MEIOB expression) by the expression of nearby testis specific ncRNAs [37]. Finally, we explored whether CTA expression is correlated with gene copy number amplification but found weak to no correlation between the expression of CTAs and gene copy number amplification (**Fig. 2.7**). The gene encoding epidermal growth factor receptor (EGFR) was utilized as a positive control, and none of the CTAs reached that level of correlation. This analysis was not resolved for tumor type, explaining the relatively low Pearson's coefficient for EGFR. Among CTAs, SYCP2 and TEX12 showed the highest Pearson coefficients, and tumor type-resolved analysis did reveal significant correlation between RNA levels and gene copy number for these and additional CTAs in certain tumor types (**Table 2.3**). We conclude that promotor demethylation, ncRNAs and gene amplification are some of the mechanisms underlying mis-expression of some CTAs in specific tumor types.

Cancer cells can become dependent ('addicted') on the expression of normally non-essential genes, which may identify cancer-specific vulnerabilities. Some genes involved in maintaining genome stability are essential, for example *BRCA1* and *BRCA2*, while other HR genes such as *RAD54* or *BLM* are not (for detailed information see [24]). Cancer gene dependency is defined as a gene whose expression is required for the proliferation or survival of cancer cells [65, 66]. We used the Dependency Map (DepMap; <https://depmap.org/portal>) database to analyze the dependency of cancer cell lines on the CTAs listed in **Table 2.1** focusing on the CRISPR knockout data as they tend to be more robust than the siRNA datasets [63]. Cancer cell lines generally showed low to no dependency on the CTAs (**Table 2.4**). We have included dependency data for the prototypical oncogene *MYC* as a positive control, and 99% of the cell lines are dependent on *MYC* (**Table 2.4**). There were some cell lines that had moderate dependency on a CTA (**Table**

2.4) and other reported dependencies [58, 67-69]). Such dependencies appeared to be cell-line specific and did not apply to a specific cancer type. We infer that CTAs do generally not assume an essential function in cancer cells, which is consistent with the overall conclusion that CTAs are not required for normal HR-mediated repair in cancer cells but rather interfere with it (see below).

Most studies on CTAs use a limited number of cell lines as models. We tried to extend these studies by database analysis of multiple cell lines of different cancer types using the Dependency Map (DepMap; <https://depmap.org/portal>) and the Broad Institute Cancer Cell Line Encyclopedia (CCLE; <https://portals.broadinstitute.org/ccle>) databases [63, 64]. Our findings indicate that there is significant variation across cell lines even within a particular cancer subtype, and it is difficult to make a generalizable conclusions or correlations based on findings from a few cell lines. For example, *Sato et al.* show that ectopic expression of HSF2BP in HELA cells led to increased sensitivity to treatment with cisplatin and PARP inhibitor olaparib [69]. But when we analyzed the effect of cisplatin or olaparib treatment across cell lines expressing HSF2BP in the Dependency Map (DepMap; <https://depmap.org/portal>) we do not find any correlation. Cell lines with high HSF2B expression do not show increased sensitivity to cisplatin or olaparib treatment. Hence findings from a few cell lines may not be generalizable to an entire cancer type.

Mutually exclusive CTA expression with inactivating mutations in the major HR genes, BRCA1 and BRCA2, that drive tumor formation may indicate functional significance. Using genomic and transcriptomic breast cancer data [70, 71], we found that somatic expression of the CTAs in **Table 2.1** was seemingly mutually exclusive of inactivating mutations in BRCA1 and BRCA2 (**Fig. 2.8**), although the results were not statistically significant due to low sample sizes of tumors containing BRCA1/BRCA2 mutation and CTA overexpression. A published study revealed mutually

exclusive expression of CTAs, including MEIOB (**Table 2.1**), with mutations in PIK3CA, the catalytic subunit of phosphatidylinositol 3-kinase [37]. Our analysis of the CTAs in **Table 2.1** identified statistical significance for expression of DMC1 and HSF2BP being mutually exclusive of PIK3CA mutations. These analyses are currently limited by low sample sizes, and there is a clear need for more cancer samples with HR gene mutations and CTA overexpression to determine statistical significance.

Apart from DNA repair by HR, CTAs can also promote oncogenesis by affecting other pathways such as transcription (TEX19 [72]), mutagenic DNA damage tolerance by trans-lesion DNA synthesis (MAGE-A4 [73]), or as oncogenes (SYCP3 [68, 74], HELLS [75]) and tumor suppressors (REC8 [76, 77]). While non-CT-Xs have specific functions in DNA metabolism (**Table 2.1**), CT-Xs tend to be intrinsically disordered proteins, lacking rigid 3D structure or enzymatic functions, and their functions in germ cells remain largely unknown [78]. CT-Xs like MAGE-A4 and the SSX family of proteins are not seemingly involved in DNA metabolism in germ cells but have been shown to affect DNA repair and genome stability when expressed in somatic cells [73, 79] (**Table 2.1**). A recent study demonstrated that MAGE genes evolved to protect the mammalian male germline against environmental stress, proposing that cancer cells exploit MAGE genes to facilitate their cell growth [80]. Thus, certain CTAs may increase the fitness in reproduction and cancer survival.

In conclusion, the CTAs in **Table 2.1** are rarely co-expressed with their meiotic partner proteins in cancer cells. Hence these proteins are unlikely to be performing their normal meiotic function in somatic cells. CTAs that are mis-expressed in cancers have varying functions in meiosis. They include structural components of the synaptonemal complex, recombinases, cofactors and

cohesins. In germline cells, meiotic proteins interact with somatic HR proteins to achieve specialized functions, including interhomolog recombination and crossing over. So, it is likely that when a given CTA is expressed in somatic cells, it will similarly interact with its somatic recombination partners. However, since other meiotic interaction partners are unavailable, this interaction could lead to dysfunction and genomic instability. For example, in a comprehensive analysis of over 1,500 cancer samples across 39 cancer types, PRDM9 was found to be mis-expressed in ~20% of tumors [81]. Interestingly, structural variant breakpoints in these tumors were significantly enriched at PRDM9 binding sites. Similar to the results of our database analysis, the authors found no evidence that SPO11 was co-expressed with PRDM9, arguing against a model wherein PRDM9 is targeting and stimulating SPO11-catalyzed DSB formation in these tumors. In a separate study, IHC analysis of 52 triple-negative breast cancers and 32 adjacent tissues found that MEIOB was significantly upregulated in the tumors [82]. Overexpression of MEIOB in the SUM1315MO2 breast cancer cell line led to significantly decreased γ H2AX foci in response to cisplatin treatment, but HR *via* a GFP-reporter assay was also decreased. These findings suggest that there may be an early defect in γ H2AX focus formation in response to MEIOB expression in the SUM1315MO2 cell line, possibly as a result of aberrant association between MEIOB and RPA. **Figure 2.9** sketches out a number of postulated and potential mechanisms that the CTAs in **Table 2.1** could employ to interfere with genomic stability, and **Table 2.1** summarizes the key observations along with the relevant primary literature.

2.6 Conclusions and Future Studies

In this section we present conclusions based on our literature review and the database analyses presented in the earlier sections. There are now significantly more CTAs than originally reported, although their status as cancer antigens has often not been validated. CTAs are a diverse group of proteins of which only some of them are exclusively expressed in germ cells [55]. CT-Xs,

including many traditional CTAs, and non-CT-Xs, including many newly discovered CTAs, are distinct groups of proteins subject to different regulation based on their chromosomal locations. Moreover, CTAs have diverse meiotic functions and thus provoke distinct impacts on somatic cells when mis-expressed.

Concerted misexpression of numerous CTAs is rarely observed. As described in Section II, tumors typically mis-express between 0 and 2 CTAs. A much greater number of proteins is required for successful meiotic recombination arguing against the germ cell state theory of cancer [4, 53, 83]. Furthermore, though many meiotic proteins function within a heterodimer or protein complex (e.g. HOP2-MND1) that can also include somatic proteins (e.g. MEIOB and SPATA22 form a complex with RPA; BRME1 and MEILB2 interact with BRCA2), CTAs are seldom co-expressed with their interaction partners. Thus, it is unlikely that misexpressed CTAs are perform their normal meiotic function in somatic cells. Instead, we propose that these CTAs may bind DNA and/or interact with core HR proteins and thereby interfere with DNA replication, chromosome segregation, and DNA repair in somatic cells (**Fig. 2.10**). Emerging evidence suggests that misexpression of a single CTA can disrupt HR and lead to genomic instability. (**Table 2.1**). Currently, it is not known at what expression level the CTAs begin to disrupt HR and functional studies are clearly needed.

Our database analysis in Section IV suggests that a majority of cancer cell lines are not dependent on expression of CTAs for survival and proliferation. There are discrepancies between the database analyses and published studies of individual CTAs in a few cell lines which may be due to technical differences (e.g. CRISPR vs. RNAi; differently scored endpoints). CRISPR-knockout is generally more rigorous than siRNA knockdown. But tumors tend to be extremely adaptable

and so CRISPR analysis may miss important transient changes in tumor cell proliferation. There is a need for rigorous studies of CTAs in specific tumor types employing both CRISPR-knockout and siRNA knockdown in order to fully understand the effects of CTAs on tumor growth and proliferation.

Our analysis indicates that it may be difficult to project the findings from individual cell lines to an entire cancer subtype. Rigorous methodologies, such as the analysis of knockout mutants, will be required to gain a definitive picture of the biological significance of these meiosis-specific proteins in somatic cells. There may also be limitations to the findings from cell line studies when compared to tumors in their natural environment in an immuno-competent organism.

An ideal CTA to be used as a marker for HR-deficiency in tumors or as a therapeutic target should have testis-restricted expression. However, transcriptional data indicate that many meiosis-specific genes are expressed in normal somatic tissues as well [55]. However, given the multiple levels of post-transcriptional control in higher eukaryotes, expression at the mRNA level does not necessarily mean translation into protein products [37, 84]. There is very limited protein expression data available for CTAs, highlighting the need for more comprehensive CTA proteomics analysis in tumors, normal tissues and cancer cell lines. These findings will help understand which CTAs have an expression pattern that is strictly restricted to germ cells, as well as the physiological consequences of expression of certain meiosis-specific proteins in somatic cells.

It may be possible to develop certain CTAs as biomarkers for deficiencies in important cellular functions, such as HR, in cancer cells. This knowledge can be exploited to determine to which

therapies the tumor is most likely to respond. For instance, PARP inhibitors may be especially effective in treating HR-defective tumors, as these cancers would be particularly vulnerable to additional disruptions in the recombination pathway.

Cohesins
 DSB formation
 Others
 Recombination
 SC components

Protein	Meiotic function	Proposed role in carcinogenesis
BJ-HCC-20A	Unknown	BRCA2 interaction, promotion of cell growth and inhibition of apoptosis [85, 86]
BRME1/ C19orf57	Required for DMC1 focus formation	Reduction in RAD51 focus formation [46, 49]
DMC1	Homologous recombination	Replication fork stability [58]; enable interhomolog biased recombination?
HELLS	Chromatin Remodeler	Interaction with E2F3 to promote tumor progression [75]
HOP2/PSMC3-IP-MND1	DMC1 accessory factor	Increase in chromosome mobility, telomere exchanges [60]; cell cycle progression by upregulating E2F1 expression through interaction with KLF6 [67]
HORMAD1	Required for DSB formation and/or resection, SC formation	Promotes CtIP mediated resection [87] and RAD51 filament formation [88]; inhibition of HR [89]; prevents MCM8-MCM9 nuclear localization and limits MLH1 mismatch repair [90]
HSF2BP/ MEILB2	Required for DMC1 focus formation	Interference with BRCA2 function and HR [48, 69]
MAGE-A4	Transcriptional repressor	Increase in trans-lesion DNA synthesis [73]
MEIOB	ssDNA binding protein required for meiosis I progression	Homologous recombination deficiency and genome instability [37, 82]
PRDM9	Designates locations of DSBs	Whole-genome rearrangements [81]

RAD21L	Sister chromatid cohesion	Promotes homolog alignment [91] ; aberrant chromosome segregation leading to genome instability [57, 92]
REC8	Sister chromatid cohesion	Tumor suppressor [76, 77]; increased cancer cell survival by facilitating ploidy reduction in endopolyploid cells [93]; interacts with Hrp3 to promote loss of mitotic kinetochores [94]
SMC1 β , STAG3	Sister chromatid cohesion	Increased expression in some cancers [57, 95]
SPO11	Catalytic component of complex that reates DSBs	Increased expression in certain cancers, induces DNA damage [59, 96]; interacts with Hrp3 to cause loss of mitotic kinetochores [94]
SSX family	Transcriptional repressor	Genome instability [79]
SYCE1, SYCP1, SYCP2	Structural components of synaptonemal complex	Genome instability [97, 98]; expression in cancers [99, 100]
SYCP3	Lateral element of synaptonemal complex	Interferes with BRCA2, RAD51 function [101, 102]; interacts with AKT to promote tumor formation [68]; upregulates VEGF-C and VEGF-D to promote metastasis in lung cancers [74]
TEX12	Central element of synaptonemal complex	Centrosome amplification [103]
TEX19	Promote normal levels of SPO11 dependent recombination	Tumor proliferation [72]

Table 2.1. Selected cancer-testis antigens and their established functions in meiotic chromosome metabolism and homologous recombination with their proposed roles in carcinogenesis.

Gene	Cancer subtypes where gene expression has moderate to strong negative correlation with promotor methylation
<i>SOX10</i> (positive control)	breast: -0.861; central nervous system: -0.882; skin: -0.935
<i>DMC1</i>	-
<i>HOP2</i>	pancreas: -0.374; ovary: -0.403
<i>MND1</i>	-
<i>HSF2BP</i>	esophagus: -0.460
<i>MAGE-A4</i>	esophagus: -0.988; bile duct: -0.997; lung: -0.395; lymphocyte: -0.570
<i>MEIOB</i>	blood: -0.392; colorectal: -0.623; gastric: -0.622; lung: -0.454; ovary: -0.603; soft tissue: -0.610; uterus: -0.858
<i>PRDM9</i>	uterus: -0.683; ovary: -0.402; lymphocyte: -0.450; kidney: -0.497; blood: -0.372; bone: -0.596; colorectal: -0.344
<i>STAG3</i>	Lymphocyte: -0.325
<i>RAD21L</i>	Lymphocyte: -0.382
<i>REC8</i>	bile duct: -0.766; bone: -0.888; lung: -0.768; ovary: -0.751; peripheral nervous system: -0.838; uterus: -0.814; thyroid: -0.746
<i>SPO11</i>	-
<i>SYCP1</i>	peripheral nervous system: -0.589; uterus: -0.504
<i>SYCP2</i>	bone: -0.587; lung: -0.539; liver: -0.617; pancreas: -0.588; peripheral nervous system: -0.712; uterus: -0.531
<i>SYCE1</i>	breast: -0.699; bile duct: -0.795; gastric: -0.743; lymphocyte: -0.706; skin: -0.558; soft tissue: -0.641; upper aerodigestive: -0.890; thyroid: -0.869
<i>SYCP3</i>	uterus: -0.512; lymphocyte: -0.397
<i>TEX12</i>	breast: -0.307; lymphocyte: -0.496;

Table 2.2. Tumor-type specific correlation of gene expression with promotor methylation.

Tumor specific analysis of data in **Supplemental Figure 6** showing cancer subtypes where gene expression has moderate to high positive correlation with promotor methylation and are statistically significant (Pearson's correlation coefficient ≥ 0.3).

Gene	Cancer subtypes where gene expression has moderate to strong positive correlation with copy number amplification
<i>EGFR</i> (positive control)	breast: 0.499; esophagus: 0.695; lung: 0.410; liver: 0.455; upper aerodigestive: 0.585; thyroid: 0.611
<i>DMC1</i>	plasma cell: 0.427
<i>HELLS</i>	upper-aerodigestive: 0.38; plasma cell: 0.404; skin: 0.35; pancreas: 0.332; central nervous system: 0.391
<i>HOP2</i>	lymphocyte: 0.453; skin: 0.376
<i>MND1</i>	urinary tract: 0.468; liver: 0.419; gastric: 0.344; breast:0.310; bile duct: 0.827
<i>HORMAD1</i>	central nervous system: 0.394
<i>HSF2BP</i>	kidney: 0.389; soft tissue: 0.73
<i>MEIOB</i>	gastric: 0.554; pancreas: 0.380
<i>PRDM9</i>	blood: 0.369; thyroid; 0.781
<i>SMC1β</i>	breast: 0.401
<i>STAG3</i>	central nervous system: 0.358; pancreas: 0.306; upper aerodigestive: 0.486
<i>RAD21L</i>	thyroid: 0.660; soft tissue: 0.622
<i>REC8</i>	central nervous system: 0.359; kidney: 0.380; pancreas: 0.425
<i>SPO11</i>	Ovary: 0.442
<i>SYCP1</i>	-
<i>SYCP2</i>	uterus: 0.577; esophagus: 0.41; skin: 0.316 upper aerodigestive: 0.399
<i>SYCE1</i>	bone: 0.529
<i>SYCP3</i>	-
<i>TEX12</i>	bile duct: 0.908; upper aerodigestive: 0.559; lymphocyte: 0.461; breast: 0.541; skin: 0.443; plasma cell: 0.478; lung: 0.348
<i>TEX19</i>	-

Table 2.3. Tumor-type specific correlation of gene expression with copy number. Tumor specific analysis of data in **Figure 7** showing cancer subtypes where gene expression has moderate to high positive correlation with copy number amplification and are statistically significant (Pearson's correlation coefficient ≥ 0.3).

Gene	Dependent cell lines based on CRISPR screens/Total cell lines	Example of Cell lines with dependency score ≤ -0.5
<i>MYC</i> (positive control)	966/978	LS1034 (colorectal cancer), BT549 (breast cancer)
<i>DMC1</i>	0/990	-
<i>HELLS</i>	0/978	-
<i>HOP2</i>	12/978	HT3 (cervical cancer), NCIH1666 (lung cancer), OAW42 (ovarian cancer), TCCSUP (bladder cancer), JHU029 (head and neck cancer), WM88 (skin cancer), CHP212 (neuroblastoma)
<i>MND1</i>	1/990	JHU029 (head and neck cancer)
<i>HORMAD1</i>	24/990	CHLA57 (bone cancer), A427 (lung cancer), MC116 (lymphoma), TTC642 (rhabdoid), SCH (gastric cancer)
<i>HSF2BP</i>	1/990	GIMEN (neuroblastoma)
<i>MAGE-A4</i>	1/987	NCIH2882 (lung cancer)
<i>MEIOB</i>	0/990	-
<i>PRDM9</i>	0/978	-
<i>SMC1β</i>	3/978	SW403 (colorectal cancer), COLO800(skin cancer), YAMATO Sarcoma)
<i>STAG3</i>	2/990	SW948 (colorectal cancer), GIMEN (neuroblastoma)
<i>RAD21L</i>	0/990	AML193 (leukemia)
<i>REC8</i>	36/990	SG231 (bile duct cancer), UACC893 (breast cancer), D283MED (brain cancer), COLO230 (colorectal cancer), SCH (gastric cancer), LI7 (liver cancer), CORL105 (lung cancer), PEO4 (ovarian cancer)
<i>SPO11</i>	1/990	SNU626 (brain cancer)

<i>SSX1</i>	80/975	DU4475 (breast cancer), LS123 (colorectal cancer), JHH2 (liver cancer), EJM (myeloma), HEC1B(uterine cancer), JR (sarcoma), HCC2935 (lung cancer)
<i>SYCP1</i>	2/990	OMM1 (eye cancer), CH157MN(brain cancer)
<i>SYCP2</i>	0/990	-
<i>SYCE1</i>	0/990	-
<i>SYCP3</i>	0/978	-
<i>TEX12</i>	0/990	-
<i>TEX19</i>	9/990	SIHA (cervical cancer), GSS (gastric cancer), WM115 (skin cancer), NS (neuroblastoma), NB5 (neuroblastoma), MC116 (lymphoma)

Table 2.4. Cell line dependency on cancer-testis antigens from Table 1. The analysis of cancer cell line dependency used the Dependency Map (DepMap; <https://depmap.org/portal>) database [63]. Dependent cell lines have a probability of dependency (probability that the dependency score is from the distribution of essential gene scores rather than non-essential gene scores) greater than 0.5 [104], and column 2 lists the number of cell lines that meet this criterion. The gene dependency scores reflect the dependency of a given cell line on a particular gene. A dependency score of 0 means the gene is not dependent, while a score of -1 indicates strong inhibition of cell survival and proliferation in the corresponding cell line. The table uses the common cutoff of ≤ -0.5 in column 3.

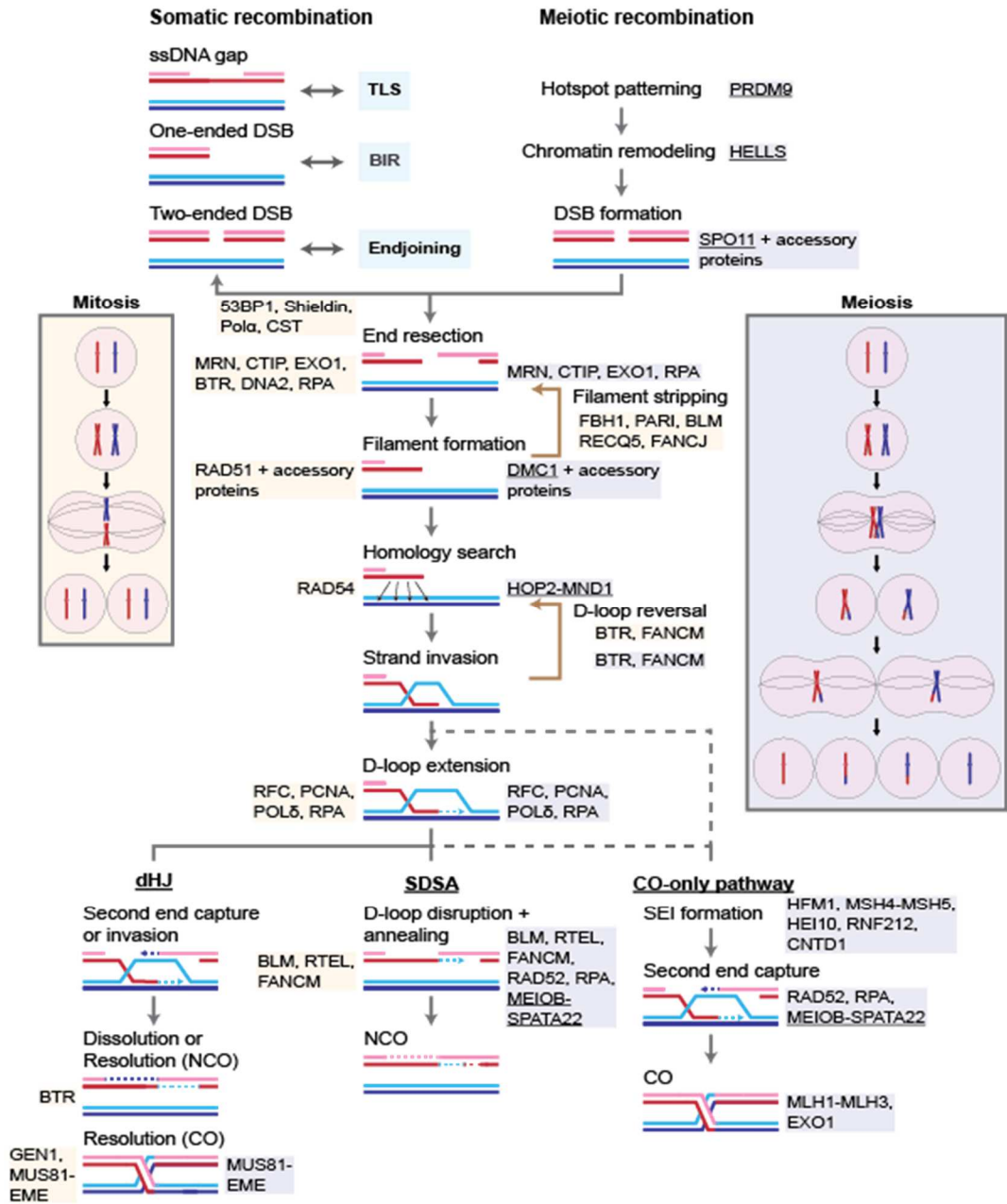


Figure 2.1. Somatic and meiotic homologous recombination pathways. Use of the somatic recombination is triggered by several types of DNA damage, including ssDNA gaps, one-ended breaks, arising from replication fork collapse or nicks in the replication template, and two-ended DSBs. In contrast, the meiotic recombination pathway is initiated by two-ended DSBs induced by SPO11 that remains covalently attached to the 5'-end of the DSB. The somatic recombination

pathway competes with other DNA damage repair/tolerance pathways in the cell (e.g., trans-lesion DNA synthesis (TLS) for repair of ssDNA gaps, break-induced replication (BIR) for repair of one-ended breaks, and endjoining pathways (non-homologous endjoining, microhomology-mediated endjoining) for repair of two-ended breaks, whereas alternative repair pathways are repressed during meiosis to promote use of the meiotic recombination pathway. Once initiated, the two homologous recombination pathways transition through similar steps, beginning with end resection. Proteins involved at each step in the recombination pathways are indicated (yellow boxes, somatic recombination; blue boxes, meiotic recombination). Note that many proteins function in both pathways, including RAD51 and its accessory factors, which act in conjunction with DMC1 during meiotic recombination. Resolution of the recombination intermediate can follow one of the three pathways indicated: a pathway that passes through a double Holiday junction (dHJ) intermediate to form crossovers (CO) and non-crossovers (NCO); a synthesis-dependent strand annealing (SDSA) pathway that gives rise exclusively to NCOs; and a meiosis-specific pathway that produces only COs. The SDSA pathway predominates during somatic recombination, whereas both the CO-only and SDSA pathways are common outcomes during meiosis. In both somatic and meiotic recombination, use of the dHJ pathway that results in both COs and NCOs is a minor pathway. The meiosis-specific CO-only pathway first transitions through a meta-stable intermediate called the single-end invasion (SEI), which is pre-destined to form a CO by forming a dHJ intermediate that is formed by second-end capture. The exact structure of the SEI and whether it includes newly synthesized DNA is unknown. Boxes depict chromosome segregation during the mitotic and meiotic cell cycles, respectively. Underlined protein names indicate that the factor has been implicated as a CTA (see **Table 1**). Additional Abbreviations: CST, CTC1-STN1-TEN1; BTR, BLM-TOPOIII α -RMI1/2.

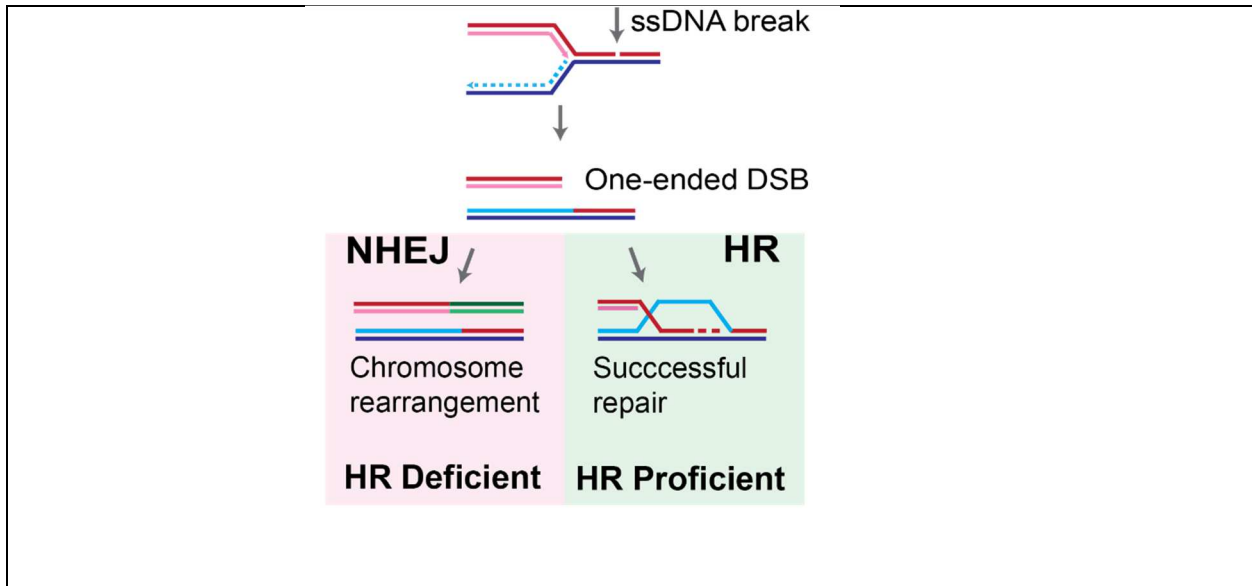


Figure 2.2. Replication-dependent formation and recovery of one-sided DNA double-stranded breaks during S-phase. Recovery of one-sided DSBs by homologous recombination (**HR**) in HR-proficient cells. In HR-deficient cells, the recovery is by non-homologous endjoining (**NHEJ**) which is joining the single end DSB to an ectopic DSB resulting in chromosome rearrangements.

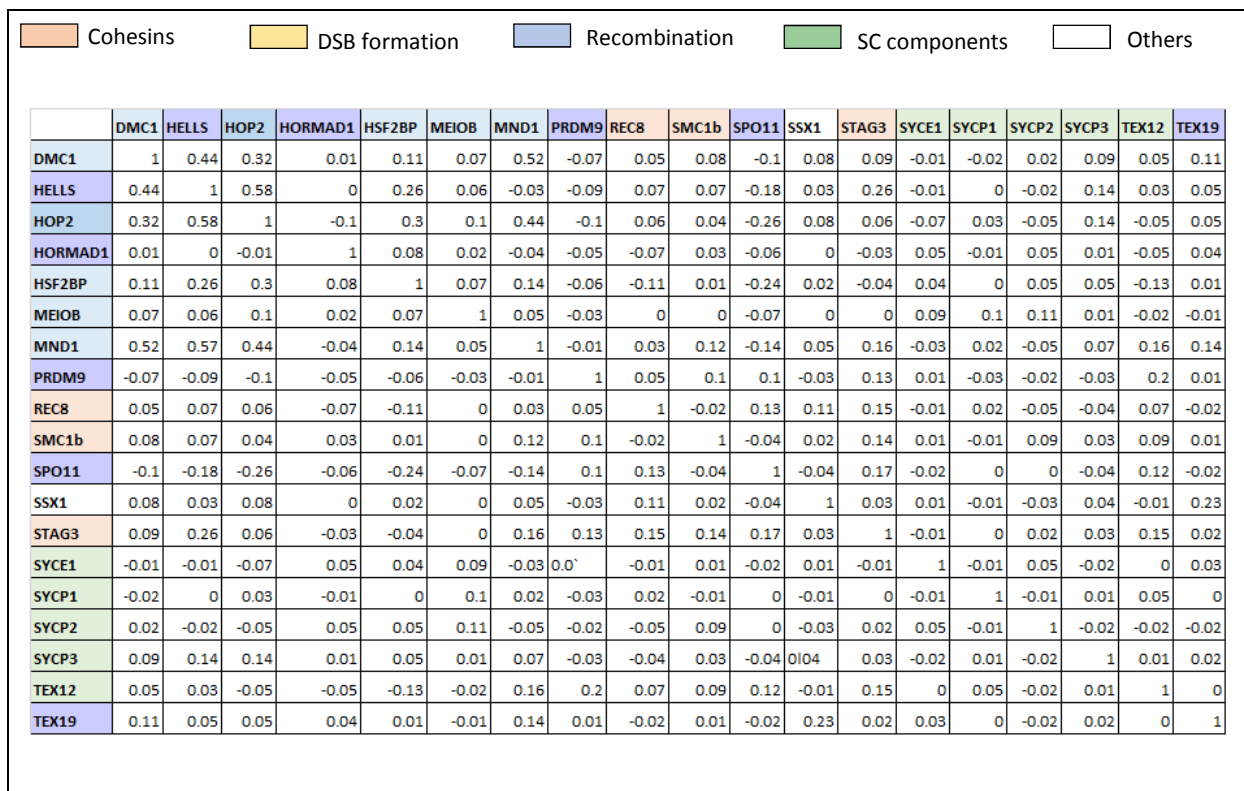


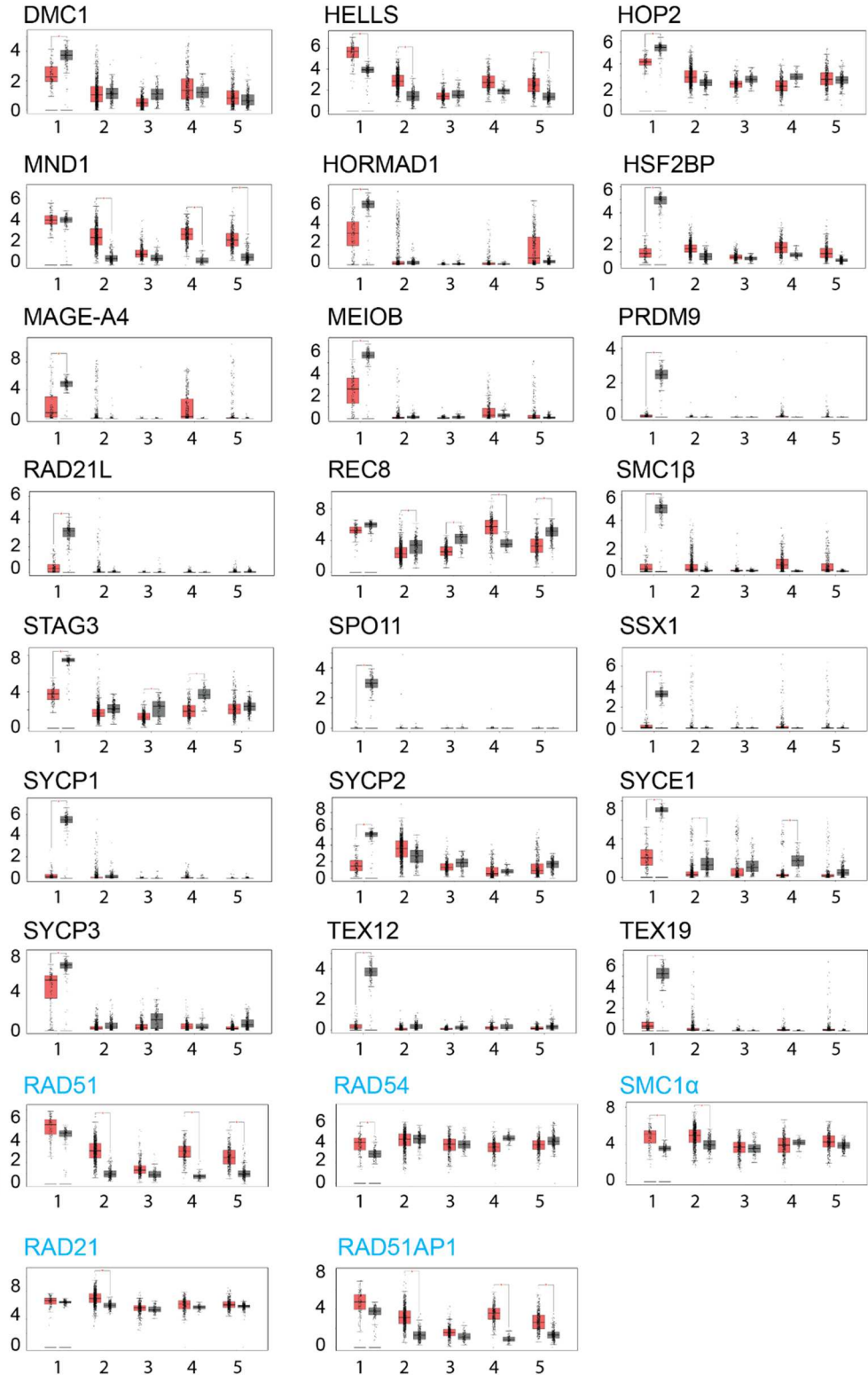
Figure 2.3. Correlation of cancer-testis antigen (CTA) expression across cancer cell lines and tumors. Pearson correlation using the Metabolic gEne RApid Visualizer (MERAV, <http://merav.wi.mit.edu>) website to calculate the association between expression of the CTAs from Table 1 [54].



Figure 2.4. Cancer-testis antigen expression in testicular cancers compared to other tumor types and corresponding normal tissues. RNA transcript expression ($\log_2(\text{TPM} + 1)$) analysis using the Gene Expression Profiling Interactive Analysis (GEPIA; <http://gepia.cancerpku.cn>) portal to analyze CTA expression in normal somatic tissues *versus* cancers from TCGA and GTEx datasets [56]. Dark blue indicates high expression while white indicates no expression.

CTAs:

Expression log₂(TPM+1)



Tumor █
Normal █

- 1. Testicular germ cell tumor
- 2. Breast Invasive Carcinoma
- 3. Prostate adenocarcinoma
- 4. Ovarian serous cystadenocarcinoma
- 5. Lung adenocarcinoma

Figure 2.5. Expression of cancer-testis antigens (CTA) and somatic HR proteins in tumors and normal somatic tissues. RNA transcript expression analysis using the Gene Expression Profiling Interactive Analysis (GEPIA; <http://gepia.cancerpku.cn>) portal to analyze CTA and somatic HR protein expression from TCGA and GTEx datasets in normal somatic tissues and cancers [56]. The Y axis is the gene expression in $\log_2(\text{TPM}+1)$ and adjusted according to the data. The X axis lists the cancers/corresponding normal tissues analyzed.

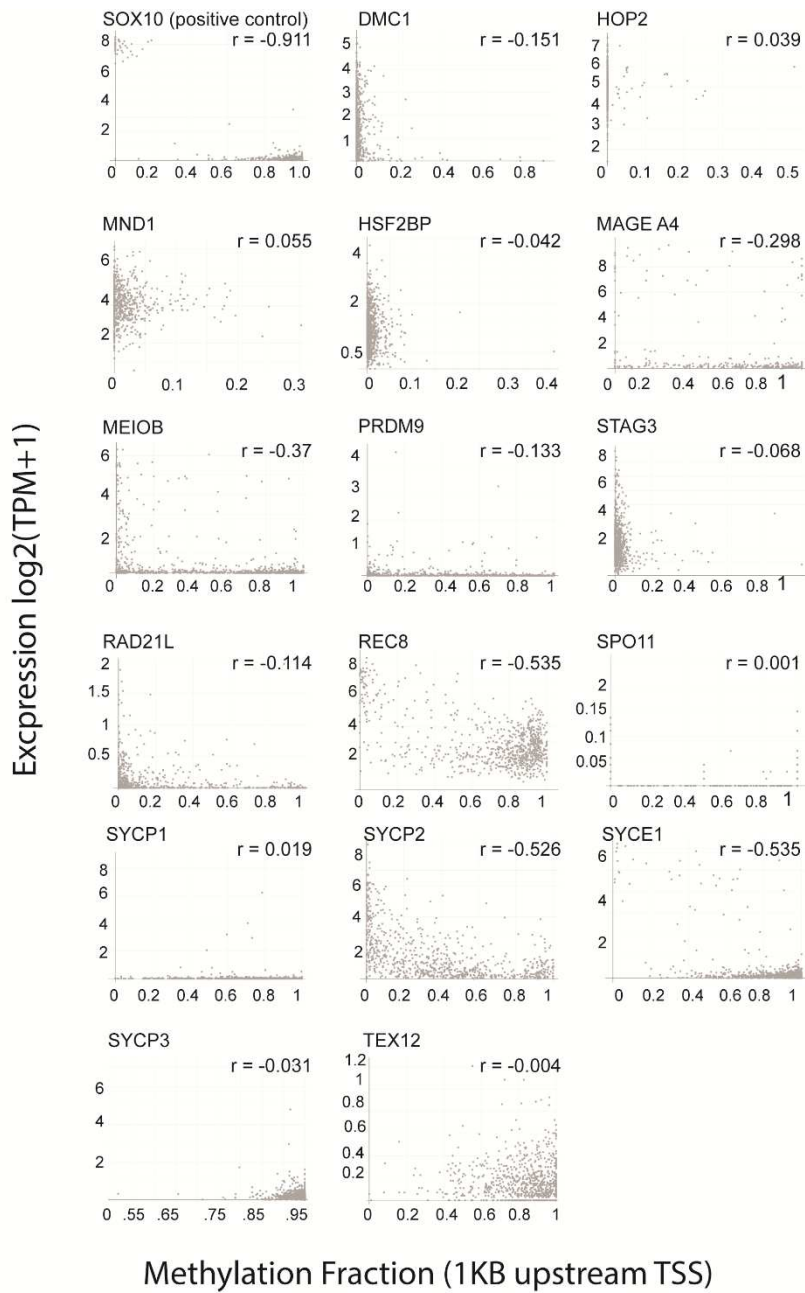


Figure 2.6. Correlation of gene expression with methylation. The analysis of cancer cell lines used the Dependency Map (DepMap; <https://depmap.org/portal>) database [63]. r is the Pearson correlation coefficient. X axis is the methylation 1 Kb upstream of transcription start site (**TSS**) for each gene. Y axis is the gene expression in $\log_2(\text{TPM}+1)$. X axis and Y axis scales are adjusted according to the data. See **Table 2.2** for cancer type-resolved analysis.

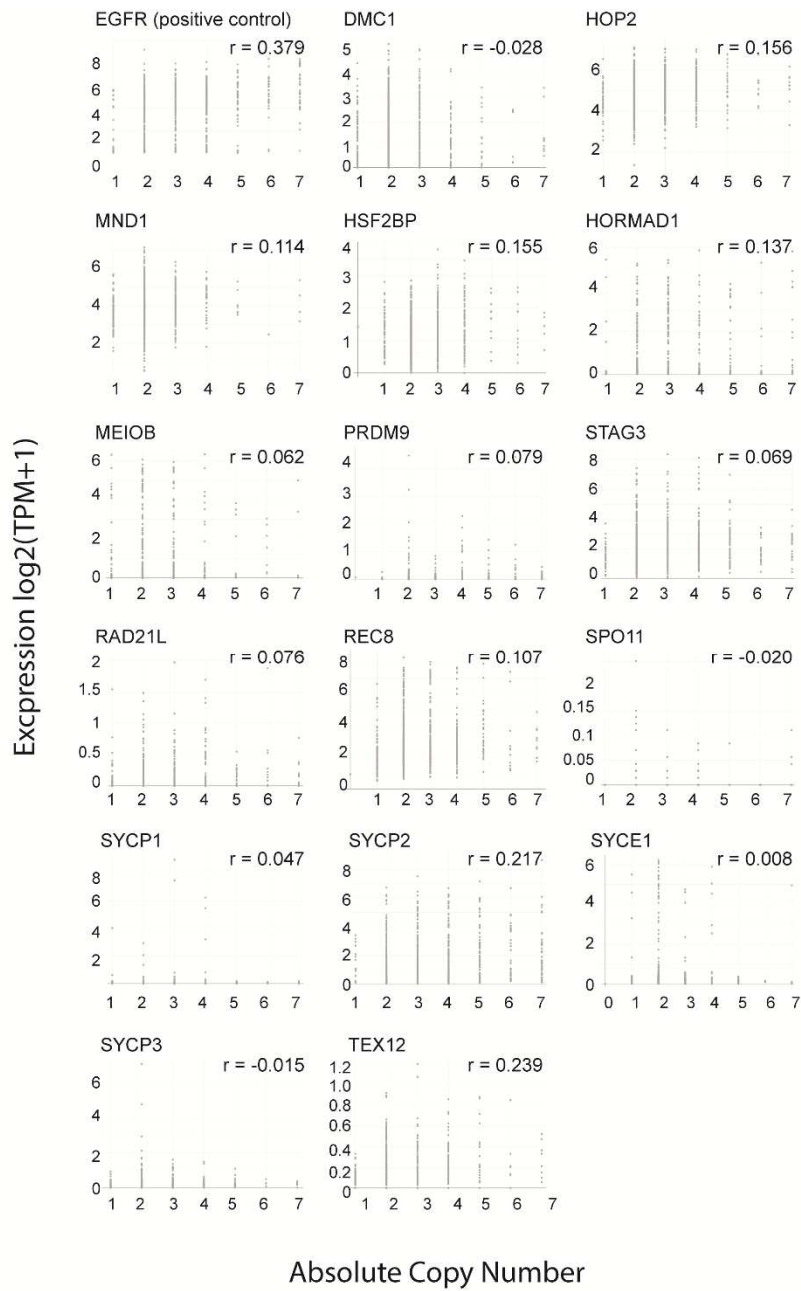


Figure 2.7. Correlation of gene expression with copy number. The analysis of cancer cell lines used the Dependency Map (DepMap; <https://depmap.org/portal>) database [63]. r is the Pearson correlation coefficient. X axis is absolute copy number. Y axis is the gene expression in $\log_2(\text{TPM}+1)$. X axis scale is adjusted according to the data. See **Table 2.3** for cancer type-resolved analysis.

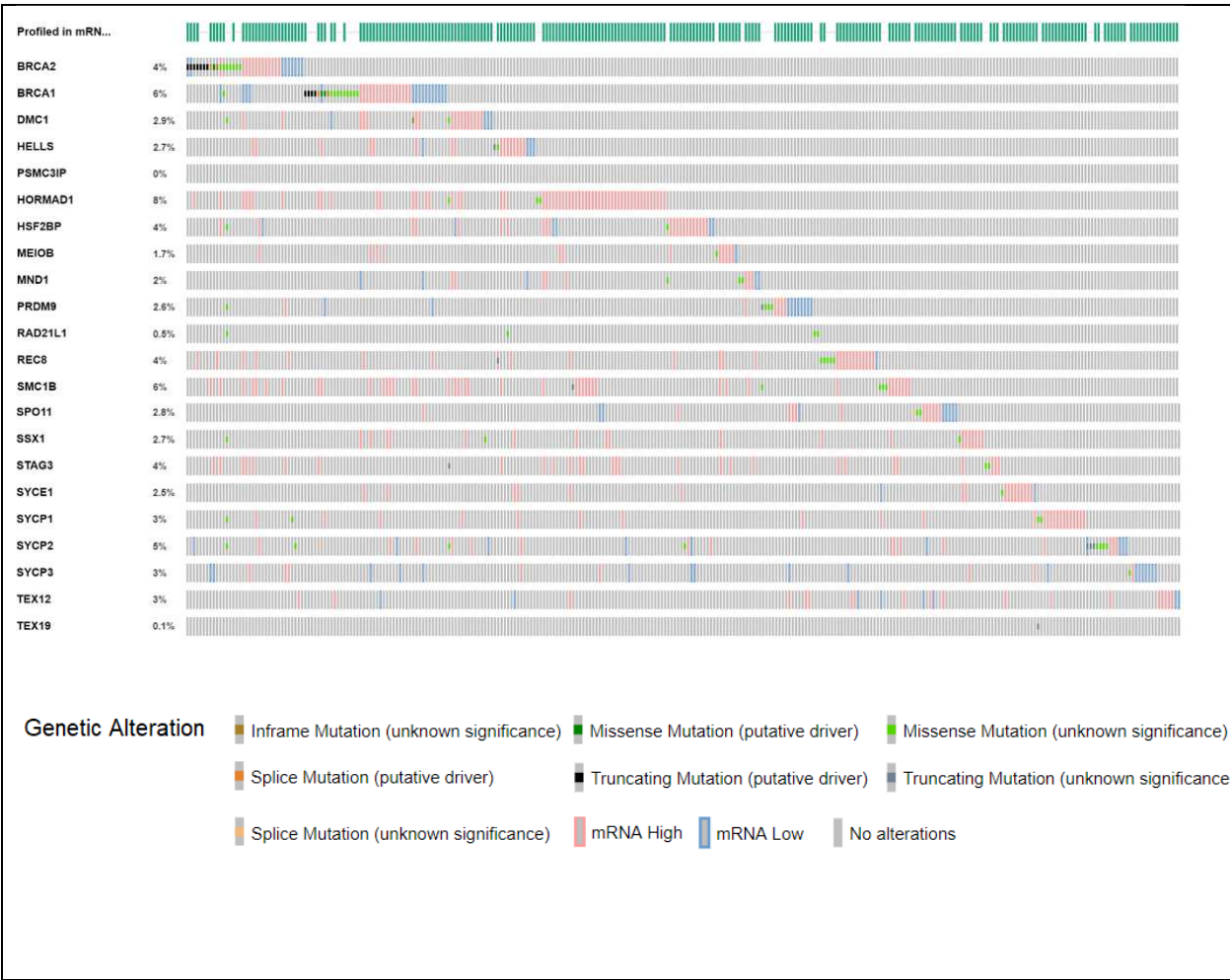


Figure 2.8. Cancer testis antigen (CTA) overexpression versus BRCA1 or BRCA2 modifications. 816 patient samples with breast invasive carcinoma (TCGA, CELL 2015 [105]) were analyzed for the correlation of CTA over-expression and mutations in the BRCA1 and BRCA2 genes using the cBioPortal for Cancer Genomics (cBioPortal; <https://www.cbioportal.org>) [70, 71].

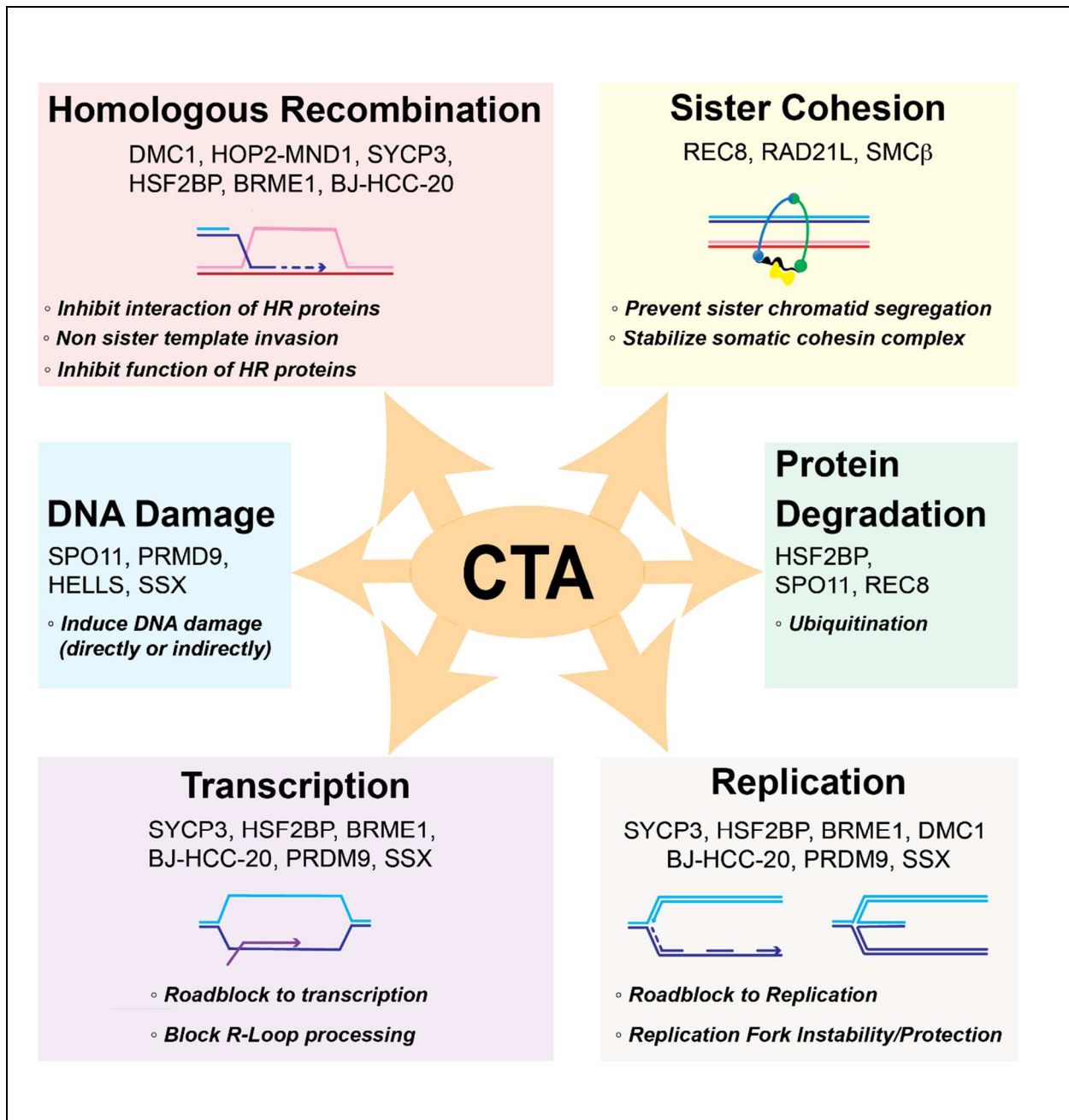


Figure 2.9. Possible mechanisms by which cancer testis antigens with a function in meiotic chromosome metabolism may affect genome stability. See **Table 1** for the list of proteins, their normal meiotic functions, and their proposed effects during in somatic cells.

2.6 References

1. Old, L.J. and Y.T. Chen, *New paths in human cancer serology*. J Exp Med, 1998. **187**(8): p. 1163-7.
2. Almeida, L.G., et al., *CTdatabase: a knowledge-base of high-throughput and curated data on cancer-testis antigens*. Nucleic Acids Res, 2009. **37**(Database issue): p. D816-9.
3. Fratta, E., et al., *The biology of cancer testis antigens: putative function, regulation and therapeutic potential*. Mol Oncol, 2011. **5**(2): p. 164-82.
4. Feichtinger, J. and R.J. McFarlane, *Meiotic gene activation in somatic and germ cell tumours*. Andrology, 2019. **7**(4): p. 415-427.
5. Simpson, A.J., et al., *Cancer/testis antigens, gametogenesis and cancer*. Nat Rev Cancer, 2005. **5**: p. 615-625.
6. Ogi, C. and A. Aruga, *Immunological monitoring of anticancer vaccines in clinical trials*. Oncoimmunology, 2013. **2**(8): p. e26012.
7. Ulloa-Montoya, F., et al., *Predictive gene signature in MAGE-A3 antigen-specific cancer immunotherapy*. J Clin Oncol, 2013. **31**(19): p. 2388-95.
8. Vansteenkiste, J., et al., *Adjuvant MAGE-A3 immunotherapy in resected non-small-cell lung cancer: phase II randomized study results*. J Clin Oncol, 2013. **31**(19): p. 2396-403.
9. D'Angelo, S.P. and e. al., *Antitumor Activity Associated with Prolonged Persistence of Adoptively Transferred NY-ESO-1 c259 T Cells in Synovial Sarcoma Cancer Discovery*, 2018. **8**: p. 944-957.
10. Wei, X.M., et al., *Cancer-Testis Antigen Peptide Vaccine for Cancer Immunotherapy: Progress and Prospects* Transl. Oncol, 2019. **12**: p. 733-738.
11. Gibbs, Z.A. and A.W. Whitehurst, *Emerging Contributions of Cancer/Testis Antigens to Neoplastic Behaviors*. Trends Cancer, 2018. **4**(10): p. 701-712.

12. DeSantis, C., et al., *Breast cancer statistics, 2013*. CA Cancer J Clin, 2014. **64**(1): p. 52-62.
13. Donepudi, M.S., et al., *Breast cancer statistics and markers*. J Cancer Res Ther, 2014. **10**(3): p. 506-11.
14. Iqbal, J., et al., *The incidence of pancreatic cancer in BRCA1 and BRCA2 mutation carriers*. Br J Cancer, 2012. **107**(12): p. 2005-9.
15. Taylor, R.A., et al., *Germline BRCA2 mutations drive prostate cancers with distinct evolutionary trajectories*. Nat Commun, 2017. **8**: p. 13671.
16. Davies, H., et al., *HRDetect is a predictor of BRCA1 and BRCA2 deficiency based on mutational signatures*. Nat Med, 2017. **23**(4): p. 517-525.
17. Turner, N., A. Tutt, and A. Ashworth, *Hallmarks of 'BRCAness' in sporadic cancers*. Nat Rev Cancer, 2004. **4**(10): p. 814-9.
18. Edwards, S.L., et al., *Resistance to therapy caused by intragenic deletion in BRCA2*. Nature, 2008. **451**: p. 1111-1115.
19. Sakai, W., et al., *Secondary mutations as a mechanism of cisplatin resistance in BRCA2-mutated cancers*. Nature, 2008. **451**: p. 1116-1120.
20. Ma, J., et al., *The therapeutic significance of mutational signatures from DNA repair deficiency in cancer*. Nature Communications, 2018. **9**.
21. Meijer, T.G., et al., *Functional homologous recombination REpair CAPacity (RECAP) test in metastatic breast cancer biopsies*. Cancer Research, 2018. **78**(4).
22. Meijer, T.G., et al., *Functional Ex Vivo Assay Reveals Homologous Recombination Deficiency in Breast Cancer Beyond BRCA Gene Defects*. Clinical Cancer Research, 2018. **24**(24): p. 6277-6287.
23. Willers, H., et al., *Utility of DNA repair protein foci for the detection of putative BRCA1 pathway defects in breast cancer biopsies*. Mol Cancer Res, 2009. **7**(8): p. 1304-9.

24. Kowalczykowski, S.C., N. Hunter, and W.-D. Heyer, eds. *DNA Recombination*. Cold Spring Harbor Perspectives in Biology Collection. 2016, Cold Spring Harbor Laboratory Press. 549 pages.
25. Bryant, H.E., et al., *Specific killing of BRCA2-deficient tumours with inhibitors of poly(ADP-ribose) polymerase*. *Nature*, 2005. **434**(7035): p. 913-7.
26. Farmer, H., et al., *Targeting the DNA repair defect in BRCA mutant cells as a therapeutic strategy*. *Nature*, 2005. **434**(7035): p. 917-21.
27. Lord, C.J. and A. Ashworth, *PARP inhibitors: Synthetic lethality in the clinic*. *Science*, 2017. **355**(6330): p. 1152-1158.
28. Fong, P.C., et al., *Inhibition of poly(ADP-ribose) polymerase in tumors from BRCA mutation carriers*. *N Engl J Med*, 2009. **361**(2): p. 123-34.
29. van der Bruggen, P., et al., *A gene encoding an antigen recognized by cytolytic T lymphocytes on a human melanoma* *Science*, 1991. **254**: p. 1643-7.
30. Chen, Y.T., et al., *A testicular antigen aberrantly expressed in human cancers detected by autologous antibody screening* *Proc Natl Acad Sci USA*, 1997. **94**: p. 1914-8.
31. Sin, H.S., et al., *Human postmeiotic sex chromatin and its impact on sex chromosome evolution*. *Genome Res*, 2012. **22**(5): p. 827-36.
32. Mueller, J.L. and e. al., *Independent specialization of the human and mouse X chromosomes for the male germ line*. *Nature Genetics*, 2013. **45**: p. 1083-7.
33. Nelson, P.T., et al., *Cancer/testis (CT) antigens are expressed in fetal ovary*. *Cancer Immun*, 2007. **7**: p. 1.
34. Hofmann, O. and e. al., *Genome-wide expression analysis of cancer/testis gene expression*. *Proc Natl Acad Sci USA*, 2008. **105**: p. 20422-7.
35. Scanlan, M.J. and e. al., *Identification of cancer/testis genes by database mining and mRNA expression analysis* *Inter J Cancer*, 2002. **98**: p. 485-92.

36. Chen, Y.T. and e. al., *Identification of cancer/testis-antigen genes by massively parallel signature sequencing* Proc Natl Acad Sci USA, 2005. **102**: p. 7940-5.
37. Wang, C., et al., *Systematic identification of genes with a cancer-testis expression pattern in 19 cancer types*. Nat Commun, 2016. **7**: p. 10499.
38. da Silva, V.L. and e. al., *Genome-wide identification of cancer/testis genes and their association with prognosis in a pan-cancer analysis* Oncotarget, 2017. **8**: p. 92966-77.
39. Hunter, N., *Meiotic Recombination: The Essence of Heredity*. Cold Spring Harb Perspect Biol, 2015. **7**(12).
40. Brown, M.S. and D.K. Bishop, *DNA strand exchange and RecA homologs in meiosis*. Cold Spring Harb Perspect Biol, 2014. **7**(1): p. a016659.
41. Baudat, F., Y. Imai, and B. de Massy, *Meiotic recombination in mammals: localization and regulation*. Nat Rev Genet, 2013. **14**(11): p. 794-806.
42. Symington, L.S. and J. Gautier, *Double-strand break end resection and repair pathway choice*. Annual review of genetics, 2011. **45**: p. 247-71.
43. Elbakry, A., et al., *ATRX and RECQ5 define distinct homologous recombination subpathways*. Proceedings of the National Academy of Sciences of the United States of America, 2021. **118**(3).
44. Luo, M., et al., *MEIOB exhibits single-stranded DNA-binding and exonuclease activities and is essential for meiotic recombination*. Nat Commun, 2013. **4**: p. 2788.
45. Souquet, B., et al., *MEIOB targets single-strand DNA and is necessary for meiotic recombination*. PLoS Genet, 2013. **9**(9): p. e1003784.
46. Zhang, J., et al., *The BRCA2-MEILB2-BRME1 complex governs meiotic recombination and impairs the mitotic BRCA2-RAD51 function in cancer cells*. Nat Commun, 2020. **11**(1): p. 2055.
47. Brandsma, I., et al., *HSF2BP Interacts with a Conserved Domain of BRCA2 and Is Required for Mouse Spermatogenesis*. Cell Rep, 2019. **27**(13): p. 3790-3798 e7.

48. Zhang, J., et al., *A meiosis-specific BRCA2 binding protein recruits recombinases to DNA double-strand breaks to ensure homologous recombination*. Nat Commun, 2019. **10**(1): p. 722.
49. Takemoto, K., et al., *Meiosis-Specific C19orf57/4930432K21Rik/BRME1 Modulates Localization of RAD51 and DMC1 to DSBs in Mouse Meiotic Recombination*. Cell Rep, 2020. **31**(8): p. 107686.
50. Reyes, J.G., et al., *The hypoxic testicle: physiology and pathophysiology*. Oxid Med Cell Longev, 2012. **2012**: p. 929285.
51. Oliveira, P.F., et al., *The Warburg effect revisited--lesson from the Sertoli cell*. Med Res Rev, 2015. **35**(1): p. 126-51.
52. Rajaraman, R., et al., *Neosis - a paradigm of self-renewal in cancer*. Cell Biol Int, 2005. **29**: p. 1084-97.
53. McFarlane, R.J. and J.A. Wakeman, *Meiosis-like Functions in Oncogenesis: A New View of Cancer*. Cancer Res, 2017. **77**(21): p. 5712-5716.
54. Shaul, Y.D., et al., *MERAV: a tool for comparing gene expression across human tissues and cell types*. Nucleic Acids Res, 2016. **44**(D1): p. D560-6.
55. Hofmann, O., et al., *Genome-wide analysis of cancer/testis gene expression*. Proc Natl Acad Sci U S A, 2008. **105**(51): p. 20422-7.
56. Tang, Z., et al., *GEPIA: a web server for cancer and normal gene expression profiling and interactive analyses*. Nucleic Acids Res, 2017. **45**(W1): p. W98-W102.
57. Feichtinger, J., et al., *Meta-analysis of clinical data using human meiotic genes identifies a novel cohort of highly restricted cancer-specific marker genes*. Oncotarget, 2012. **3**(8): p. 843-53.
58. Rivera, M., et al., *Acquisition of meiotic DNA repair regulators maintain genome stability in glioblastoma*. Cell Death Dis, 2015. **6**: p. e1732.

59. Romanienko, P.J. and R.D. Camerini-Otero, *Cloning, characterization, and localization of mouse and human SPO11*. Genomics, 1999. **61**(2): p. 156-69.
60. Cho, N.W., et al., *Interchromosomal homology searches drive directional ALT telomere movement and synapsis*. Cell, 2014. **159**(1): p. 108-121.
61. Lindsey, S.F., et al., *Potential role of meiosis proteins in melanoma chromosomal instability*. J Skin Cancer, 2013. **2013**: p. 190109.
62. Hammoud, S.S., et al., *Chromatin and Transcription Transitions of Mammalian Adult Germline Stem Cells and Spermatogenesis*. Cell Stem Cell, 2014. **15**: p. 239-53.
63. *DepMap, Broad (2019): DepMap 19Q3 Public. figshare. Dataset doi:10.6084/m9.figshare.*
64. Barretina, J., et al., *The Cancer Cell Line Encyclopedia enables predictive modelling of anticancer drug sensitivity*. Nature, 2012. **483**(7391): p. 603-7.
65. Lin, A. and J.M. Sheltzer, *Discovering and validating cancer genetic dependencies: approaches and pitfalls*. Nat Rev Genet, 2020. **21**(11): p. 671-682.
66. Tsherniak, A., et al., *Defining a Cancer Dependency Map*. Cell, 2017. **170**(3): p. 564-576 e16.
67. Zhang, Q., et al., *Meiotic nuclear divisions 1 (MND1) fuels cell cycle progression by activating a KLF6/E2F1 positive feedback loop in lung adenocarcinoma*. Cancer Commun (Lond), 2021.
68. Cho, H., et al., *Synaptonemal complex protein 3 is a prognostic marker in cervical cancer*. PLoS One, 2014. **9**(6): p. e98712.
69. Sato, K., et al., *HSF2BP negatively regulates homologous recombination in DNA interstrand crosslink repair*. Nucleic Acids Res, 2020. **48**(5): p. 2442-2456.
70. Cerami, E., et al., *The cBio cancer genomics portal: an open platform for exploring multidimensional cancer genomics data*. Cancer Discov, 2012. **2**(5): p. 401-4.

71. Gao, J., et al., *Integrative analysis of complex cancer genomics and clinical profiles using the cBioPortal*. *Sci Signal*, 2013. **6**(269): p. p11.
72. Planells-Palop, V., et al., *Human germ/stem cell-specific gene TEX19 influences cancer cell proliferation and cancer prognosis*. *Mol Cancer*, 2017. **16**(1): p. 84.
73. Gao, Y., et al., *A neomorphic cancer cell-specific role of MAGE-A4 in trans-lesion synthesis*. *Nat Commun*, 2016. **7**: p. 12105.
74. Kitano, H., et al., *Synaptonemal complex protein 3 is associated with lymphangiogenesis in non-small cell lung cancer patients with lymph node metastasis*. *J Transl Med*, 2017. **15**(1): p. 138.
75. von Eyss, B., et al., *The SNF2-like helicase HELLS mediates E2F3-dependent transcription and cellular transformation*. *EMBO J*, 2012. **31**(4): p. 972-85.
76. Zhao, J., et al., *REC8 inhibits EMT by downregulating EGR1 in gastric cancer cells*. *Oncol Rep*, 2018. **39**(4): p. 1583-1590.
77. Liu, D., et al., *REC8 is a novel tumor suppressor gene epigenetically robustly targeted by the PI3K pathway in thyroid cancer*. *Oncotarget*, 2015. **6**(36): p. 39211-24.
78. Rajagopalan, K., et al., *A majority of the cancer/testis antigens are intrinsically disordered proteins*. *J Cell Biochem*, 2011. **112**(11): p. 3256-67.
79. Greve, K.B., et al., *Ectopic expression of cancer/testis antigen SSX2 induces DNA damage and promotes genomic instability*. *Mol Oncol*, 2015. **9**(2): p. 437-49.
80. Fon Tacer, K., et al., *MAGE cancer-testis antigens protect the mammalian germline under environmental stress*. *Sci Adv*, 2019. **5**(5): p. eaav4832.
81. Houle, A.A., et al., *Aberrant PRDM9 expression impacts the pan-cancer genomic landscape*. *Genome Res*, 2018. **28**(11): p. 1611-1620.
82. Gu, Y., et al., *The cancer-testis gene, MEIOB, sensitizes triple-negative breast cancer to PARP1 inhibitors by inducing homologous recombination deficiency*. *Cancer Biol Med*, 2021. **18**(1): p. 74-87.

83. Simpson, A.J., et al., *Cancer/testis antigens, gametogenesis and cancer*. Nat Rev Cancer, 2005. **5**(8): p. 615-25.
84. Maggi, L.B., Jr. and J.D. Weber, *Forget transcription: translation is where the action is*. Mol Cell Biol, 2013. **33**(10): p. 1884-5.
85. Tomiyoshi, G., et al., *Novel BRCA2-interacting protein BJ-HCC-20A inhibits the induction of apoptosis in response to DNA damage*. Cancer Sci, 2008. **99**(4): p. 747-54.
86. Dong, X.Y., et al., *BJ-HCC-20, a potential novel cancer-testis antigen*. Biochem Cell Biol, 2004. **82**(5): p. 577-82.
87. Gao, Y., et al., *The Cancer/Testes (CT) Antigen HORMAD1 promotes Homologous Recombinational DNA Repair and Radioresistance in Lung adenocarcinoma cells*. Sci Rep, 2018. **8**(1): p. 15304.
88. Nichols, B.A., et al., *HORMAD1 Is a Negative Prognostic Indicator in Lung Adenocarcinoma and Specifies Resistance to Oxidative and Genotoxic Stress*. Cancer Res, 2018. **78**(21): p. 6196-6208.
89. Watkins, J., et al., *Genomic Complexity Profiling Reveals That HORMAD1 Overexpression Contributes to Homologous Recombination Deficiency in Triple-Negative Breast Cancers*. Cancer Discov, 2015. **5**(5): p. 488-505.
90. Liu, K., et al., *Aberrantly expressed HORMAD1 disrupts nuclear localization of MCM8-MCM9 complex and compromises DNA mismatch repair in cancer cells*. Cell Death Dis, 2020. **11**(7): p. 519.
91. Rong, M., S. Miyauchi, and J. Lee, *Ectopic expression of meiotic cohesin RAD21L promotes adjacency of homologous chromosomes in somatic cells*. J Reprod Dev, 2017. **63**(3): p. 227-234.
92. Strunnikov, A., *Cohesin complexes with a potential to link mammalian meiosis to cancer*. Cell Regen, 2013. **2**(1): p. 4.

93. Folco, H.D., et al., *Untimely expression of gametogenic genes in vegetative cells causes uniparental disomy*. Nature, 2017. **543**(7643): p. 126-130.
94. Hou, H., et al., *Centromeres are dismantled by foundational meiotic proteins Spo11 and Rec8*. Nature, 2021.
95. Wolf, P.G., et al., *Studying meiotic cohesin in somatic cells reveals that Rec8-containing cohesin requires Stag3 to function and is regulated by Wapl and sororin*. J Cell Sci, 2018. **131**(11).
96. Rossi, F., et al., *An in vivo genetic screen in Drosophila identifies the orthologue of human cancer/testis gene SPO11 among a network of targets to inhibit lethal(3)malignant brain tumour growth*. Open Biol, 2017. **7**(8).
97. Masterson, L., et al., *Deregulation of SYCP2 predicts early stage human papillomavirus-positive oropharyngeal carcinoma: A prospective whole transcriptome analysis*. Cancer Sci, 2015. **106**(11): p. 1568-75.
98. Kubuschok, B., et al., *Expression of cancer testis antigens in pancreatic carcinoma cell lines, pancreatic adenocarcinoma and chronic pancreatitis*. Int J Cancer, 2004. **109**(4): p. 568-75.
99. Taguchi, A., et al., *A search for novel cancer/testis antigens in lung cancer identifies VCX/Y genes, expanding the repertoire of potential immunotherapeutic targets*. Cancer Res, 2014. **74**(17): p. 4694-705.
100. Wu, X., et al., *A 10-gene signature as a predictor of biochemical recurrence after radical prostatectomy in patients with prostate cancer and a Gleason score ≥ 7* . Oncol Lett, 2020. **20**(3): p. 2906-2918.
101. Hosoya, N., et al., *Synaptonemal complex protein SYCP3 impairs mitotic recombination by interfering with BRCA2*. EMBO Rep, 2011. **13**(1): p. 44-51.
102. Kobayashi, W., et al., *SYCP3 regulates strand invasion activities of RAD51 and DMC1*. Genes Cells, 2017. **22**(9): p. 799-809.

103. S Sandhu, L.S., JE Hunter, CL Wilson, ND Perkins, N Hunter, OR Davies, UL McClurg, *A pseudo-meiotic centrosomal function of TEX12 in cancer*. bioRxiv, 2019.
104. Joshua M. Dempster, J.R., Mariya Kazachkova, Joshua Pan, Guillaume Kugener, David E. Root, Aviad Tsherniak, *Extracting Biological Insights from the Project Achilles Genome-Scale CRISPR Screens in Cancer Cell Lines*. bioRxiv, 2019.
105. Ciriello, G., et al., *Comprehensive Molecular Portraits of Invasive Lobular Breast Cancer*. Cell, 2015. **163**(2): p. 506-19.

Chapter 3: SYCP3 as a Potential Biomarker for HR Deficiency in Human Breast Cancers

This work has not been published yet and includes contributions from:

Ash Jay, Matthew Wong, Qian Chen, Kenneth Leung, Jie Liu, Alexander Borowsky
and Wolf-Dietrich Heyer

3.1 Abstract

SYCP3 is a cancer testis antigen (CTA) that is expressed in a variety of cancers including breast cancers. Recent findings show that SYCP3 mis-expression leads to functional BRCA2 deficiency which is a key factor associated with many breast cancers. The studies that evaluate SYCP3 expression in cancers are based on RNA transcript levels which may not be indicative of the protein levels. SYCP3 protein expression in breast cancers and its prognostic significance has not been studied yet. We assess SYCP3 protein expression in tumor samples from a cohort of 213 patients by immunohistochemistry. Our findings show that about 33 % of breast cancers express SYCP3 to some degree at the protein level. Finally, we assess the prognostic effect of SYCP3 protein expression on patient survival, and our results show that high SYCP3 expression is associated with better survival outcomes of patients as these tumors are defective in HR and might hence respond better to chemotherapeutics.

3.2 Introduction

SYCP3 is a structural component of the meiosis-specific synaptonemal complex (**SC**) which connects homologous chromosomes along their lengths and is required for chiasmata formation and accurate chromosome segregation during prophase I of meiosis [1]. The SC is comprised of two lateral elements or homolog axes connected by a central element comprising transverse filaments. SYCP3 is an essential part of the lateral elements of the SC. It is a small protein with a molecular weight of ~28 KD containing a central coiled-coil region that mediates assembly into anti-parallel tetramers [2]. SYCP3 also binds DNA *via* its N terminal region and is thought to bridge chromatin loops to help organize meiotic chromosome structure [3]. In mice and humans, mutations in SYCP3 lead to infertility in males due to meiotic arrest and subfertility in females with increased fetal deaths [4-7]. In addition, there is inefficient DSB repair and decreased crossing

over in oocytes of SYCP3 knockout female mice leading to increases in aneuploid gametes [8, 9]. These observations suggest that SYCP3 directly or indirectly facilitates meiotic recombination and Schimenti and colleagues provided evidence that SYCP3 promotes recombination between homologs instead of sister chromatids [9].

SYCP3 is typically expressed only in germline cells (*e.g.*, in testis, fetal ovary) but not in somatic cells. Emerging evidence indicates that SYCP3 is mis-expressed in certain cancer cells and primary tumors, and hence SYCP3 has been termed a cancer/testis antigen (**CTA**) [10-14]. CTAs are a class of proteins that were targeted as potential tumor-specific neo-antigens [15]. Surprisingly, recent data showed that when SYCP3 is ectopically expressed in somatic cells, it disrupts the high-fidelity DNA repair pathway, homologous recombination (**HR**) [11]. A central protein in HR is BRCA2 which localizes to the site of DNA damage and recruits other proteins such as RAD51 in somatic cells and DMC1 and RAD51 in germline cells to function in homology search and DNA strand invasion [16]. SYCP3 has been shown to interact with BRCA2, RAD51, and DMC1 in both cell-based assays and *in vitro* [17, 18] [17, 18] (unpublished data, Dr. Jie Liu in Heyer laboratory) . The structural role of SYCP3 in the SC during meiosis is relatively well understood but not much is known about its potential effects following misexpression in somatic cells. In germline cells, SYCP3, BRCA2, and RAD51 facilitate meiotic recombination which is induced by SPO11-mediated DNA double-stranded breaks. However, in somatic cells, SYCP3 expression results in a DNA repair defect [11]. This pathology is thought to result from out of context interactions between SYCP3, BRCA2 and RAD51 that impair their functions in DNA repair by HR [11, 17].

Breast cancer is a commonly diagnosed cancer in women, and it is a leading cause of cancer associated deaths [19]. BRCA1 and BRCA2 are recognized as susceptibility proteins for breast cancer. Only a small fraction (~5%) of cancers are caused by inherited germline mutations in BRCA1 or BRCA2 [20]. However, the “BRCA-ness” phenotype is characterized by defects in HR that can be caused by mutations in many factors including the BRCA1/BRCA2 interacting partner PALB2 [21-26]. Clinical studies show that about 20% of breast cancers exhibit the BRCA-ness phenotype [20, 27, 28]. Since SYCP3 affects BRCA2 and RAD51 function its misexpression in somatic cells could lead to a BRCA-ness phenotype, defective repair of DNA damage and increased risk of cancer over time. Indeed, cells with engineered expression of SYCP3 show defects in recombinational DNA repair and chromosomal instability [11].

Tumors deficient in HR are specifically sensitive to poly (ADP-ribose) polymerase inhibitors (**PARPi**) allowing selectively killing of tumor cells while sparing non-tumor tissue [29-32]. One of the functions of PARP is in the repair of ssDNA breaks. PARP inhibitors trap PARP at the site of DNA damage and block the repair of ssDNA breaks. During DNA replication these ssDNA breaks convert into one-sided DNA double-stranded breaks (DSB) which are normally repaired by the HR repair pathway. In cells deficient in HR, such one-sided DSBs are repaired by end joining which can result in genomic rearrangements that lead to mitotic catastrophe and cell death. Hence cells defective in HR are more sensitive to PARPi than HR-proficient cells. Conceptually, HR-deficiency could also be induced by the expression of proteins such as SYCP3 that impede HR. Hence, SYCP3 expression in cancers could serve as biomarkers for HR deficiency to help determine whether patients are eligible for treatment with PARP inhibitor therapy. In fact, cells with experimentally controlled SYCP3 expression show enhanced sensitivity to PARPi [11].

Recent studies show that about ~ 14% of breast cancers have SYCP3 misexpression [33]. This analysis is based on RNA transcript analysis, and it remains unclear whether these cells express SYCP3 at the protein level. In fact, cases have been described where the presence of mRNA does not result in translation and detectable protein levels, in particular for genes that undergo the exquisite regulation seen for germ cell-specific expression [34, 35]. Hence, there is a gap in knowledge regarding SYCP3 protein levels in cancers that could help more accurately identify tumors with a potential HR defect.

SYCP3 has been shown to have both nuclear and cytoplasmic localization in somatic cells. SYCP3 self-assembled into fibers in nucleus and cytoplasm when ectopically expressed in a mouse fibroblast cell line (Swiss-3T3) [36]. SYCP3 expression was detected in nuclear and cytoplasmic fractions of H1299, a lung carcinoma cell line [14]. Cytoplasmic expression of SYCP3 was detected by IHC analysis in tissue sections of cervical cancers and non-small cell lung cancers [12, 14]. In breast cancers, IHC analysis reveals both nuclear and cytoplasmic expression of SYCP3 [37]. We are interested in both nuclear and cytoplasmic expression because SYCP3 in the nucleus could directly affect HR by binding to BRCA2, RAD51 or DNA; while cytoplasmic SYCP3 could sequester BRCA2 and RAD51 to limit their nuclear entry potentially leading to an HR defect.

In this study, we performed immunohistochemistry (IHC) analysis of human breast tumors to detect SYCP3 protein expression in breast cancers. Our findings indicate that about 33% of human breast cancers have SYCP3 misexpression in the nucleus while 27% of the breast cancers have SYCP3 expression in the cytoplasm. There is a strong positive correlation between nuclear and cytoplasmic SYCP3 expression in the tumors (Spearman correlation; $r = 0.8331$). In a 2.5–

15-year period, patients with high SYCP3 expression show a better overall survival rate than patients with low SYCP3 expression ($p = 0.0356$ by MANTEL-COX log rank test). We speculate this is because tumors with SYCP3 expression may have HR defects and hence a better response to chemotherapeutics, similar to BRCA-deficient tumors [11, 17]. The difference in overall survival and disease-free survival curves for a period of 20 years was not statistically significant due to low sample sizes and presence of some outliers. This highlights the need for continued studies to increase sample size and independently confirm our results.

3.3 Materials and Methods

Tumor Specimens

Tissue microarrays (**TMA**s) with sections of paraffin-embedded primary breast tumor samples were obtained from Yale Tissue Microarray Facility (<https://www.tissuearray.org/Aquamine>).

Clinical information including age, race, survival status, survival time, surgery and chemotherapy were associated with the TMA's, as was pathology information including stage, grade, tumor characteristics and hormone receptor status. The TMA's also contained controls of 7 normal human breast sections and 8 breast cancer cell lines.

IHC Analysis

TMA's were baked at 60°C overnight and then deparaffinized in xylene and rehydrated in decreasing concentrations of ethanol. The slide was incubated in 3% H₂O₂ for 10 minutes to squelch endogenous peroxidase activity. We used a steam rice cooker for antigen retrieval in citrate buffer (pH 6.0) for 5 minutes at 125°C. Nonspecific immunoglobulin binding was blocked using 10 % fetal bovine serum for 30 minutes at room temperature (**RT**). The slides were

incubated overnight at RT in a humidified chamber with anti-SYCP3 antibody (1:6,000, SIGMA ATLAS antibody, HPA039635, lot# R37957) followed by incubation with an biotinylated anti-rabbit secondary antibody (Vector laboratories, BA-1000) for 1 hour. For immunohistochemical detection, slides were incubated with avidin and biotinylated horseradish peroxidase (Vector laboratories, PK-6100) and developed using a diaminobenzidine (DAB) substrate kit (Vector laboratories, SK-4100). The slides were counterstained in hematoxylin, dehydrated, and cover slipped. Images were acquired using an Aperio AT2 scanner and analyzed using Qupath [38] open-source software. The tumors were assigned a semiquantitative h-score based on the percentage and intensity of staining using the following equation:

h-score: (3 x percentage of strongly staining nuclei) + (2 x percentage of moderately staining nuclei) + percentage of weakly staining nuclei [38]. We classified high SYCP3 expression levels as h-score values in the upper quartile of the population (nucleus ≥ 4.4 ; cytoplasm ≥ 0.67).

Cell Pellet Controls

The human SYCP3 cDNA was inserted into the mammalian expression vector pcDNA5 under a tetracycline-inducible promoter. Following the Lipofectamine 3000 reagent protocol (Invitrogen), pcDNA5-SYCP3 was transiently transfected into HEK293 cells. We converted the HEK293 cells to pseudo-tissue blocks by pelleting the cells followed by formalin fixation and paraffin embedding (FFPE) of the pellet.

Immunoblot Analysis

The cells were lysed in lysis buffer (2 % SDS) and heated at 90 °C for 10 minutes before freezing at -20 °C. The lysate was solubilized in Laemmli buffer (1 X 6.25 mM Tris-Cl (pH 6.8), 2 % SDS,

10 % glycerol, 5 % beta-mercaptoethanol, 0.005 % bromophenol blue), boiled for 5 minutes, and proteins were separated by polyacrylamide gel electrophoresis (4-15 % Bio-Rad Mini-PROTEAN precast protein gel). The separated proteins were transferred to a PVDF membrane (Bio-Rad) and the membrane blocked with 5 % milk (Safeway, non-fat dry milk) for one hour. The membrane was incubated overnight at 4 °C with primary SYCP3 antibody (1:500, SIGMA ATLAS antibody, HPA039635, lot R37957) followed by secondary antibody incubation for 1 hour (1:10,000, polyclonal goat anti rabbit, Dako, P0448). SYCP3 bands were visualized by enhanced chemiluminescence (ECL, PerkinElmer) and exposed to X-ray film.

SYCP3 purification

The human SYCP3 cDNA sequence fused to a self-cleavable intein tag was cloned into the pet28b+ vector and transformed into Rosetta *Escherichia coli* cells. The *E. coli* cells were grown at 37 °C until the OD₆₀₀ reached 0.6, and then 0.5 mM IPTG was added to induce SYCP3 expression overnight at 18 °C. Cells from 10 L culture were suspended in lysis buffer containing 20 mM Tris-Cl (pH 7.5), 500 mM NaCl, 1 mM EDTA, 1 mM PMSF, 0.1 % Triton X-100 and 10 % glycerol. The cells were disrupted by sonication and crude lysate was clarified by centrifugation at 45,000 rpm for 1 hour in a Beckman Ti 70 rotor. The protein lysate was added to chitin resin equilibrated with 20 mM Tris-Cl (pH 7.5), 500 mM NaCl, 1 mM EDTA, 1 mM pMSF, 0.1 % Triton X-100 and 10 % glycerol. After extensive washing, on column cleavage of SYCP3 was induced by adding 50 mM DTT to the column buffer and incubating for 48 hrs. The eluent was applied to Mono Q column with buffer containing 20 mM Tris-Cl (pH 7.5), 100 mM NaCl, 1 mM EDTA, 10 % glycerol and 0.5 mM TCEP. After washing, SYCP3 was recovered by gradient elution from 200 mM NaCl – 1M NaCl. Peak fractions were pooled and dialyzed against storage buffer containing 20 mM Tris-Cl (pH 7.5), 100 mM NaCl, 1 mM EDTA, 10 % glycerol and 0.5 mM TCEP. The protein was aliquoted, flash frozen in liquid nitrogen and stored at -80 °C.

Statistical analysis

All statistical analysis was performed using Prism 9.1.0 for Windows. SYCP3 expression across various clinical and pathological features were compared by the Kruskal-Wallis [39] and Mann-Whitney tests [40]. Relationship between SYCP3 nuclear and cytoplasmic expression was analyzed by the non-parametric Spearman correlation test [41]. Kaplan-Meier survival analysis was used to analyze the effect of SYCP3 expression levels on overall survival times and disease-free survival times. The survival curves were compared by the MANTEL-COX log-rank test [42].

3.4 Results

Antibody Validation

SYCP3 is expressed in the germ cells of seminiferous tubules in the testis. We show IHC detection of SYCP3 in the seminiferous tubules of human testis which corresponds exactly to the expected expression pattern of this protein [37, 43] (**Fig. 3.1 A**). As negative controls, we used testis sections incubated with only the primary SYCP3 antibody or only the secondary rabbit antibody (**Fig. 3.1 B, C**). Since the primary antibody was developed in rabbits, we used rabbit serum instead of primary antibody to monitor non-specific binding of rabbit immunoglobulins and verified that IHC staining was negative (**Fig. 3.1 D**).

As further controls, we used HEK293 cells as they do not show spontaneous SYCP3 expression (**Fig. 3.2**). The SYCP3 cDNA was inserted into pcDNA5 vector under a tetracycline inducible promoter and transiently transfected into HEK293 cells. SYCP3 expression was induced by titrating tetracycline concentrations to regulate the expression level. As negative controls we used non-transfected HEK293 cells and cells transfected with the empty pcDNA5 vector. SYCP3

expression in these cell lines was monitored by immunoblotting using purified SYCP3 protein as a positive control (**Fig. 3.2 A**). In immunoblots, the SYCP3 antibody also recognizes higher molecular weight bands in addition to the one co-migrating with purified SYCP3. This very likely represents non-specific binding, as these signals are also present in the negative controls of cells without vector or with empty vector.

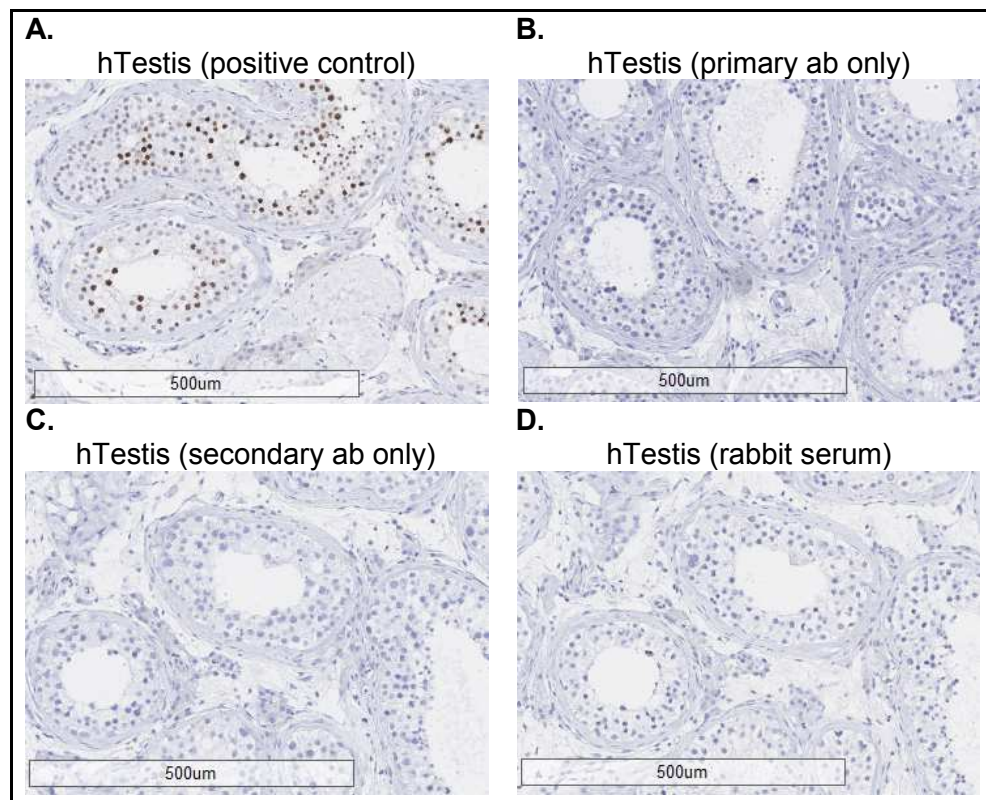


Figure 3.1: SYCP3 antibody validation on human testis sections. A. Positive control; **B.** Human testis section stained with only primary SYCP3 antibody (no secondary antibody); **C.** Human testis section stained with only secondary rabbit antibody (no primary antibody); **D.** Human testis section stained with rabbit serum instead of SYCP3 primary antibody to

test for non-specific binding of immunoglobulins. Images were taken at 5x magnification.

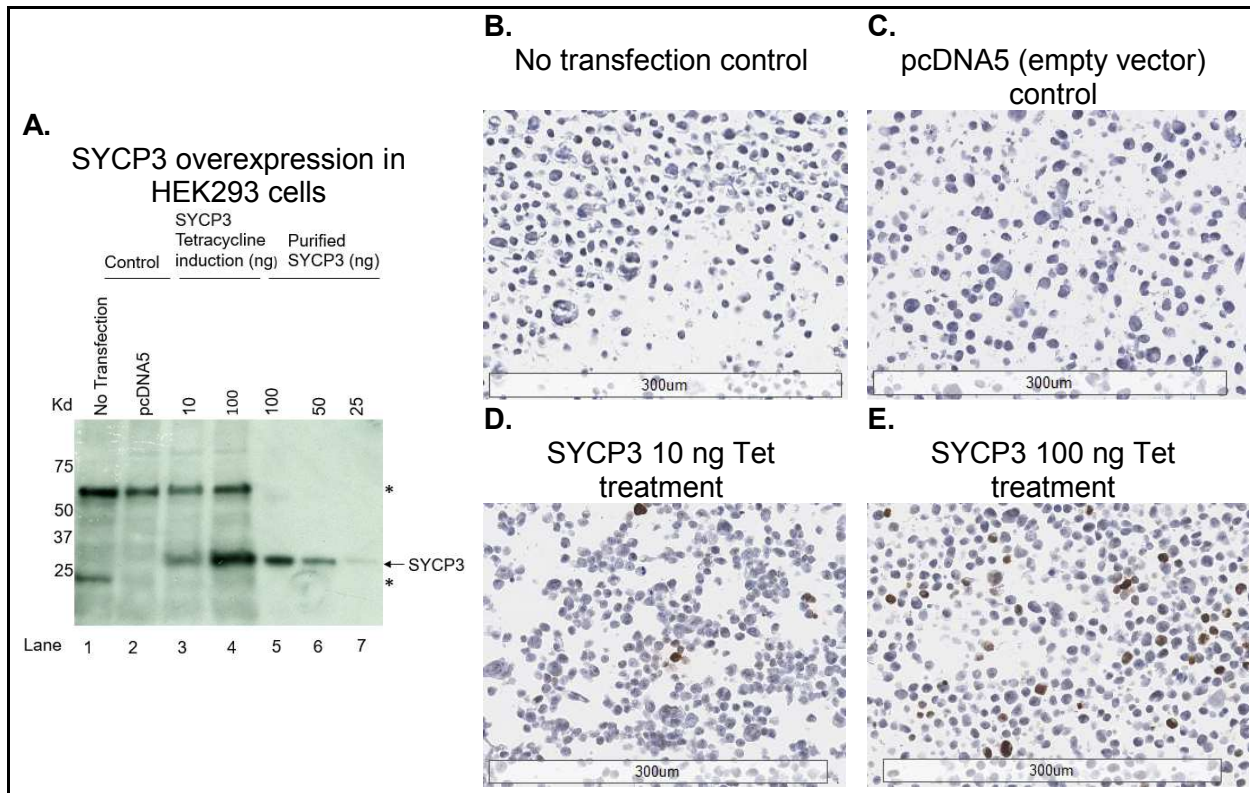


Figure 3.2: Immunoblot and IHC analysis of transient SYCP3 over-expression in HEK293 cells. **A.** Immunoblot analysis: Lane 1: No transfection control; Lane 2: Empty vector, pcDNA5 control; Lane 3: 10 ng tetracycline induction of SYCP3 expression; Lane 4: 100 ng tetracycline induction of SYCP3 expression; Lane 5-7: 100 ng, 50 ng and 25 ng of purified SYCP3 protein; **B-E.** IHC analysis in of SYCP3 expression in HEK293 cells: **B.** non-transfected HEK293 cells; **C.** HEK293 cells transfected with empty pcDNA5 vector; **D.** HEK293 cells transfected with pcDNA5-SYCP3 vector and treated with 10 ng tetracycline; **E.** HEK293 cells transfected with pcDNA5-SYCP3 vector and treated with 100 ng tetracycline. Images were taken at 10x magnification. (*) Non-specific binding.

Next, we performed IHC analysis on sections of cell pellets derived from the same cells used for immunoblot analysis to correlate both analytical methods. By IHC analysis we detect an increase in SYCP3 expression in the transfected HEK293 cell pellets with increasing concentrations of tetracycline induction (**Fig. 3.2 D, E**). There was no SYCP3 signal in negative controls including non-transfected HEK293 cells and those transfected with empty pcDNA5 vector (**Fig. 3.2 B, C**). The non-specific bands detected by the SYCP3 antibody in immunoblots are apparently not detected as staining signal in the IHC analysis. In human testis and HEK293 cells with transient SYCP3 over-expression we observed only nuclear staining and no cytoplasmic SYCP3 localization.

Finally, we performed IHC analysis on normal human breast tissues. Existing studies show that there is some SYCP3 expression in normal tissues including breasts by RNA transcript analysis (**Fig.3.3 A**) [44]. We stained 5 normal breast tissue sections from UC Davis Cancer Repository. Our findings indicate little to no SYCP3 protein expression in normal breast tissues (**Fig. 3.3 B**).

In sum, we have validated the specificity of the SYCP3 antibody in the IHC setting and optimized the IHC protocol conditions including antigen retrieval, antibody selection and antibody concentrations.

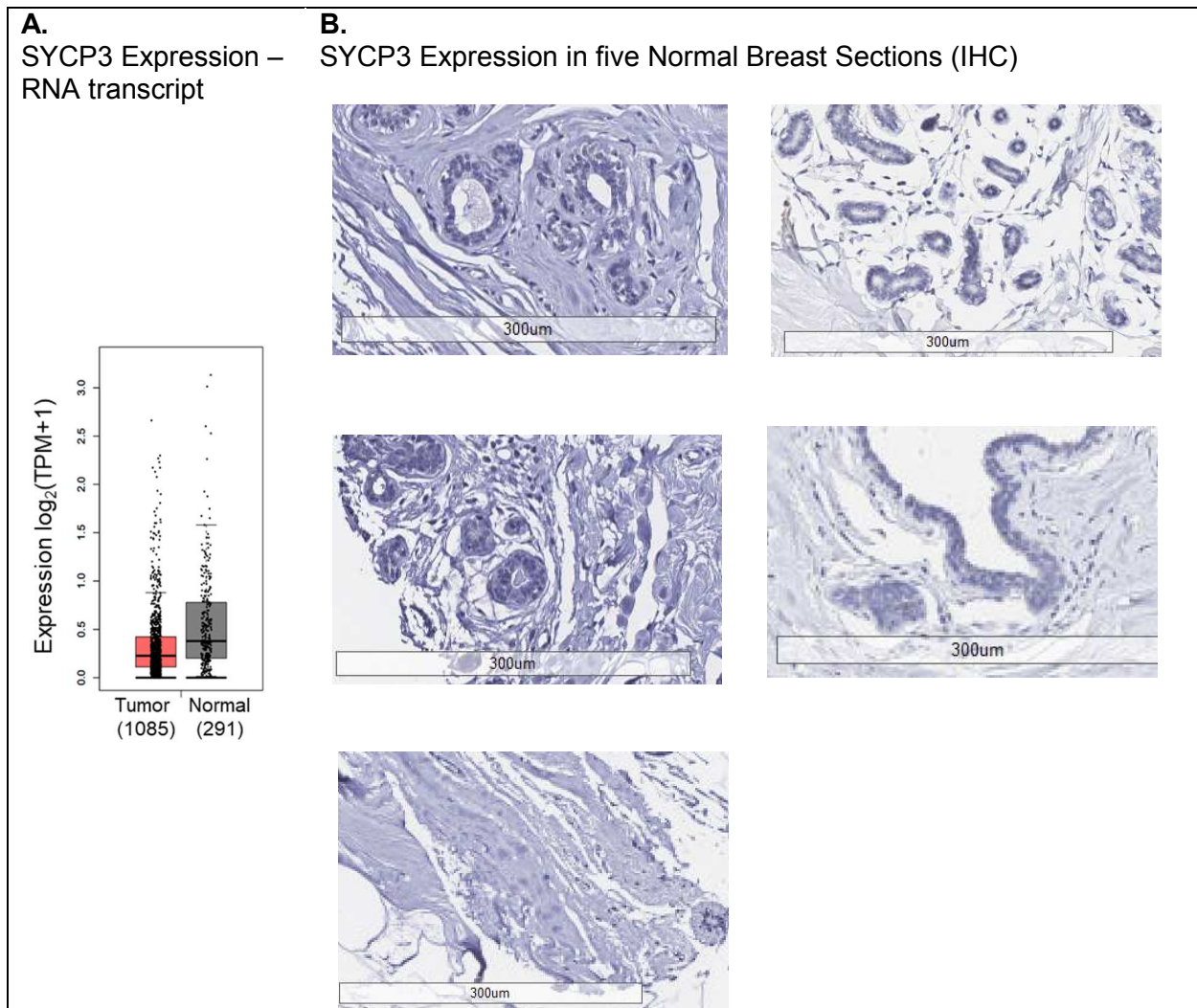


Figure 3.3: SYCP3 expression in normal breast tissue. **A.** SYCP3 RNA transcript levels in normal human breast vs. breast cancer from GEPIA [42]; **B.** IHC image of 5 normal human breast sections with no SYCP3 protein expression (10x magnification).

SYCP3 expression in 33 % of breast cancers

After establishing reliable IHC conditions for SYCP3, we performed IHC analysis of tissue microarrays (TMA) containing sections of human breast tumors. The TMAs also included 7 normal breast sections and 9 breast cancer cell lines. We show representative images of normal breast

sections from the TMA in **Figure 3.4 A, B**. Of the 9 cancer cell lines we evaluated for spontaneous SYCP3 expression, four (BTB474, MB351, SKBR, MB157) are positive for SYCP3 expression, while the remaining five (MB468, BTB549, BT20, MB435, MB231) are negative (**Fig 3.4 C-G**). We analyzed breast cancer sections from 213 patients and representative images of breast cancer tissue sections negative and positive for SYCP3 protein expression are shown in **Figure 3.4 H and 3.4 I** respectively.

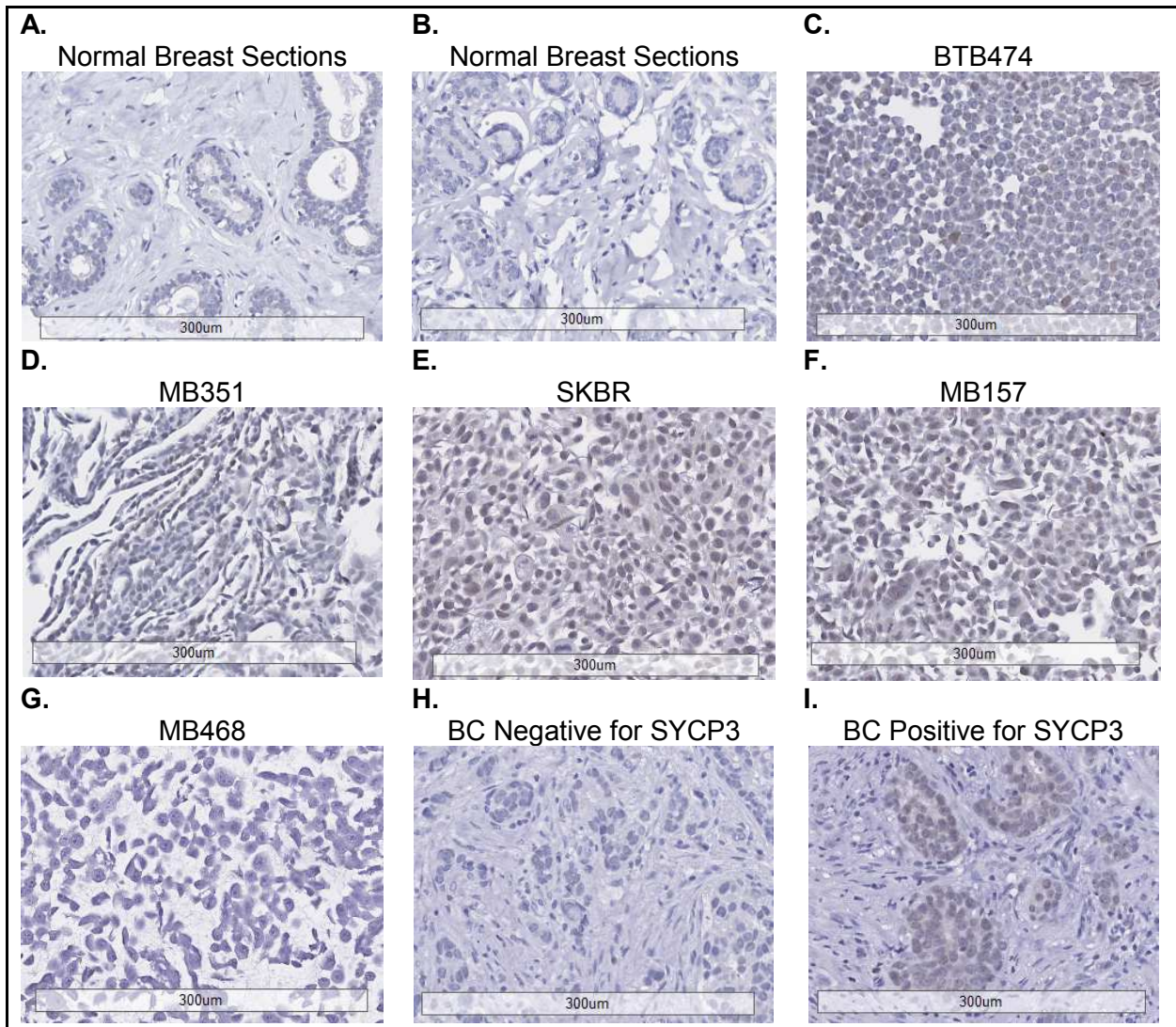


Figure 3.4: SYCP3 IHC analysis in normal breast tissue sections, breast cancer cell lines, and breast cancer (BC) tissue sections from YALE TMA. A. and B. IHC images

representative of normal human breast sections, both negative for SYCP3 expression; **C-F.** IHC staining of breast cancer cell lines positive for SYCP3 expression: **C.** BTB474, **D.** MB351, **E.** SKBR, **F.** MB157; **G.** MB468 Representative image of cell line negative for SYCP3 expression; **H.** and **I.** Representative IHC staining of human breast cancer tissue sections negative (**H.**) and positive (**I.**) for SYCP3 expression. Images were taken at 10x magnification.

QUPATH open-source software was used for semiquantitative analysis of the tissue sections in the TMA, and the sections were assigned an h-score based on the percentage and intensity of positive staining. The h-score distribution for normal breast tissues, cancer cell lines, and cancer tissue sections are shown in **Figure 3.5**. For normal tissues, the distribution of nuclear h-scores was less than 2 while the cytoplasmic h-scores were less than 0.5. We attribute this faint staining to be non-specific staining. Hence, to exclude non-specific staining of SYCP3, we considered tumor tissues with nuclear h-score less than 2 and cytoplasmic h-score less than 0.5 to be negative. About 33 % of the breast cancers showed SYCP3 expression in the nucleus, while about 27 % show expression in the cytoplasm. There is a strong positive correlation between the nuclear and cytoplasmic SYCP3 expression in tumors (Spearman correlation; $r = 0.8331$).

Tumor characteristics grouped by clinical and pathologic features of patients.

We have grouped the tumor SYCP3 expression (h-score) in the nucleus and cytoplasm based on clinical and pathologic features of the 213 patients in the study in **Table 1.1**. There is a higher expression of SYCP3 in patients with triple positive cancers (tumors positive for HR, ER and HER2 hormone receptors) than patients with triple negative cancers, and this difference is statistically significant (Mann-Whitney test, p -value = 0.01). There is no statistical significance in the distribution of h-scores based on other parameters tested.

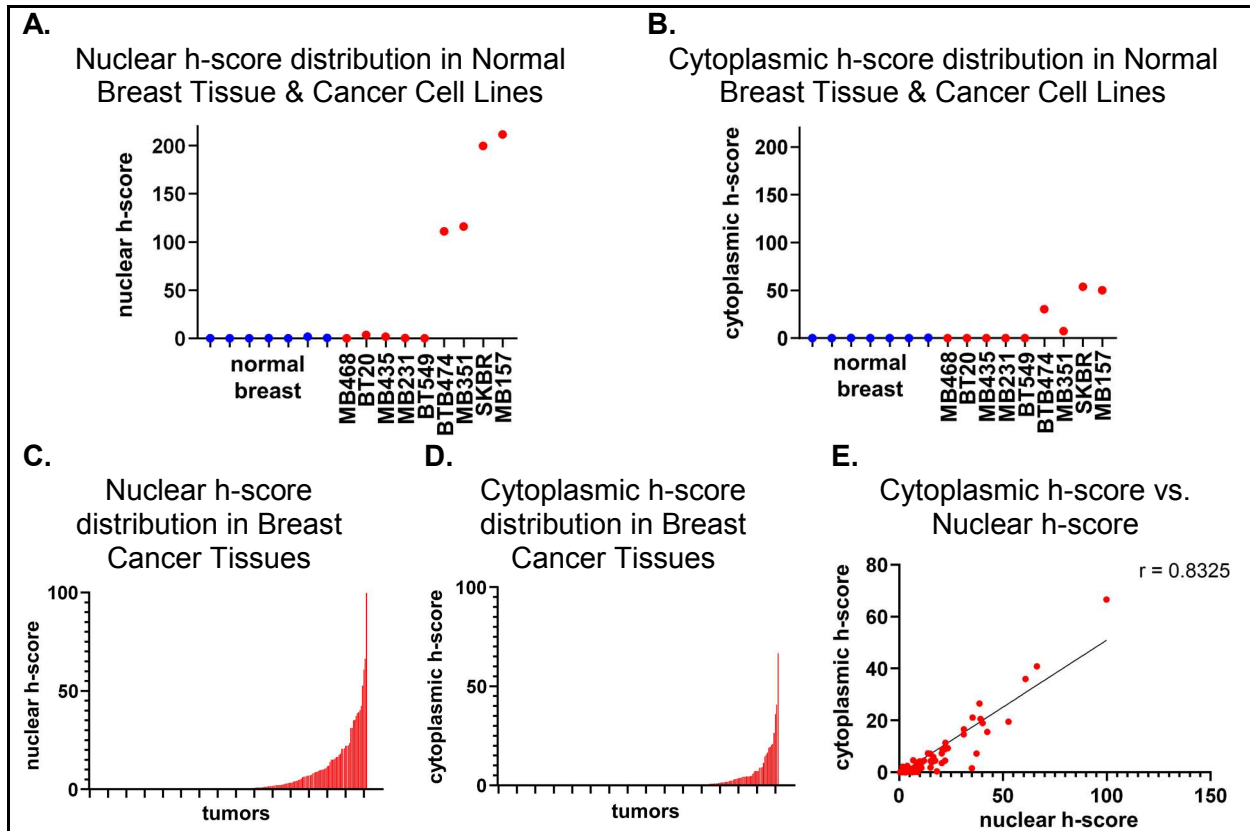


Figure 3.5: Semiquantitative analysis of SYCP3 protein levels by IHC. **A.** Nuclear h-score distribution in normal breast tissue and cancer cell lines (MB468, BT20, MB435, MB231, BT549, BTB474, MB351, SKBR, MB157). **B.** Cytoplasmic h-score distribution in normal breast tissue and cancer cell lines (MB468, BT20, MB435, MB231, BT549, BTB474, MB351, SKBR, MB157). **C.** Nuclear h-score distribution in breast cancer tissues. **D.** Cytoplasmic h-score distribution in breast cancer tissues. **E.** Cytoplasmic h-score vs. nuclear h-score analyzed using Spearman correlation coefficient ($r = 0.8331$).

Table 3.1 Tumor SYCP3 expression (h-score) in nucleus & cytoplasm grouped by patient clinical and pathological features

	SYCP3 nuclear h-score			SYCP3 cytoplasmic h-score		
	High	Low	p *	High	Low	p *
	n (%)	n (%)		n (%)	n (%)	
Age at Diagnosis						
Across all ages			ns			ns
≤ 60	6 (9)	60 (91)		4 (6)	62 (94)	
> 60	1 (5)	19 (95)		1 (5)	19 (95)	
Ethnicity						
Across all ethnicities			ns !			ns !
White	14 (19)	59 (81)		13 (18)	60 (82)	
Black	5 (15)	28 (85)		5 (15)	28 (85)	
Spanish/Hispanic	1 (17)	5 (83)		2 (33)	4 (67)	
Hormone Receptor status						
TN vs. TP			0.0100			0.0020
TN	9 (10)	80 (90)		7 (8)	82 (92)	
TP	6 (50)	6 (50)		4 (33)	8 (67)	
Cancer Stage						
Across all stages			ns !			ns !
I	8 (36)	14 (64)		8 (36)	14 (64)	
II	6 (15)	35 (85)		4 (10)	37 (90)	
III	0 (0)	5 (100)		0 (0)	5 (100)	
IV	1 (14)	6 (86)		1 (14)	6 (86)	
Histological Grade						
Across all grades			ns			ns
Poor Diff-Medium grade	9 (13)	60 (87)		11 (16)	58 (84)	
Mod Diff-Low grade	11 (27)	30 (73)		8 (20)	33 (80)	
Recurrence status						
Recurrence vs. No Recurrence			ns			ns
Recurrence	5 (36)	9 (64)		4 (29)	10 (71)	
No Recurrence	15 (32)	32 (68)		16 (34)	31 (66)	
Chemotherapy Received						
Yes vs. No			ns			ns
Yes	18 (37)	30 (63)		18 (37)	30 (63)	
No	2 (29)	5 (71)		3 (43)	4 (57)	
Type of Surgery						
Mastectomy vs. Lumpectomy			ns			ns
Mastectomy	12 (36)	21 (64)		13 (39)	20 (61)	
Lumpectomy	10 (29)	24 (71)		12 (35)	22 (65)	

Abbreviations: *TN*, Triple Negative; *TP*, Triple Positive; Diff, Differentiation

(!) Kruskal-Wallis; all else by Mann-Whitney

Prognostic analysis of patients with high expression of SYCP3

We examined the effect of high SYCP3 expression on patient overall survival and disease-free survival through Kaplan-Meier plots. Patients were grouped into high expression and low expression based on h-score values determined by IHC. A cohort of 213 patients were analyzed and followed for a period of about 20 years.

There is no difference in overall survival curves between patients with high *versus* low SYCP3 nuclear expression. However, it is noticeable that between 2.5 to 15 years, there is higher overall survival for patients with high SYCP3 expression (80% survival, 132.6 months) than patients with low SYCP3 expression (80% survival, 58.6 months) ($p = 0.0356$ by MANTEL-COX log rank test, **Fig. 3.6 A, B**). SYCP3 expression has been shown to inhibit DNA repair in experimental cell systems which is required to recover from DNA damage induced by chemotherapy [11]. So, patients with high SYCP3 expression in tumors may respond better to chemotherapy. We suspect that most of the patients received chemotherapy, but this information was available to us for only for a subset of the patients. For the patients known to have received chemotherapy, we repeated the survival analysis. Our findings in patients who received chemotherapy indicate that between 2.5-15 years there is significantly higher overall survival for patients with high SYCP3 expression (80% survival, 168.2 months) than patients with low SYCP3 expression (80% survival, 58.6 months) ($p = 0.0466$ by MANTEL-COX log rank test, **Fig. 3.6 C**). For disease free survival curves there is no statistically significant difference in patients with high *versus* low SYCP3 expression (**Fig. 3.6 D**) due to the small sample sizes.

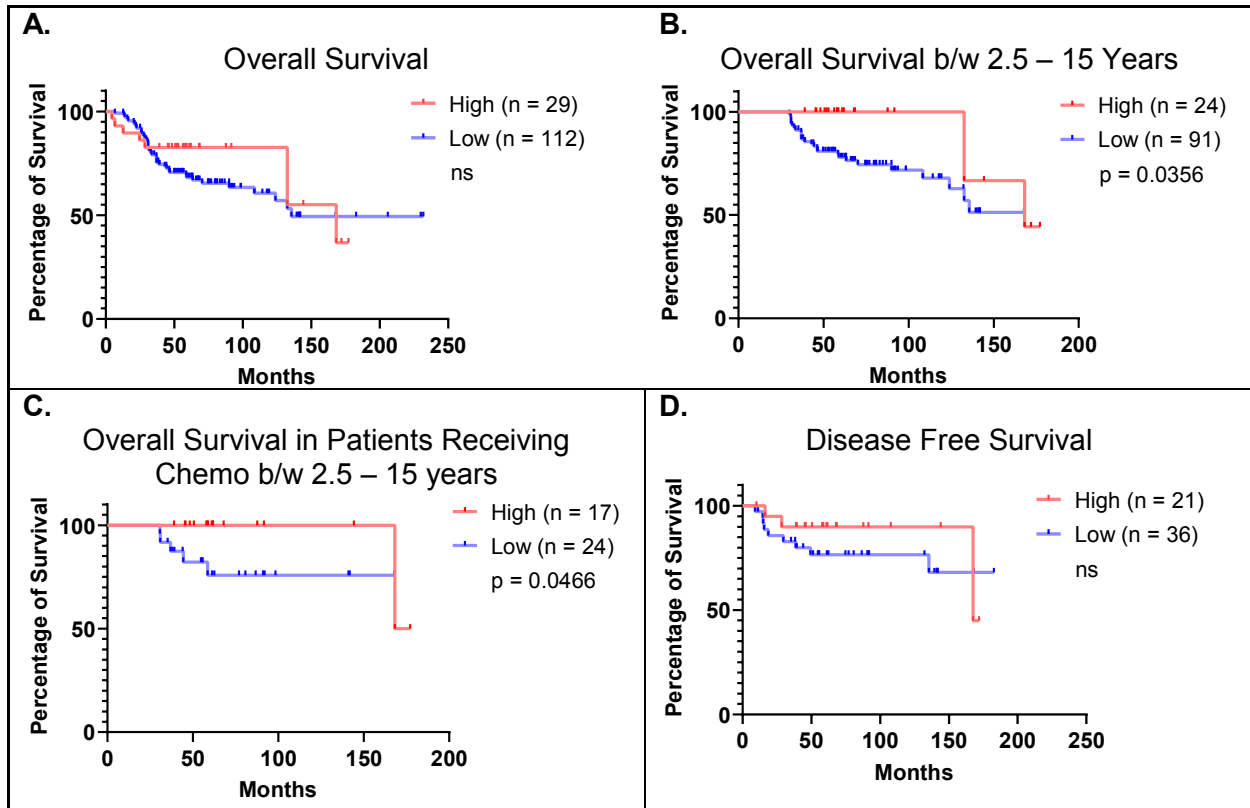


Figure 3.6: Kaplan-Meier survival curves of patients considering censored data separated by high vs. low nuclear SYCP3 expression. Curves are compared by log-rank test (Mantel-Cox). A. Overall survival; B. Overall survival b/w 2.5 – 15 years; C. Overall survival in patients receiving chemotherapy b/w 2.5 – 15 years; D. Disease free survival.

3.5 Conclusions

SYCP3 misexpression has been shown to disrupt BRCA2-mediated HR leading to a cellular DNA repair defect [11]. Though there have been some studies evaluating the misexpression of SYCP3 in different types of primary tumors, there has not been a systematic study to determine the extent of SYCP3 misexpression in breast cancers. The studies so far have only evaluated SYCP3 expression by RNA transcript levels which may not be indicative of the protein levels [10, 45].

We validated the SIGMA ATLAS antibody with a variety of positive and negative controls and optimized an IHC protocol for SYCP3 detection in human tissues. Our findings indicate little to no SYCP3 expression in normal human breast tissue. About 33% of breast cancers show SYCP3 protein expression in the nucleus and 27% of breast cancers show SYCP3 protein expression in the cytoplasm detectable by IHC. There is a strong positive correlation between nuclear and cytoplasmic SYCP3 expression which indicates that in these cancer cells SYCP3 could potentially both directly affect HR in the nucleus as well as sequester essential HR proteins in the cytoplasm.

We analyzed SYCP3 expression using the semi-quantitative h-score against a variety of clinical and pathologic features. Our analysis shows significantly higher SYCP3 expression in triple positive cancers compared to triple negative cancers (Mann-Whitney test, $p = 0.01$). Both triple positive and triple negative cancers are considered aggressive though the triple negative cancers seem to have a shorter survival and poorer prognosis [46]. Higher levels of SYCP3 in triple positive cancers could serve as a biomarker for HR defects in these cancers. To determine this, we need to perform IHC analysis on a larger cohort of triple positive cancers.

We performed Kaplan-Meier survival analysis for patients with high *versus* low SYCP3 expression in the tumors. We compared the survival curves of patients followed for about 20 years. However, ~ 80% of the cases in this study were between 2.5 – 15 years with some outliers present before 2.5 years and after 15 years. There is no difference in overall survival curves of the patients followed for about 20 years likely due to the presence of these outliers. However, in a 2.5–15-year period there is a statistically significant higher overall survival in patients with high SYCP3 expression (80% survival, 132.6 months) than low SYCP3 expression (80% survival, 58.6 months) ($p = 0.0356$ by MANTEL-COX log rank test). Since SYCP3 expression has been shown

to cause HR defect in somatic cells, tumors with SYCP3 expression could respond better to chemotherapy which would explain the higher survival in patients with high SYCP3 expression. To test this interpretation, we repeated the survival analysis for patients who were known to have received chemotherapy and among these patients there is also higher survival (80% survival, 168.2 months) for those with high SYCP3 expression than low SYCP3 expression (80% survival, 58.6 months)($p = 0.0466$ by MANTEL-COX log rank test). To strengthen our findings, future studies are needed to analyze more cases of breast cancer for SYCP3 protein expression

This is the first study analyzing SYCP3 protein expression in breast cancers and investigating the prognostic effect of SYCP3 protein expression on patient survival and response to chemotherapy. SYCP3 expression in somatic cells is shown to disrupt the activity of BRCA2 in HR [11]. In addition, unpublished data from Heyer laboratory show that SYCP3 also disrupts RAD51 activity in HR by inhibiting RAD51 binding to DNA. However, at present it is not known what level of SYCP3 expression leads to HR defects and tumor formation. To determine this, functional HR assays, such as evaluating RAD51 focus formation in response to damage, in tumors expressing different levels of SYCP3 expression are required. So, while all SYCP3 expressing tumors may not be HR defective, it could be one of the mechanisms causing a BRCA-ness phenotype and hence may serve as a valuable biomarker for HR deficiency.**3.5**

3.6 References

1. Dobson, M.J., et al., *Synaptonemal complex proteins: occurrence, epitope mapping and chromosome disjunction*. J Cell Sci, 1994. **107 (Pt 10)**: p. 2749-60.
2. Syrjanen, J.L., L. Pellegrini, and O.R. Davies, *A molecular model for the role of SYCP3 in meiotic chromosome organisation*. Elife, 2014. **3**.
3. Syrjanen, J.L., et al., *Single-molecule observation of DNA compaction by meiotic protein SYCP3*. Elife, 2017. **6**.
4. Miyamoto, T., et al., *Male infertility and its causes in human*. Adv Urol, 2012. **2012**: p. 384520.
5. Bolor, H., et al., *Mutations of the SYCP3 Gene in Women with Recurrent Pregnancy Loss*. American Journal of Human Genetics, 2009. **84**(1): p. 14-20.
6. Yuan, L., et al., *The murine SCP3 gene is required for synaptonemal complex assembly, chromosome synapsis, and male fertility*. Molecular Cell, 2000. **5**(1): p. 73-83.
7. Yuan, L., et al., *Female germ cell aneuploidy and embryo death in mice lacking the meiosis-specific protein SCP3*. Science, 2002. **296**(5570): p. 1115-1118.
8. Wang, H. and C. Hoog, *Structural damage to meiotic chromosomes impairs DNA recombination and checkpoint control in mammalian oocytes*. Journal of Cell Biology, 2006. **173**(4): p. 485-495.
9. Li, X.C., E. Bolcun-Filas, and J.C. Schimenti, *Genetic evidence that synaptonemal complex axial elements govern recombination pathway choice in mice*. Genetics, 2011. **189**(1): p. 71-82.
10. Mobasheri, M.B., R. Shirkoohi, and M.H. Modarressi, *Synaptonemal Complex Protein 3 Transcript Analysis in Breast Cancer*. Iran J Public Health, 2016. **45**(12): p. 1618-1624.
11. Hosoya, N., et al., *Synaptonemal complex protein SYCP3 impairs mitotic recombination by interfering with BRCA2*. EMBO Rep, 2011. **13**(1): p. 44-51.

12. Cho, H., et al., *Synaptonemal complex protein 3 is a prognostic marker in cervical cancer*. PLoS One, 2014. **9**(6): p. e98712.
13. Kitano, H., et al., *Synaptonemal complex protein 3 is associated with lymphangiogenesis in non-small cell lung cancer patients with lymph node metastasis*. J Transl Med, 2017. **15**(1): p. 138.
14. Chung, J.Y., et al., *Synaptonemal complex protein 3 as a novel prognostic marker in early stage non-small cell lung cancer*. Hum Pathol, 2013. **44**(4): p. 472-9.
15. Fratta, E., et al., *The biology of cancer testis antigens: putative function, regulation and therapeutic potential*. Mol Oncol, 2011. **5**(2): p. 164-82.
16. Martinez, J.S., et al., *BRCA2 regulates DMC1-mediated recombination through the BRC repeats*. Proc Natl Acad Sci U S A, 2016. **113**(13): p. 3515-20.
17. Kobayashi, W., et al., *SYCP3 regulates strand invasion activities of RAD51 and DMC1*. Genes Cells, 2017. **22**(9): p. 799-809.
18. Tarsounas, M., et al., *RAD51 and DMC1 form mixed complexes associated with mouse meiotic chromosome cores and synaptonemal complexes*. J Cell Biol, 1999. **147**(2): p. 207-20.
19. Coughlin, S.S., *Epidemiology of Breast Cancer in Women*. Adv Exp Med Biol, 2019. **1152**: p. 9-29.
20. Davies, H., et al., *HRDetect is a predictor of BRCA1 and BRCA2 deficiency based on mutational signatures*. Nat Med, 2017. **23**(4): p. 517-525.
21. Marsit, C.J., et al., *Inactivation of the Fanconi anemia/BRCA pathway in lung and oral cancers: implications for treatment and survival*. Oncogene, 2004. **23**(4): p. 1000-4.
22. Matsuda, M., et al., *Mutations in the RAD54 recombination gene in primary cancers*. Oncogene, 1999. **18**(22): p. 3427-30.

23. Macedo, G.S., B. Alemar, and P. Ashton-Prolla, *Reviewing the characteristics of BRCA and PALB2-related cancers in the precision medicine era*. Genet Mol Biol, 2019. **42**(1 suppl 1): p. 215-231.
24. Polak, P., et al., *A mutational signature reveals alterations underlying deficient homologous recombination repair in breast cancer*. Nat Genet, 2017. **49**(10): p. 1476-1486.
25. van den Tempel, N., et al., *The effect of thermal dose on hyperthermia-mediated inhibition of DNA repair through homologous recombination*. Oncotarget, 2017. **8**(27): p. 44593-44604.
26. Xia, F., et al., *Deficiency of human BRCA2 leads to impaired homologous recombination but maintains normal nonhomologous end joining*. Proc Natl Acad Sci U S A, 2001. **98**(15): p. 8644-9.
27. Oei, A.L., et al., *Enhancing synthetic lethality of PARP-inhibitor and cisplatin in BRCA-proficient tumour cells with hyperthermia*. Oncotarget, 2017. **8**(17): p. 28116-28124.
28. Turner, N., A. Tutt, and A. Ashworth, *Hallmarks of 'BRCAness' in sporadic cancers*. Nat Rev Cancer, 2004. **4**(10): p. 814-9.
29. Bryant, H.E., et al., *Specific killing of BRCA2-deficient tumours with inhibitors of poly(ADP-ribose) polymerase*. Nature, 2005. **434**(7035): p. 913-7.
30. Farmer, H., et al., *Targeting the DNA repair defect in BRCA mutant cells as a therapeutic strategy*. Nature, 2005. **434**(7035): p. 917-21.
31. Fong, P.C., et al., *Inhibition of poly(ADP-ribose) polymerase in tumors from BRCA mutation carriers*. N Engl J Med, 2009. **361**(2): p. 123-34.
32. Lord, C.J. and A. Ashworth, *PARP inhibitors: Synthetic lethality in the clinic*. Science, 2017. **355**(6330): p. 1152-1158.
33. Goldman, M.J., et al., *Visualizing and interpreting cancer genomics data via the Xena platform*. Nat Biotechnol, 2020. **38**(6): p. 675-678.

34. Liu, Y., A. Beyer, and R. Aebersold, *On the Dependency of Cellular Protein Levels on mRNA Abundance*. Cell, 2016. **165**(3): p. 535-50.
35. Vogel, C. and E.M. Marcotte, *Insights into the regulation of protein abundance from proteomic and transcriptomic analyses*. Nat Rev Genet, 2012. **13**(4): p. 227-32.
36. Yuan, L., et al., *The synaptonemal complex protein SCP3 can form multistranded, cross-striated fibers in vivo*. J Cell Biol, 1998. **142**(2): p. 331-9.
37. *Human Protein Atlas* <http://www.proteinatlas.org>.
38. Bankhead, P., et al., *QuPath: Open source software for digital pathology image analysis*. Sci Rep, 2017. **7**(1): p. 16878.
39. *Kruskal-Wallis test was performed using GraphPad Prism version 9.1.0 for Windows, GraphPad Software, San Diego, California USA, www.graphpad.com*.
40. *Man-Whitney was performed using GraphPad Prism version 9.1.0 for Windows, GraphPad Software, San Diego, California USA, www.graphpad.com*.
41. *Nonparametric Spearman correlation test was performed using GraphPad Prism version 9.1.0 for Windows, GraphPad Software, San Diego, California USA, www.graphpad.com*.
42. *Kaplan-Meier survival plot followed by MANTEL-COX log-rank test was performed using GraphPad Prism version 9.1.0 for Windows, GraphPad Software, San Diego, California USA, www.graphpad.com*
43. Ponten, F., K. Jirstrom, and M. Uhlen, *The Human Protein Atlas--a tool for pathology*. J Pathol, 2008. **216**(4): p. 387-93.
44. Tang, Z., et al., *GEPIA: a web server for cancer and normal gene expression profiling and interactive analyses*. Nucleic Acids Res, 2017. **45**(W1): p. W98-W102.
45. *DepMap, Broad (2019): DepMap 19Q3 Public. figshare. Dataset doi:10.6084/m9.figshare*.

46. Negi, P., et al., *Survival of Triple Negative versus Triple Positive Breast Cancers: Comparison and Contrast*. Asian Pac J Cancer Prev, 2016. **17**(8): p. 3911-6.

Chapter 4: Biochemical Analysis of SYCP3 and its Potential Role in Homologous Recombination

This work has not been published yet and includes contributions from:

Ash Jay conducted the experiments. Hang Phuong Le and Jie Liu contributed critical reagents.

4.1 Abstract

SYCP3 is an essential structural component of the meiosis-specific synaptonemal complex. SYCP3 is typically expressed only in germline cells and not in somatic cells. Emerging evidence indicates that SYCP3 is misexpressed in a variety of cancers, and hence it is called a cancer testis antigen. The structural role of SYCP3 in meiosis is well understood but not much is known about its potential effects when misexpressed in somatic cells. Recently, it was reported that in somatic cells SYCP3 interacts with RAD51 and BRCA2, impairing HR involving mechanisms that remain to be defined. Here we establish the biochemical mechanism by which SYCP3 leads to functional loss of RAD51 and HR in somatic cells by *in vitro* assays using purified proteins. Our findings indicate that SYCP3 directly disrupts RAD51 mediated strand invasion. This disruption is not due an effect on the ATPase activity of RAD51 by SYCP3. Instead, SYCP3 affects RAD51 activity *via* direct interaction which inhibits DNA binding by RAD51 and dissociates preformed RAD51 filaments. Another critical recombination protein, RAD54, can overcome SYCP3-mediated inhibition of RAD51 function, likely by out-competing SYCP3 for interaction with RAD51.

4.2. Introduction

DNA repair and genome maintenance define major cellular pathways to suppress tumor formation. BRCA2 is a tumor suppressor that functions in a pathway called homologous recombination (**HR**), to accurately repair DNA double-stranded breaks (DSBs) and other types of complex DNA damages, which is key to maintaining genomic integrity. HR involves two signature steps: 1. search for a homologous DNA template; 2. DNA strand invasion. BRCA2 recruits other key recombination proteins such as RAD51 in somatic cells and DMC1 as well as RAD51 in meiotic cells to enable the homology search and DNA strand invasion reactions [1, 2]. Loss of BRCA2 leads to accumulation of unrepaired DNA damage and aberrant repair increasing the risk

of cancer over time [3]. BRCA2 deficiencies are associated with increased risk for cancers including breast, ovarian, pancreatic, and prostate cancer [4-8].

BRCA2 is a large, complex protein of 3,418 amino acids containing two DNA binding regions, a nuclear localization signal at the C terminus and several protein interaction motifs [9-12]. Of particular relevance are the 8 conserved repeats in exon 11, called the BRC repeats [13], which are the primary sites of interaction with RAD51 and DMC1 [14-16]. The repeats have differential binding affinities for RAD51 and DMC1 and, based on these affinities, they are grouped into two classes with repeats 1-4 in class 1 and repeats 5-8 in class 2 [14]. Class 1 repeats have high binding affinity for free RAD51 and enable BRCA2 to nucleate the RAD51 filament on ssDNA but not on double stranded DNA. Class 2 repeats bind RAD51-ssDNA nucleoprotein filaments with high affinity and are thought to stabilize the filaments and enable them to lengthen by displacing RPA. Furthermore, BRC repeats 6-8 from class 2 bind with higher affinity to DMC1 than RAD51 [15], probably enabling DMC1 to assemble on DSB ends to repair meiotic DSBs. The C-terminal RAD51 binding domain is not involved in RAD51 filament formation [17] but is required for RAD51 filament stabilization [18, 19] and plays a specific role in replication fork protection [20].

SYCP3 is a structural component of the synaptonemal complex (**SC**) [21] which connects homologous chromosomes along their lengths during prophase I of meiosis and facilitates chiasmata formation (crossover recombination) and consequently chromosome segregation [22]. The SC is comprised of two parallel lateral elements or chromosome axes connected by a central region comprising transverse filaments. SYCP3 forms a part of the lateral elements of the SC [23]. SYCP3 assembles via its coiled-coil domain into antiparallel tetramers, where the N terminal ends bind DNA and are thought to act as a strut bringing together distant sites of DNA to assemble

meiotic chromosomes into linear arrays of chromatin loops [24]. In mice and humans, mutations in SYCP3 lead to infertility in males and increased fetal deaths in females [25-28]. In SYCP3 knockout female mice, there is inefficient meiotic DSB repair and decreased crossing over in oocytes [29, 30], indicating that SYCP3 might facilitate HR during meiosis.

SYCP3 is generally expressed only in germline cells and not in somatic cells. However, SYCP3 mis-expression has been found in many cancers and for this reason it is classified as a cancer testis antigen (**CTA**) [31-35]. CTAs are a class of proteins that are normally expressed in the adult testis and show sporadic expression in some human cancers [36]. Surprisingly, recent data show that when SYCP3 is ectopically expressed in somatic cells, it disrupts the high-fidelity DNA repair pathway homologous recombination. *Hosoya et al.* [33] reported a decrease in radiation induced RAD51 focus formation in somatic cells with SYCP3 expression, indicative of an HR-defect. Results from co-immunoprecipitation (Co-IP) experiments in cell lysates indicated that SYCP3 interacts with BRCA2 thereby inhibiting its interaction with RAD51. Cells with ectopic SYCP3 expression showed reduced HR efficiency as measured by a GFP-reporter system and increased sensitivity to DNA damage inducing agents such as cisplatin and Poly (ADP-ribose) polymerase (**PARP**) inhibitors [33]. However, it is unclear whether the interaction between BRCA2 and SYCP3 is direct or indirect. Unpublished data of protein pull-down experiments using purified BRCA2, SYCP3, and RAD51 by Dr. Jie Liu in the Heyer laboratory show that there is a direct interaction between SYCP3 and BRCA2 and that SYCP3 impairs the BRCA2-RAD51 interaction. *Kobayashi et al.* [37] performed *in vitro* experiments with purified proteins to determine whether SYCP3 impacts the strand exchange activities of RAD51 or DMC1 during HR. They show that SYCP3 interacts directly with RAD51 and DMC1, with the interaction being much weaker with DMC1. In reconstituted D-loop experiments that assay DNA strand invasion *in vitro*, SYCP3 suppresses RAD51-mediated D-loop formation that is stimulated by HOP2-MND1 but not that of

DMC1 [37]. These results suggest that SYCP3 may specifically inhibit RAD51-mediated HR by two distinct mechanisms: first, by interference with the BRCA2-RAD51 interaction, and second by direct inhibition of RAD51 function.

In meiotic cells, SYCP3, BRCA2, DMC1 and RAD51 function in the same pathway to repair programmed meiotic DSBs between homologous chromosomes. However, SYCP3 expression in somatic cells results in a DNA repair defect [33]. My hypothesis is that when SYCP3 is expressed in somatic cells, which lack the normal meiotic environment containing other interaction partners, SYCP3 binds BRCA2 and RAD51 and limits their participation in HR. This leads to an HR repair defect and increased risk of cancer.

My goal is to establish the mechanisms by which SYCP3 affects HR, first focusing on its interactions with RAD51 and DMC1 through *in vitro* functional recombination assays with purified proteins. Next, I plan to establish the affinity of SYCP3 with the BRCA2 BRC repeats and determine how SYCP3 could affect the interactions of the repeats with RAD51 and DMC1 through pull down assays with purified proteins or protein fragments.

4.3. Experimental Procedures:

Thin Layer Chromatography (TLC) ATPase assay

RAD51 or DMC1 (2 μ M) was incubated with single stranded DNA (**ssDNA**; 6 μ M nucleotides) for 2 minutes at 37 °C and then increasing concentrations of SYCP3 were added and incubated for another 40 minutes in buffer containing 20 mM Tris-HCl (pH 7.5), 4 mM MgCl₂, 100 μ g/mL bovine serum albumin (**BSA**), 0.5 mM ATP, 20 μ Ci/ml [γ ³²P] ATP and 1 mM DTT. The reactions were

terminated by adding a stop buffer containing 5 mM ATP, 5 mM ADP and 20 mM EDTA. Aliquots of 2 μ L were spotted on a polyethyleneimine (PEI) Cellulose TLC plate (Baker-flex) and separated in a buffer containing 1 M formic acid and 0.5 M LiCl. The plates were imaged in a Molecular Dynamics Storm 840 PhosphorImager. 3ImageQuant software was used to quantify hydrolyzed 32 P and [γ 32 P] ATP.

Displacement Loop Assay (D-Loop)

Rad51 (0.4 μ M) was incubated with a 100mer ssDNA [5'-CTGGTCATAATCATGGTGGCGAATAAGTACGCGTTCTTGCAAATCACCCAGAAGGCGGTTCC TGAATGAATGGGAAGCCTTCAAGAAGGTGATAAGCAGGA-3'] (labeled with 32 P at the 5'-end, 12 nM molecules) for 10 minutes at 30 $^{\circ}$ C in a buffer containing 30 mM Tris-HCl pH 7.5, 1 mM ATP, 2 mM MgCl₂, 2 mM CaCl₂, 50 mM KCl, 0.25 mg/mL BSA, 0.5 mM tris(2-carboxyethyl) phosphine (**TCEP**), 10 mM phosphocreatine and 0.1 mg/mL phosphocreatine kinase. SYCP3 at the indicated concentrations was titrated and incubated for another 10 minutes. The reactions were started by adding supercoiled double stranded DNA (**dsDNA**; 96 nM molecules) with or without RAD54 (1.05 μ M) such that there were 11 molecules of RAD54 for every molecule of supercoiled dsDNA. After 15 minutes, the reactions were stopped by treating with proteinase K (Roche) for 30 minutes at 37 $^{\circ}$ C. The reaction products were resolved by 0.8% agarose gel electrophoresis in TBE buffer (Tris-borate ETA buffer) at 73 V for 2 hours. The gel was dried and imaged using Molecular Dynamics Storm 840 PhosphorImager. The results were quantified using ImageQuant software. The % D-Loop formed was calculated as a percentage of the strand invasion products relative to the total DNA in the same lane.

Electrophoretic Mobility-Shift Assay (EMSA)

RAD51 or DMC1 (0.4 μ M unless indicated otherwise) was incubated with 5' fluorescently labelled 80mer ssDNA [5'-Cy5-ATCAACATCATAGCCAGATGCCAGAGATTAGAGCGCATGACAAGTAAAGGACGGTTGTCAGCGTCATAAGAGGTTTTAC-3'] for 10 minutes at 37 °C to form filaments in a buffer containing 30 mM Tris-HCl (pH 7.5), 30 mM KCl, 1 mM CaCl₂, 1 mM MgCl₂, 100 μ g/mL BSA and 0.5 mM TCEP. Increasing concentrations of SYCP3 were added to the reaction and incubated for another 15 minutes. The reaction products were resolved on a 6 % polyacrylamide gel (**PAGE**) at room temperature (**RT**) in 1XTB buffer (Tris-Borate pH 8.0, 2 mM MgCl₂). The gels were imaged using an Amersham Imager 600, and the results were quantified with ImageJ software. A negative control without added protein defines 100% unbound DNA, and the percentage of DNA dissociated was calculated relative to the 100% unbound DNA. Nuclease contamination can result in the loss of DNA which could appear on the gels as an artifact that there is less free/unbound DNA. To make sure that our samples do not contain a nuclease contamination, we add a control in our assays where we allow for the maximum filament formation and digest the proteins with proteinase K before loading the reaction products on the gel. We can then compare the unbound DNA with the no protein negative control lane to confirm that there is no loss of DNA caused by a potential nuclease contamination.

GST Pull Down Assay

Glutathione-Agarose 4B beads (GE) were equilibrated with binding buffer 'B' containing 20 mM Tris-HCl (pH 7.5), 100 mM NaCl, 1 mM EDTA, 50 μ L/mL and 1 mM DTT, 10 % glycerol, 0.01 % NP-40. GST-BRC peptides were incubated with SYCP3, the SYCP3 coiled-coil domain (SYCP3 cc), the SYCP3 N-terminal region (SYCP3 NT), or the SYCP3 C-terminal region (SYCP3 CT) at indicated concentrations 60 min at 37 °C in buffer B and then batch bound to glutathione beads

in a final volume of 40 μ L for 60 min at 37 °C. The complexes were then washed with buffer B containing 0.1% NP-40 and loaded onto an SDS-PAGE gel and stained with SYPRO-Orange (Invitrogen). The gel was imaged using Molecular Dynamics Storm 840 PhosphorImager and protein bands were quantified by ImageQuant software.

Far Western Immunoblot Analysis

The proteins from the PAGE gel were transferred to a nitrocellulose membrane (Bio-Rad) and the membrane was blocked with 5 % milk (Safeway, non-fat dry milk) for one hour. The membrane was incubated overnight at 4 °C with a primary RAD51 antibody (1:1,000, GeneTex RAD51 antibody, GTX70230, lot 11300) followed by a secondary antibody incubation for 1 hour (1:10,000, polyclonal goat anti-mouse, Dako P0447). Protein bands were visualized by enhanced chemiluminescence (ECL, PerkinElmer) and imaged using an Amersham Imager 600. The membrane was then stripped of primary and secondary antibodies by incubating in a stripping buffer containing 10 % SDS, β -mercaptoethanol and 60 mM Tris-HCl (pH 6.8). After extensive washing the above immunoblotting procedure was repeated for the SYCP3 primary antibody (1:100, SIGMA ATLAS antibody HPA039635, lot R37957) followed by the secondary antibody incubation (1:10,000, polyclonal goat anti-rabbit, Dako P0448).

Protein Purifications

BRC Repeat Purifications. The 8 BRC repeats including the surrounding spacer regions were cloned into the pet28b+ vector. The repeats were flanked by two tags – a GST tag at the N-terminus and a HIS6 tag at the C-terminus. Initially, the constructs were expressed in Rosetta *Escherichia coli* at 37 °C but at this temperature there was significant protein degradation probably due to misfolding. Expression at 25 °C and 18 °C did not improve the recovery of soluble proteins.

Finally, expression in Arctic *E. coli* allowed for better protein recovery at low temperatures. Arctic *E. coli* has cold adapted chaperonins that allows for better protein processing at temperatures of 10-12 °C. The *E. coli* cells were grown at 37 °C to OD₆₀₀ = 0.5 and then 1 mM IPTG was added to induce SYCP3 expression over 24 hours at 10°C. Cells from 10 L culture were suspended in lysis buffer containing 50 mM Tris-HCl pH 8.0, 250 mM NaCl, 1 mM EDTA, 10 % glycerol, 0.5 % NP-40, 5 mM DTT and 1 mM PMSF. The cells were disrupted by sonication and crude lysate was clarified by centrifugation at 45,000 rpm for 1 hour in a Beckman Ti 70 rotor. The cleared lysate was added to glutathione agarose resin equilibrated with Buffer A containing 50 mM Tris-HCl pH 8.0, 250 mM NaCl, 1 mM EDTA, 10 % glycerol and 1 mM DTT with gentle shaking overnight at 4 °C. The BRC repeats were eluted with Buffer A containing 50 mM reduced glutathione. In the case of BRC repeats 2,4,5,7 the eluted fractions were pooled and stored at -80 °C. For BRC repeats 1,3,6 the eluent from glutathione column was applied to a Mono Q column in buffer containing 20 mM Tris-HCl pH 7.5, 100 mM NaCl, 0.2 mM EDTA, 10 % glycerol and 1 mM DTT. The proteins were eluted by a gradient of 200 mM -1M NaCl. The proteins were pooled and stored at -80 °C. The BRC8 repeat expression construct affected the viability of the *E. coli* cells and could not be purified. Hence, a new approach needs to be developed for the purification of the BRC8 repeat.

SYCP3 Purification

The human SYCP3 cDNA sequence with a self-cleavable intein tag was cloned into pTYB11 vector and transformed into Rosetta *E. coli* cells. The *E. coli* cells were grown at 37 °C until the OD₆₀₀ reached 0.6 and then 0.5 mM IPTG was added to induce SYCP3 expression overnight at 18 °C. Cells from 10 L culture were suspended in lysis buffer containing 20 mM Tris-HCl pH 7.5, 500 mM NaCl, 1 mM EDTA, 1 mM PMSF, 0.1 % Triton X-100 and 10 % glycerol. The cells were disrupted by sonication and crude lysate was clarified by centrifugation at 45,000 rpm for 1 hour

in a Beckman Ti 70 rotor. The protein lysate was added to chitin resin equilibrated with 20 mM Tris-HCl pH 7.5, 500 mM NaCl, 1 mM EDTA, 1 mM PMSF, 0.1 % Triton X-100 and 10 % glycerol. After extensive washing, on column cleavage of SYCP3 was induced by adding 50 mM DTT to the column buffer and incubating for 48 hours. The eluent was applied to Heparin agarose equilibrated with 20 mM Tris-HCl pH 7.5, 150 mM NaCl, 1 mM EDTA, 10 % glycerol and 0.5 mM TCEP. The column was washed extensively with 20 column volumes of column buffer containing 250 mM NaCl and eluted with buffer containing 400 mM NaCl. The protein was then applied to a Mono Q column with buffer containing 20 mM Tris-HCl pH7.5, 100 mM NaCl, 1 mM EDTA, 10 % glycerol and 0.5 mM TCEP. After washing, SYCP3 was recovered by gradient elution from 200 mM NaCl – 1M NaCl. The fractions were pooled and stored at -80 °C.

Purification of SYCP3 coiled coil (SYCP3 cc), N-terminal (SYCP3 NT) and C-terminal Fragments (SYCP3 CT). The SYCP3 coiled coil sequence (aa 77 – aa 207) with a self-cleavable intein tag was cloned into pet28b+ vector and transformed into Rosetta *E. coli* cells. The *E. coli* cells were grown at 37 °C till OD₆₀₀ reached 0.6 and then 0.5 mM IPTG was added to induce SYCP3 expression overnight at 18°C. Cells from 10 L culture was suspended in lysis buffer containing 20 mM Tris-HCl pH7.5, 500 mM NaCl, 1 mM EDTA, 1 mM PMSF, 0.1 % Triton X-100 and 10 % glycerol. The cells were disrupted by sonication and crude lysate was clarified by centrifugation at 45,000 rpm for 1 hour in a Beckman Ti 70 rotor. The protein lysate was added to chitin resin equilibrated with 20 mM Tris-HCl pH 7.5, 500 mM NaCl, 1 mM EDTA, 1 mM PMSF, 0.1 % Triton X-100 and 10 % glycerol. After extensive washing, on column cleavage of SYCP3 was induced by adding 50 mM DTT to the column buffer and incubating for 48 hours. The eluent was concentrated using Amicon Ultra Centrifugal Filter Units, pooled, and stored at -80 °C. SYCP3 NT (aa 1 – aa 77) and CT (residues aa 207 – aa 236) were previously purified in the Heyer laboratory using the same protocol.

4.4. Results

Purification of BRC repeats

The BRC repeats represent the main interaction sites of BRCA2 with RAD51 and DMC1 to enable them to form filaments on ssDNA and function in homologous template pairing [14-16]. Our initial goal was to first determine how SYCP3 affects the interaction of each BRC repeat with RAD51 and DMC1. Next, the intent was to extend our observations to the context of full-length BRCA2 protein, to determine how SYCP3 affects the interaction of BRCA2 with RAD51 and DMC1. Hence, we purified individual BRC repeats for the initial interaction studies with SYCP3. Previous studies have performed interaction and functional *in vitro* assays with purified fragments of BRC repeats. The findings from these studies with individual BRC repeats show certain inconsistencies regarding whether the repeats promote RAD51-DNA binding and stimulate RAD51 strand exchange. These discrepancies could be related to the presence of different amounts of spacer regions in the repeat constructs (**Fig.4.1 A-C**) [14, 16, 38, 39]. Carreira *et al.* did not include the spacer regions and their findings showed that while all the repeats promoted RAD51 binding to ssDNA, Class 2 repeats had the strongest effect. Class 1 BRC repeats simulated RAD51 D-Loop reactions only when RAD51 was present in excess of the concentration needed to saturate ssDNA [14, 16] while Class 2 repeats displayed no effect. Chatterjee *et al.* [38] grouped together the two classes of repeats including the spacer regions fused to the DNA binding domain (DBD) of BRCA2 and their results indicated that BRC5-8-DBD preferentially binds and stabilizes RAD51 filaments and also promotes RAD51 catalyzed strand exchange activity much more strongly than BRC1-4-DBD [38]. Davies *et al.* focused on the BRC3, BRC4 and BRC7 repeats with a part of the spacer sequences. They showed that repeats BRC3 and BRC4 inhibited RAD51 binding to ssDNA while BRC7 partially reduced RAD51 filament formation [39]. The spacer regions could alter the folding of the BRC repeats and affect their interaction with RAD51 and DMC1 [13]. For

this reason, we decided to purify the BRC repeats with the spacer regions (**Fig.4.1 D**). The expression construct for the BRC8 repeat affected the viability of the *E. coli* host cells and was poorly expressed. Hence, a new approach will need to be developed for the purification of the BRC8 repeat. **Figure 4.2** shows the purification results for the BRC1-7 repeats.

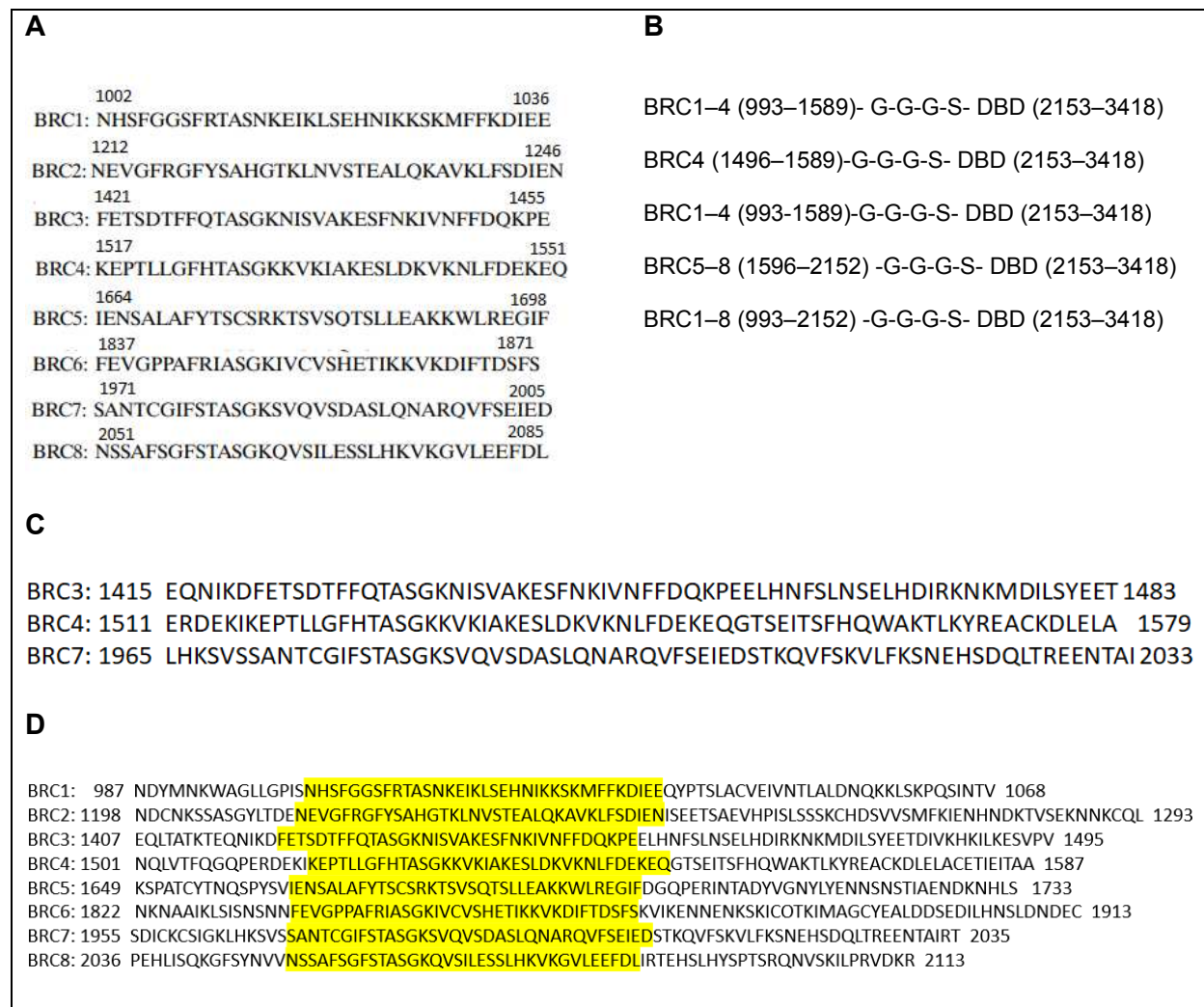


Figure 4.1: BRC repeat constructs used in this study compared with the different BRC repeat constructs studied in the past. A. BRC repeat constructs not containing spacer regions of *Carreira et al.* [14]. **B.** BRC repeat fusion constructs with the C-terminal DNA binding domain of *Chatterjee et al.* [38]; **C.** BRC repeat constructs for BRC3, BRC4 and BRC7

containing parts of the spacer region of *Davies et al.* [39]; **D.** BRC repeat constructs containing spacer regions of this study [13]. Highlighted in yellow are the BRC repeat sequences while the remainder are spacer sequences.

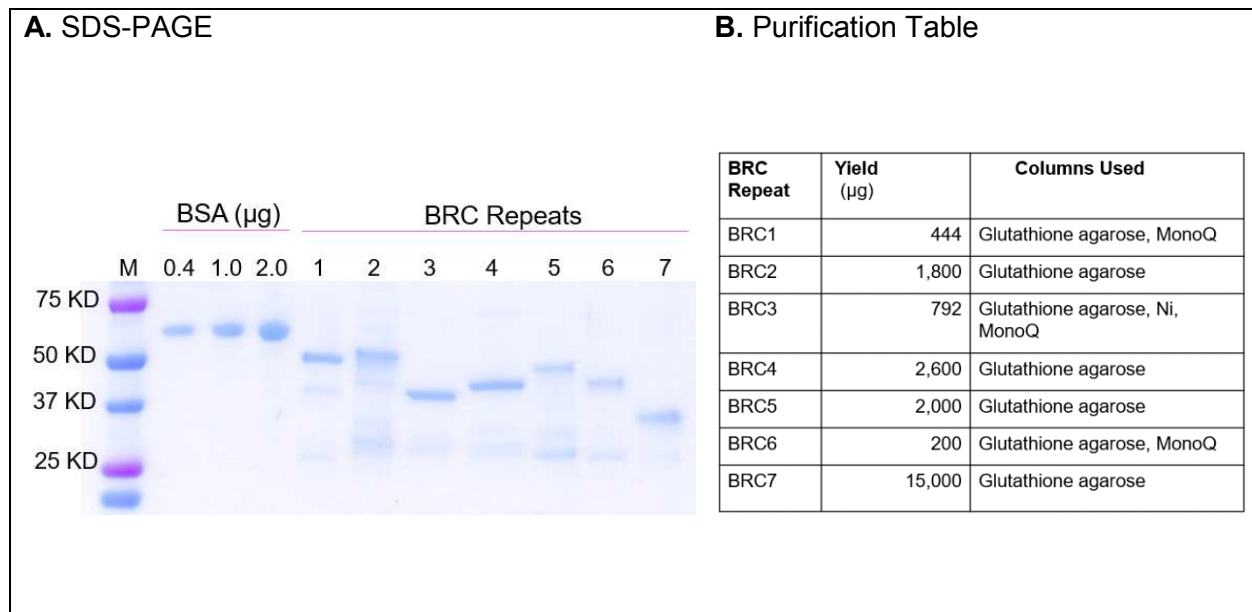


Figure 4.2: Purification of BRC repeat fragments. **A.** SDS/PAGE gel of purified BRC fragments stained with Denville Blue loading 0.5 µg each. **B.** Chromatography columns used for the purification and purification yields for the BRC repeats in **A.**

SYCP3 purification

We cloned the SYCP3 cDNA sequence with an intein tag that can be cleaved to enable SYCP3 protein purification in its native form. After SYCP3 purification using Mono Q as the last column, we performed quality control to monitor for potential ATPase contamination using a sensitive TLC-based ATPase assay on fractions of the recovered protein. SYCP3 does not contain an ATPase domain [23] and is not expected to exhibit intrinsic ATPase activity. The results from the TLC

assay indicated that the fractions had a minor ATPase contamination with k_{cat} of 0.23 - 0.29 min^{-1} (**Fig. 4.3**). Human RAD51 served as a positive control, and it exhibits the expected low ATPase activity of k_{cat} of 0.07 min^{-1} [40]. Since the ATPase contamination in fractions of SYCP3 is about 3 to 4-fold greater than the RAD51 ATPase activity, we cannot use them used in biochemical assays that requires RAD51 ATPase activity. To eliminate this contamination, we tried different elution patterns from the Mono Q column, including a shallow gradient elution over 100 column volumes (**CV**) followed by rapid elution from Mono Q column over 5 CV. However, these protocols failed to separate the ATPase contamination from SYCP3.

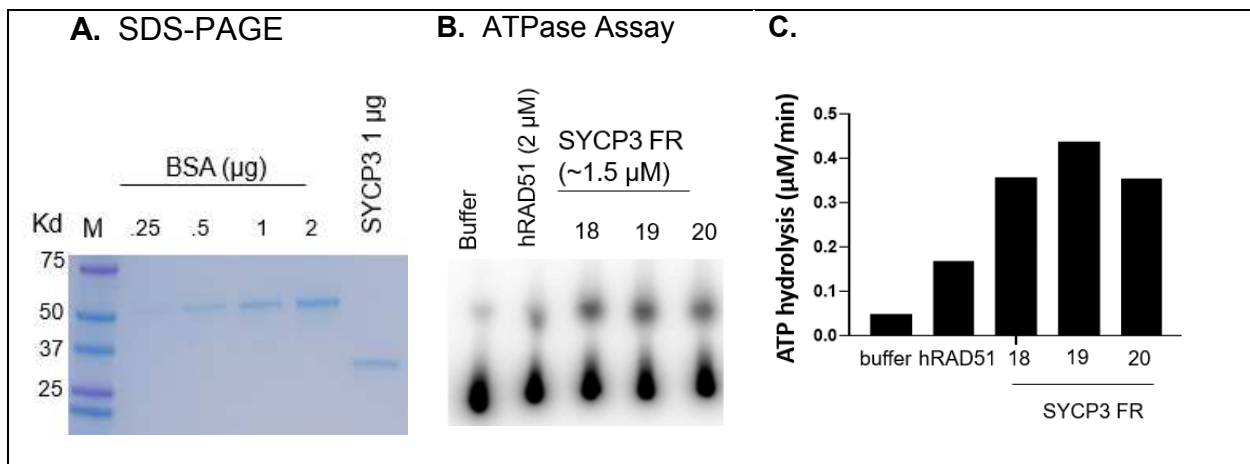


Figure 4.3: SYCP3 purified with Chitin, Heparin and Mono Q columns has ATPase contamination. **A.** SDS/PAGE gel stained with Denville Blue. Yield: 1.5 mg. **B.** TLC assay of SYCP3 fractions (~1.5 μM) eluted from Mono Q column. **C.** Quantification of TLC assay in B. TLC reactions was incubated for 40 minutes. Abbreviations: FR: Fractions.

Since the Mono Q column could not eliminate the ATPase contamination, in another attempt the fraction eluted from the Mono Q column was further purified using a Mono S column with buffer containing 20 mM Tris-HCl pH 7.5, 100 mM NaCl, 1 mM EDTA, 10 % glycerol and 0.5 mM TCEP.

After washing, SYCP3 was recovered by gradient elution from 200 mM NaCl – 1M NaCl (**Fig. 4.4**). TLC assays were used to monitor the ATPase activity of the recovered protein fractions. SYCP3 fractions contained less ATPase contamination with k_{cat} of 0.05 min^{-1} after the Mono S column (**Fig. 4.4 B**). However, as discovered much later in the course of this work, the SYCP3 protein recovered from the Mono S column did not exhibit DNA binding activity, unlike the Mono Q fraction, which readily bound DNA as expected from the literature (**Fig. 4.4 D**) [23, 24].

In another effort to remove the ATPase contamination, we supplemented the wash buffer for the heparin column with 5 mM ATP and 2.5 mM MgCl_2 with the intent to cause a conformational change in the possible ATPase contaminant and weaken its interaction with SYCP3 and/or the chromatography matrix. However, this approach was also not successful in separating SYCP3 from the ATPase activity.

A. SDS-PAGE	B. ATPase Assay

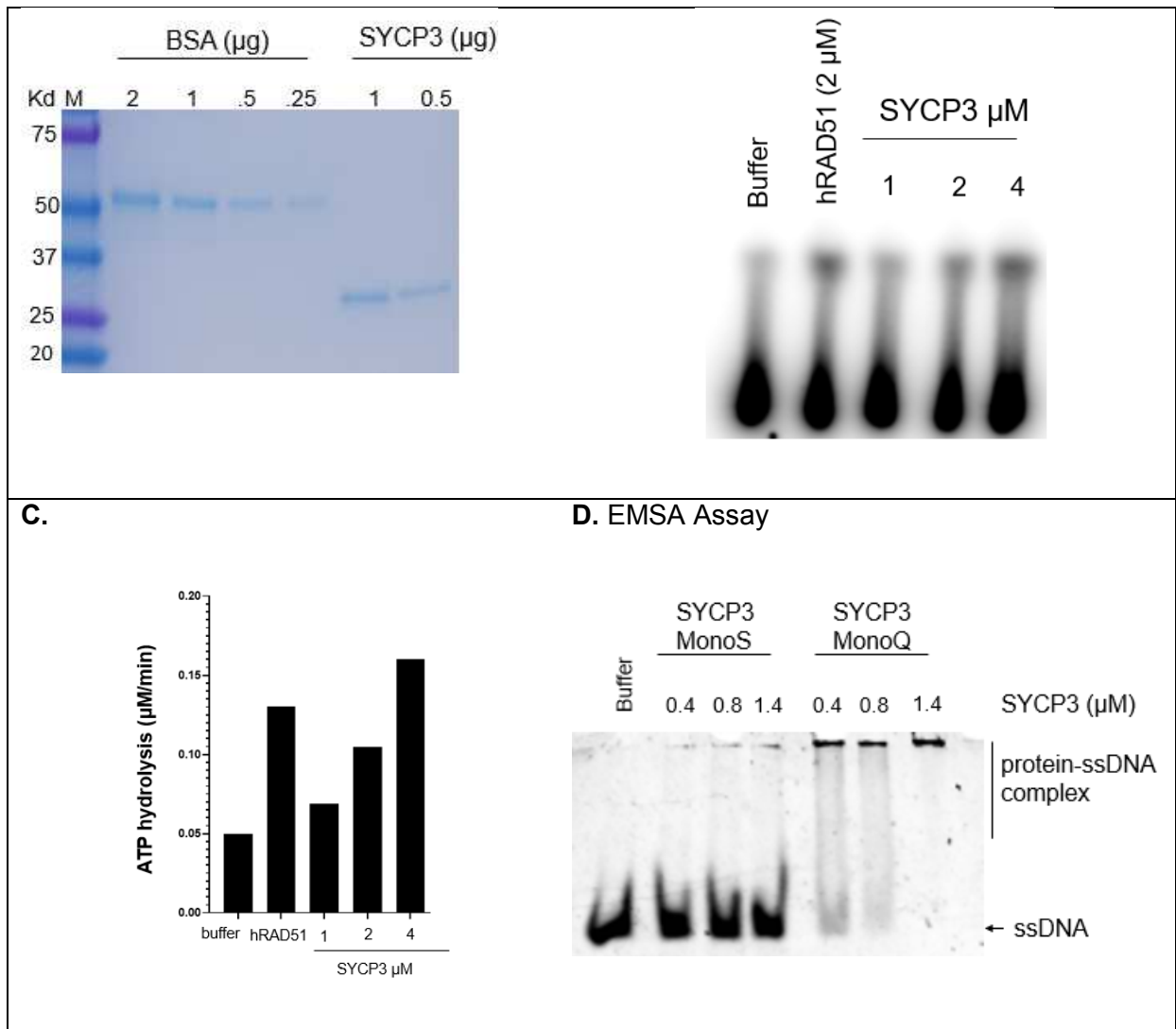


Figure 4.4: SYCP3 purified with Chitin, Heparin, Mono Q and Mono S columns has much lower ATPase contamination but lacks DNA binding. A. SDS/PAGE gel stained with Denville Blue. Yield: 2 mg. **B.** TLC assay of SYCP3 fractions eluted from a Mono Q column. **C.** Quantification of TLC assay in B. TLC reactions were incubated for 60 minutes. **D.** EMSA assay comparing DNA binding activity of SYCP3 purified by protocol B (Mono S) versus protocol A (Mono Q) using 80mer ssDNA (7.5 nM molecules)

To summarize, we used two different approaches to eliminate ATPase contamination and purify SYCP3:

- A. Chitin column, Heparin column and Mono Q column
- B. Chitin column, Heparin column, Mono Q column and Mono S column

With Approach A, the purified SYCP3 fraction contained an ATPase contamination with k_{cat} of 0.23 - 0.29 min^{-1} when compared with human RAD51 ATPase activity ($k_{cat} = 0.07 \text{ min}^{-1}$). With Approach B, ATPase contamination was much lower with k_{cat} of 0.05 min^{-1} .

Kobayashi et al. showed that SYCP3 interacts with RAD51 and blocks its interactions with HOP2-MND1. Thereby, SYCP3 inhibits stimulation of RAD51 strand invasion activity by HOP2-MND1 in D-Loop assays. However, the D-Loop assays containing only RAD51 had low efficiency, and hence, did not distinguish whether SYCP3 could directly affect RAD51 D-Loop activity [37]. The activity of SYCP3 purified from Approach B was tested in D-Loop assays with RAD51. Instead of HOP2-MND1 we used RAD54 to stimulate the D-Loop reactions by RAD51 and asked if SYCP3 inhibits this stimulation. Our results show that SYCP3 directly inhibits RAD51 D-Loop activity but the presence of RAD54 was able to overcome this inhibition (**Fig. 5**). The difference between our findings to those published [37] could be explained by the different proteins (RAD54 vs HOP2-MND1) used to stimulate the RAD51-mediated D-Loop reactions. SYCP3 was shown to bind RAD51 and thereby inhibit its interaction with HOP2-MND1 [37], while in our experiments, RAD54 was probably able to compete with the SYCP3–RAD51 interaction. Since our findings build on the previously published data, which validated the activity of the protein we proceeded to use the SYCP3 protein purified by Approach B in our biochemical assays. We later discovered that this protein was deficient in DNA binding activity. Since purified SYCP3 was immediately aliquoted and stored at $-80 \text{ }^{\circ}\text{C}$, it is unlikely that this preparation was initially active in DNA binding and then lost this activity due to repeated thawing and freezing. Also, an independent preparation using Mono Q and Mono S columns yielded the same results in ATPase and DNA binding assays, confirming that SYCP3 purified by Approach B was deficient in DNA binding and contained a

lower levels of ATPase contamination. Hence, the experiments with SYCP3, presented below, must be repeated with a new preparation of SYCP3 protein that does not have ATPase contamination and is proficient in DNA binding.

SYCP3 inhibits RAD51-mediated D-Loop formation and this effect is suppressed by RAD54

SYCP3 has been shown to directly interact with RAD51 and inhibit stimulation of the RAD51 D-loop forming activity by HOP2-MND1. SYCP3 mutants defective in the interaction with RAD51 showed no effect on the stimulation of RAD51 D-loop activity by HOP2-MND1 [37]. However, it is not known if SYCP3 can directly impede RAD51-mediated D-Loop formation. To address this question, D-Loop formation was reconstituted *in vitro*. RAD51 was incubated with ssDNA at optimal concentrations to saturate ssDNA (1:3 nucleotides) and then titrated with increasing concentrations of SYCP3. The strand-exchange reaction was initiated with the addition of dsDNA in the presence or absence of another critical recombination protein, RAD54 (**Fig. 5A**).

When the concentration of SYCP3 is up to 2-fold lower than that of RAD51, there was no noticeable effect on RAD51 D-Loop formation (**Fig. 4.5 B, C**). However, as the SYCP3 concentration became stoichiometric or higher than RAD51, D-Loop formation was significantly inhibited. These results along with earlier findings by Koyabashi *et al.* demonstrate that SYCP3 directly inhibits RAD51-mediated D-Loop formation.

The observed inhibition of RAD51-mediated D-Loop formation by SYCP3 was reversed by the presence of RAD54 (**Fig. 4.5 B, C**). RAD54 has been shown to initially stimulate RAD51-catalyzed D-Loop formation and then disrupt D-loops at later time points [41]. Previous findings show that

RAD54 forms a complex with the RAD51-ssDNA filament and stabilizing it [42]. To analyze the effect of RAD54 on D-loop formation in the presence of SYCP3, D-Loop reactions were incubated for 15 minutes after addition of RAD54. In the absence of SYCP3, a strong stimulation of RAD51-mediated D-Loop formation was observed, consistent with earlier findings [41]. In the presence of SYCP3, inhibition of RAD51-catalyzed D-Loop formation was no longer observed, and the RAD54-dependent stimulation of strand exchange dominated. The concentration of RAD54 used in these D-Loop reactions was 11x the concentration of dsDNA, greater than the concentrations of both RAD51 and SYCP3.

These results can be interpreted in the following ways. Given that SYCP3 binds dsDNA though with a lower affinity than ssDNA [37], our first hypothesis was that SYCP3 binds dsDNA and prevents strand invasion by RAD51 filaments. It is well known that RAD51 bound to the duplex DNA partner inhibits RAD51-mediated DNA strand invasion, and that this inhibition is overcome by RAD54 which displaces RAD51 from dsDNA [43, 44]. However, it was shown that when SYCP3 is preincubated with dsDNA it does not affect RAD51-catalyzed strand exchange in the D-loop assay [37]. Together, these observations suggest that the mechanism of inhibition by SYCP3 is not related to binding the duplex DNA target. Alternatively, SYCP3 may inhibit RAD51 by directly binding to RAD51 and RAD54 counteracts this effect.

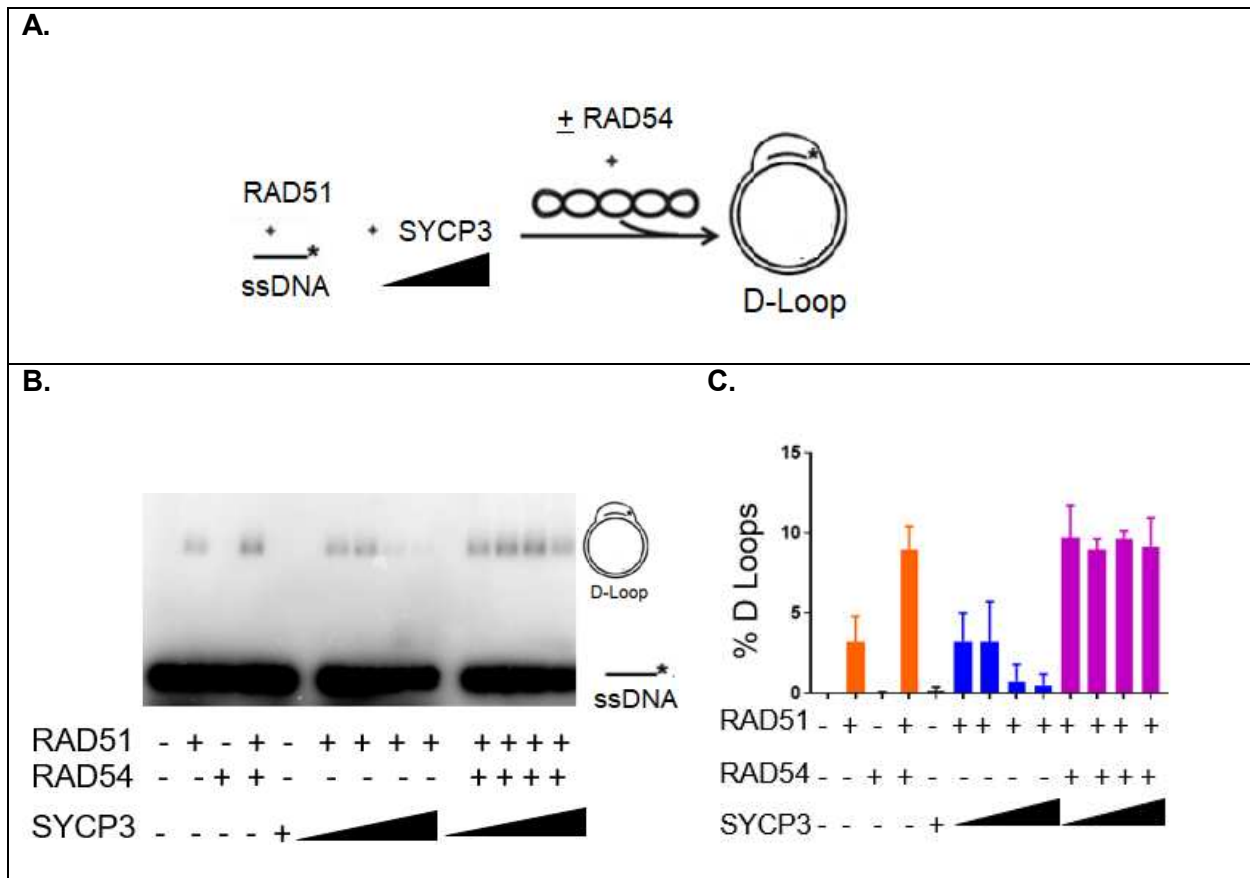


Figure 4.5: Inhibition of RAD51 strand exchange activity by SYCP3 is suppressed by the presence of RAD54. **A.** Scheme of D-loop assay. **B.** RAD51 (0.4 μ M) D-loop reactions in the absence or presence of RAD54 (1.05 μ M) with SYCP3 titration from 0, 0.1 μ M, 0.2 μ M, 0.4 μ M, 0.6 μ M. **C.** Quantification of the results in **B.** Reported are means from n=2 with standard deviation.

We conclude that SYCP3 directly inhibits RAD51-mediated D-Loop formation. The stoichiometry of inhibition suggests a 1:1 interaction between RAD51 and SYCP3, as D-Loop formation is significantly inhibited when RAD51 and SYCP3 are present in equimolar concentrations. This inhibition is reversed by the addition of RAD54, a protein that associates with the presynaptic RAD51-ssDNA filament [42, 43] and can dissociate RAD51 from dsDNA [44]. RAD54 has been

shown to form a stoichiometric complex with RAD51-ssDNA filaments to increase their stability and stimulate DNA strand exchange [42]. In our reactions RAD54 was present at ~2.5x concentration of RAD51 allowing it to form stoichiometric complexes with RAD51-ssDNA filaments. As SYCP3 binding to dsDNA has been excluded as a possible mechanism of strand-exchange inhibition [37], I suggest that RAD54 may compete with SYCP3 for binding to RAD51 and thereby antagonize its inhibitory effect. This model predicts that the rescue of the D-loop formation will be independent of the RAD54 ATPase activity, which can be tested with an ATPase-defective mutant RAD54 protein. To further corroborate this interpretation, higher concentrations of SYCP3 could be used with the intent to outcompete RAD54 in the interaction with RAD51. Such experiments will determine the stoichiometric relationship between RAD54 and SYCP3 in their competition to interact with RAD51 .

SYCP3 does not affect RAD51 and DMC1 ATPase activities

SYCP3 inhibits the D-loop activity of RAD51 but does not affect the activity of DMC1 [37]. Our hypothesis is that SYCP3 could interfere with the RAD51 strand invasion activity by stimulating its ATPase activity resulting in inactive ADP-bound RAD51 filaments. To test this idea, we performed TLC ATPase assays (**Fig. 4.6 A**) . In these experiments, we used the SYCP3 preparation from Approach B, described above. The ATPase activity of the purified SYCP3 protein fraction was at background level, similar to the level of spontaneous ATP hydrolysis observed with the negative control containing only ssDNA. I conclude that SYCP3-only reactions have negligible ATPase activity. RAD51 was then incubated with ssDNA, followed by the addition of increasing concentrations of SYCP3. In our experiments, RAD51 alone had ATPase activity with k_{cat} of 0.54 min^{-1} which is higher than the expected activity based on previous analysis ($k_{cat} = 0.07 \text{ min}^{-1}$) [40]. However, as expected, the ATPase activity of RAD51 was strongly stimulated by ssDNA. In presence of ssDNA, the k_{cat} of RAD51 ATPase activity was 3.4 min^{-1} which is also

higher than the k_{cat} observed in previous studies, which ranged from 0.2 -1 min^{-1} [16, 40, 45, 46]. The reason for the high RAD51 ATPase activity in our experiments is not clear. When SYCP3 was titrated into such reactions, the overall ATPase activity did not significantly change. The observed slight decrease in activity was well within the margin of error and not statistically significant. Next, we varied the order of addition of proteins and DNA to determine if SYCP3 could affect the RAD51 ATPase activity when: i) RAD51 was preassembled into filaments on ssDNA; ii) RAD51 was free in solution and not bound to DNA; iii) SYCP3 was bound to ssDNA before RAD51 was added. Since the SYCP3 protein preparation from Approach B was subsequently found to be deficient in DNA binding activity, our experiment does not test for case iii and hence will have to be repeated with SYCP3 preparation that is proficient for DNA binding. There was a slight variation in RAD51 ATPase activity with the different orders of addition of proteins and DNA, but these differences were not statistically significant. In sum, these results showed that SYCP3 does not have a detectable effect on the ATPase activity of RAD51 (**Fig. 4.6**).

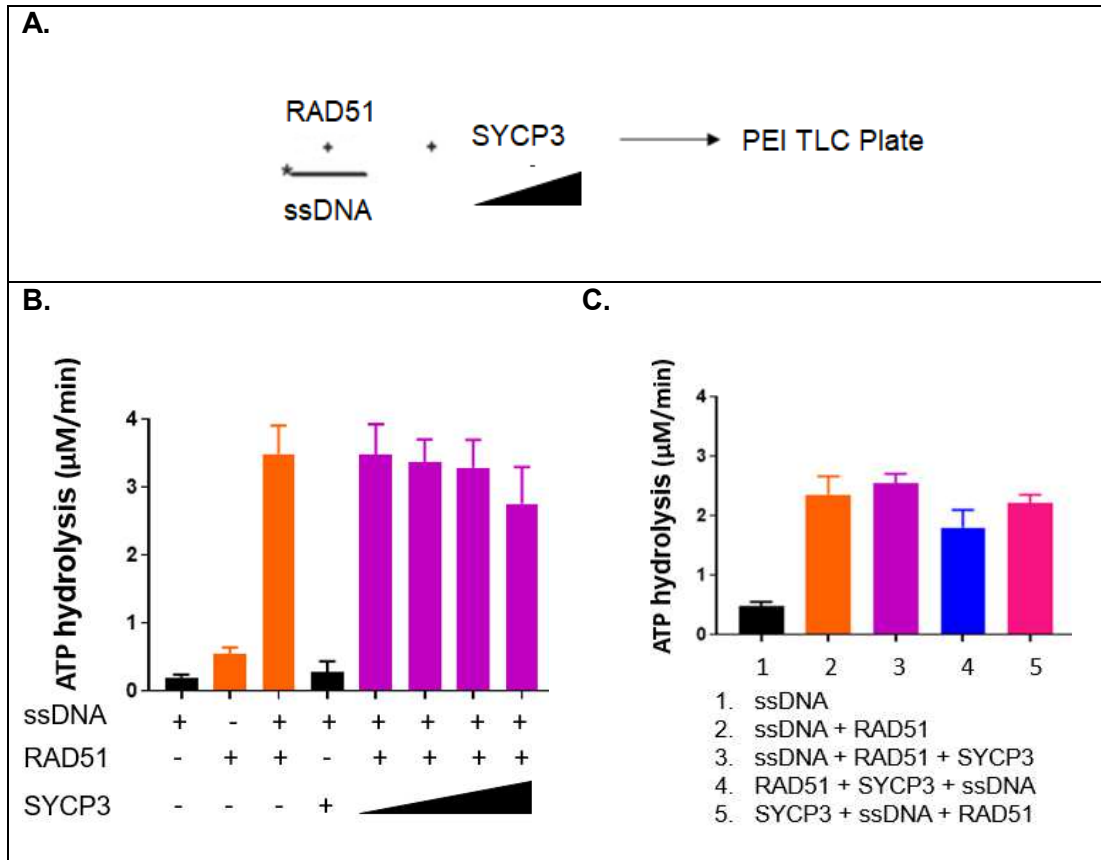


Figure 4.6. SYCP3 does not have a significant effect on the ATPase activity of RAD51. Quantification of TLC Assay with RAD51-ssDNA and SYCP3. **A.** Scheme of TLC Assay. **B.** RAD51 (2 µM) was incubated with ssDNA (6 µM nucleotides) followed by addition of increasing concentrations of SYCP3. **C.** Different order of addition of proteins in TLC assay. Proteins, DNA (6 µM nucleotides) are listed in the order added from left to right. TLC reactions were incubated for 40 minutes. SYCP3 titration is 0 µM, 0.5 µM, 1 µM, 2 µM and 4 µM. Reported are means from n=3 with standard deviation.

Next, to determine if SYCP3 affects the ATPase activity of DMC1, we performed TLC reactions in which DMC1 was incubated with ssDNA followed by the addition of increasing concentrations of SYCP3 (**Fig. 4.7 A**). The k_{cat} of the DMC1 ATPase activity was of 1.6 min^{-1} which is higher than

the expected activity ($k_{\text{cat}} = 0.6 \text{ min}^{-1}$) [47]. The reason for this higher ATPase activity is not clear. As expected, the ATPase activity of DMC1 was strongly stimulated by ssDNA [47], with a k_{cat} of 2.14 min^{-1} which is higher than what is reported by some studies (k_{cat} of $0.2 - 1.5 \text{ min}^{-1}$) [15, 48] but similar to the k_{cat} of 2.5 min^{-1} reported by *Sharma et al.* [47].

The overall DMC1 ATPase activity did not change significantly when SYCP3 was titrated into to these reactions. Although a slight decrease in the ATPase activity was suggested with increasing SYCP3 concentrations, but this was well within the margin of error and not statistically significant. Next, we varied the order of addition of proteins and DNA to determine if SYCP3 could affect the ATPase activity of DMC1 when: i) DMC1 was preassembled into filaments on ssDNA; ii) DMC1 was free in solution and not bound to DNA; iii) SYCP3 was bound to ssDNA before DMC1 was added. Since the SYCP3 protein used in these experiments was later found to be deficient in DNA binding activity, our experiments did not test for case iii and will have to be repeated with SYCP3 proficient in DNA binding. There was slight variation in the DMC1 ATPase activity depending on the order of addition of the proteins and DNA, but none of the differences were statistically significant. These results show that SYCP3 does not have a detectable effect on the ATPase activity of DMC1 (**Fig. 4.7**).

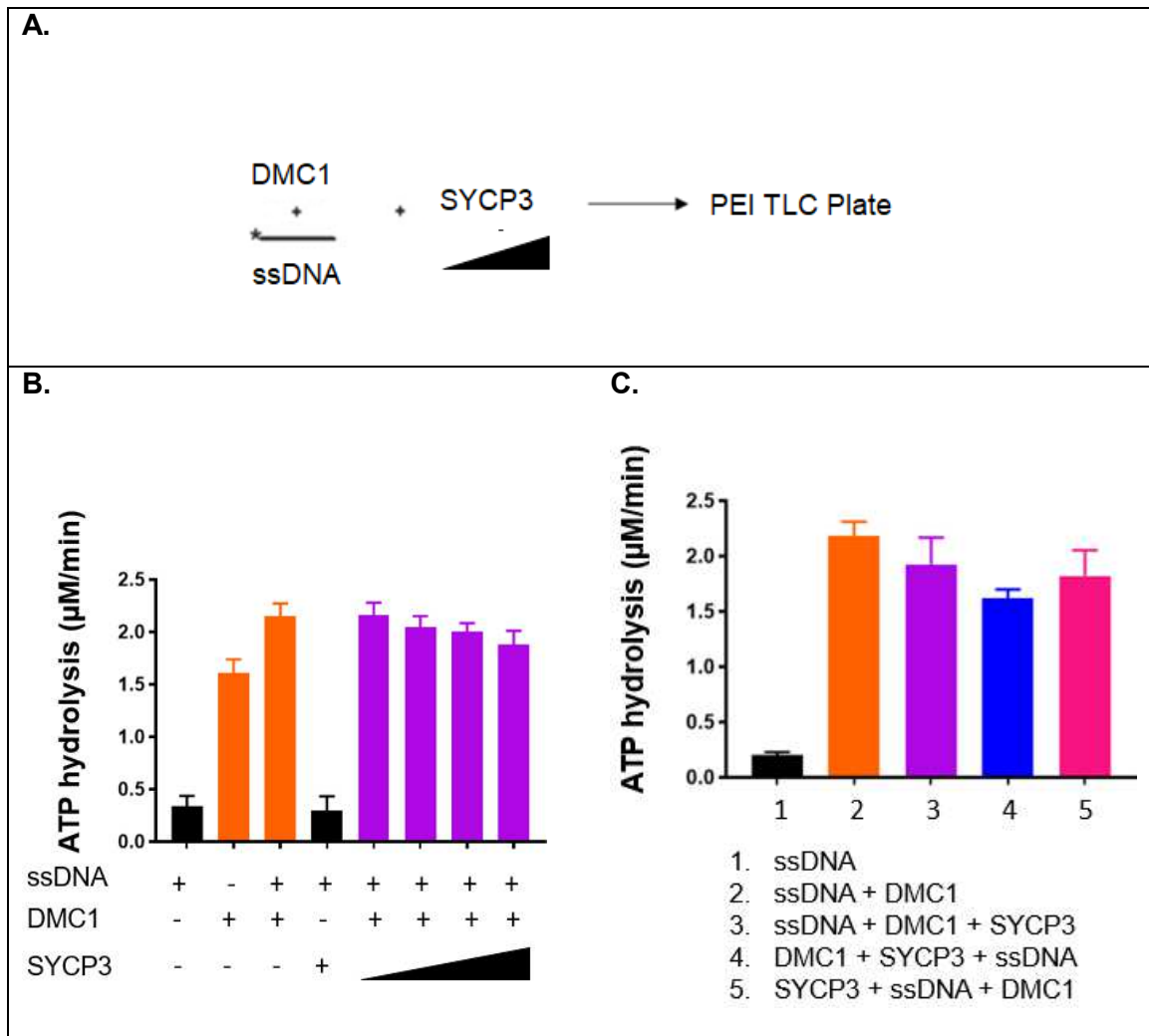


Figure 4.7. SYCP3 does not have significant effect on ATPase activity of DMC1.

Quantification of TLC Assay with DMC1-ssDNA and SYCP3. **A.** Scheme of TLC Assay **B.** DMC1 (2 µM) is incubated with ssDNA (6 µM nucleotides) followed by addition of increasing concentrations of SYCP3. **C.** Different order of addition of proteins in TLC assay. Proteins, DNA (6 µM nucleotides) are listed in the order added from left to right. TLC reactions were incubated for 40 minutes. SYCP3 titration is 0 µM, 0.5 µM, 1 µM, 2 µM and 4 µM. Reported are means from n=4 with standard deviation.

From the above experiments, I conclude that SYCP3 does not have a significant effect on the ATPase activity of both RAD51 and DMC1. Previous published data showed that SYCP3 affects the activity of RAD51, but not the DMC1, in D-loop assays and that this was not due to SYCP3 dsDNA binding [37]. Our data shows that SYCP3 does not affect the D-loop forming activity of RAD51 by modulating its ATPase activity. In aggregate, the results lead to a model in which SYCP3 affects RAD51 strand exchange activity by direct interaction with RAD51. Failure to inhibit DMC1 may be explained by the observation that SYCP3 binds DMC1 with much lower affinity than RAD51 [37].

SYCP3 disrupts pre-formed RAD51 but not DMC1 filaments:

SYCP3 inhibits RAD51 activity in D-Loop reactions, and the above results from the ATPase assays show that this inhibition is not mediated through an effect on the RAD51 ATPase activity. Another way that SYCP3 could inhibit RAD51 strand-exchange activity is by altering the formation or stability of RAD51 filaments. To test these possibilities, we performed Electrophoretic Mobility Shift Assays (EMSA).

In a first step, we optimized the conditions for EMSA assays of RAD51 and DMC1 filament formation on ssDNA. Increasing concentrations of RAD51 or DMC1 were incubated with ssDNA to form filaments at 37 °C. The reaction products were then resolved by PAGE at room temperature (**Fig. 4.8**). The buffer only lane indicates the migration position of the unbound ssDNA. As RAD51 and DMC1 concentrations were increased, there was a shift in the migration position up to the protein-DNA complex 1, which represents saturated protein-bound DNA. Since the reaction products were not crosslinked, there was some dissociation of the proteins from DNA as they were separated in the gel, which is labeled as protein-DNA complex 2. When the protein to ssDNA ratio was 1:3 most of the unbound DNA shifted to the protein-bound forms, either

protein-DNA complex1 or protein DNA complex 2. At a protein to DNA ratio of 1.5:1 for RAD51 and 1:1 for DMC1, most of the free DNA was saturated with the proteins and present as protein-DNA complex 1 with minimal dissociation into protein DNA complex 2. Since RAD51 and DMC1 form saturated protein-ssDNA filaments at a ratio of 1 monomer:3 nucleotides, we used corresponding concentrations of 15 nM ssDNA and 0.4 μ M RAD51 and DMC1 for subsequent EMSAs.

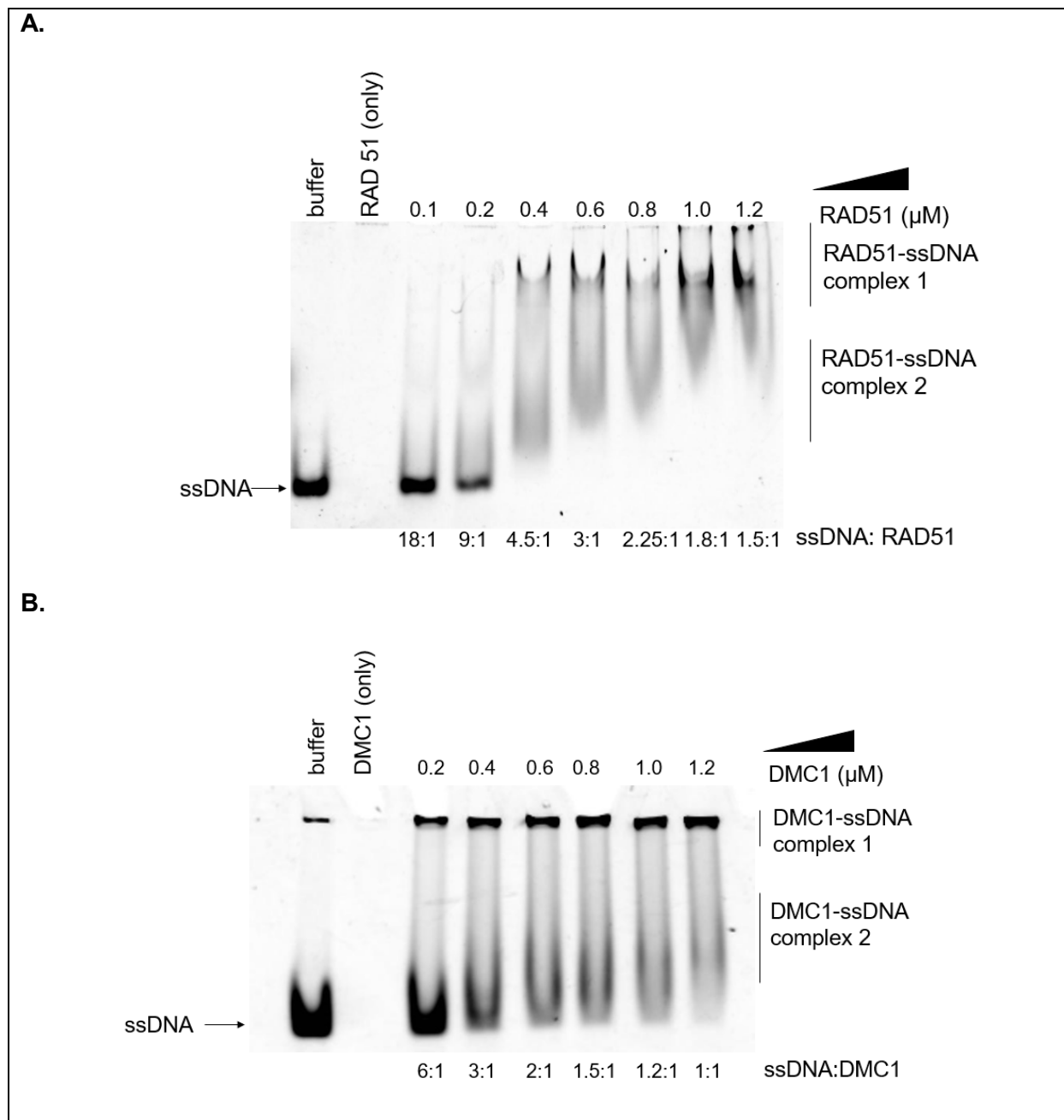


Figure 4.8: Optimization for RAD51 and DMC1 filament formation. A. RAD51 filaments formed on ssDNA (23 nM molecule) with increasing concentrations of RAD51 (4% PAGE). **B.** DMC1 filaments formed on ssDNA (15 nM molecule) with increasing concentrations of DMC1 (6% PAGE).

Next, to determine if SYCP3 affects RAD51 filament stability, we titrated in SYCP3 and analyzed the protein-DNA complexes by EMSAs. RAD51 was first incubated with ssDNA at a ratio of 1:3 nucleotides for 10 minutes to form saturated RAD51-ssDNA filaments. SYCP3 was then added, starting with a 4-fold lower concentration than that of RAD51 and going up to slightly less than a 4-fold higher concentration. The reactions were then further incubated for another 15 minutes before resolving DNA and DNA-protein complexes by 6 % PAGE (Fig. 4.9 A).

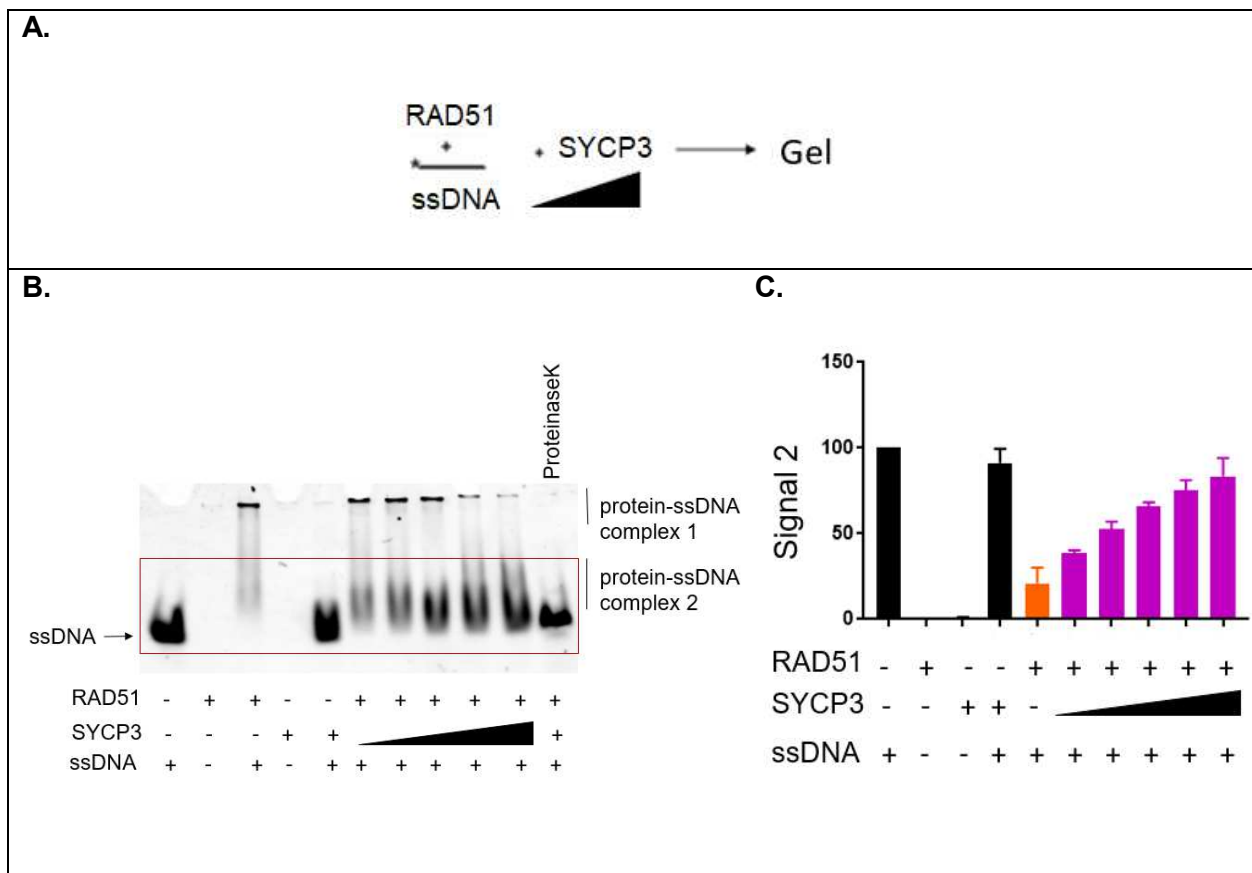


Figure 4.9: SYCP3 increases RAD51 filament instability. **A.** Scheme of EMSA assay. **B.** PAGE gel of EMSA assay of SYCP3 titration with RAD51 (0.4 μ M) filaments formed on ssDNA (15 nM molecule) with SYCP3 titration from 0.1 μ M, 0.2 μ M, 0.4 μ M, 0.8 μ M, 1.4 μ M. **C.**

Quantification of the DNA signal within the red box in **A**. Signal 2 includes % free DNA and % of DNA in protein-ssDNA complex 2. Reported are means from n=3 with standard deviation. Protein-ssDNA complex 1 indicates the saturated RAD51 filaments formed on the ssDNA and is retained in the wells. Protein-ssDNA complex 2 migrates above the position of free DNA and is inferred to represent filaments where some of the RAD51 has dissociated. To corroborate this inference, additional experiments, such as two-dimensional gel electrophoresis, will be required. In the proteinase K control lane, the final reaction products were treated with proteinase K to digest the proteins before loading them on the gel. This control monitors for any nuclease contamination which could mimic the disappearance of free DNA in a similar way to when RAD51 binds ssDNA binding. The amount of free DNA recovered in the proteinase K control was the same as the free DNA in the buffer-only lane (Lane 1 in **Fig. 4.9 B**), confirming that there is no nuclease contamination. As SYCP3 concentration increased, there was a decrease in the protein-ssDNA complex 1 and a corresponding increase in protein-ssDNA complex 2 and free ssDNA (**Fig. 4.9 B, C**) indicating that SYCP3 stimulates dissociation of RAD51 dissociation from the filaments. When the SYCP3:RAD51 ratio was 1:1, about 60% of the RAD51 filaments were dissociated. This stoichiometry suggests that direct binding of SYCP3 to RAD51 leads to filament instability and dissociation of RAD51.

To verify these results, EMSAs with RAD51 and SYCP3 titration were repeated using lower concentrations of RAD51, SYCP3 and ssDNA. Using half the concentration of proteins and DNA the expectation was that RAD51 filament dissociation would follow a similar pattern as observed in (**Fig. 4.9 B**) with the SYCP3 titration. The data (**Fig. 4.10**) confirm the earlier findings showing that when the SYCP3:RAD51 ratio is 1:1, 60% of RAD51 filaments are dissociated.

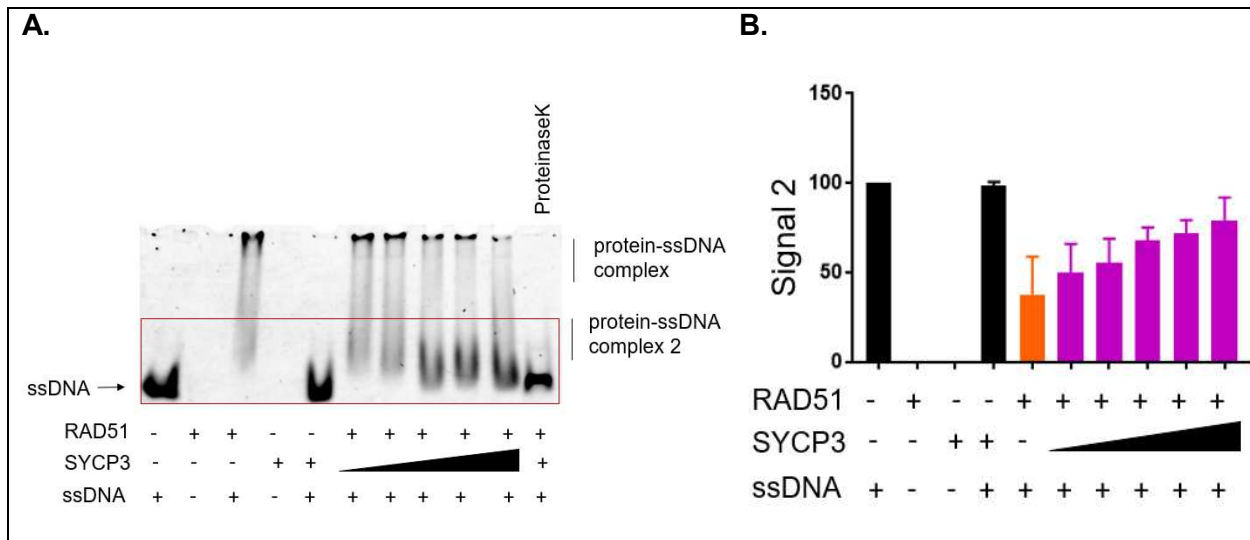


Figure 4.10: SYCP3 increases RAD51 filament instability at lower concentration of proteins and DNA. **A.** PAGE gel of EMSA assay of SYCP3 titration with RAD51 (0.2 μM) filaments formed on ssDNA (7.5 nM molecule) with SYCP3 titration from 0.05 μM, 0.1 μM, 0.2 μM, 0.8 μM. **B.** Quantification of the DNA signal within the red box in **A.** Signal 2 includes % free DNA and % of DNA in protein-ssDNA complex 2. Reported are means from n=3 with standard deviations.

To establish the mechanism of how SYCP3 leads to RAD51 filament dissociation, the migration pattern of the RAD51 protein was followed in the presence of SYCP3. Towards this goal, Far-Western immunoblot assays of EMSA gels similar to the one shown in (**Fig 4.9**) were conducted. The goal was to separate free RAD51 from RAD51:DNA and RAD51-SYCP3 complexes and detect RAD51 and SYCP3 by Far-Western assays so that we can then correlate RAD51 migration with the labelled DNA and SYCP3 to define the RAD51:DNA and RAD51:SYCP3 complexes. Our expectation was that while RAD51:DNA complex would be retained near the wells, free RAD51 and RAD51:SYCP3 complex would enter the gel, with free RAD51 migrating further ahead into the gel than RAD51:SYCP3 complex. But the results show that free SYCP3, free RAD51, SYCP3:RAD51 complex and RAD51:DNA complex are all retained near the wells (**Fig. 4.11**).

Hence, no differences in the migration pattern of RAD51 when it was DNA bound, free or bound to SYCP3 could be identified. Also, the SYCP3 SIGMA antibody works poorly for detection by Western blots (**Fig. 4.11 B**). In conclusion, it was not possible to gain insights from the Far-Western immunoblots into the mechanism by which SYCP3 led to RAD51 filament dissociation.

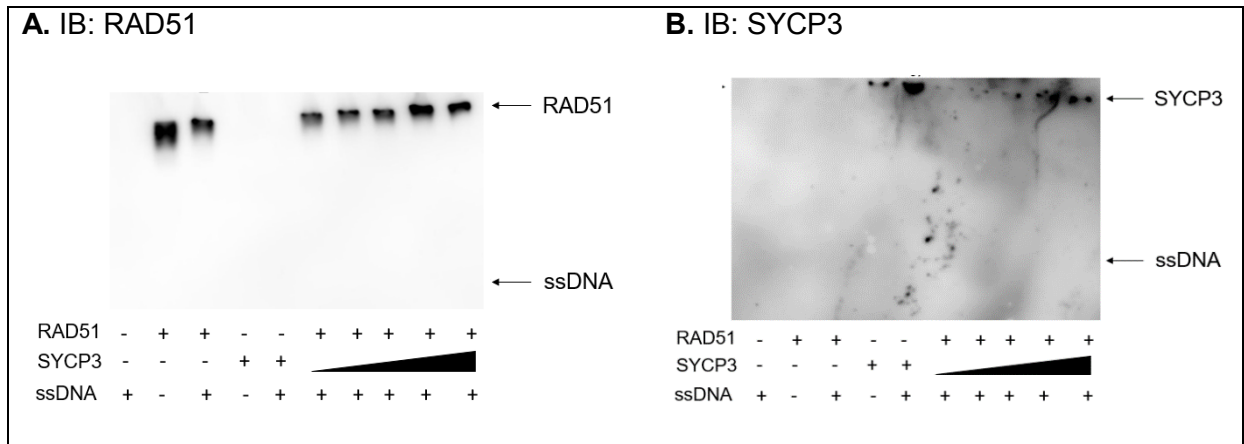


Figure 4.11: FAR Western Immunoblot Analysis (IB) of EMSA does not provide insight on the mechanism by which SYCP3 leads to RAD51 filament dissociation. A. Immunoblot of RAD51 antibody (1:1,000). **B.** Immunoblot of SYCP3 antibody (1:100). Protein and DNA concentrations: ssDNA 15 nM molecule; RAD51 0.4 μ M; SYCP3 titrations are 0.1 μ M, 0.2 μ M, 0.4 μ M, 0.8 μ M, 1.4 μ M. n=1.

Finally, we repeated the EMSAs with crosslinking to address whether more discrete protein-DNA complexes could be detected on the gel. To crosslink, 0.25% glutaraldehyde was added to completed reactions and incubated for 5 minutes at RT before loading on the PAGE gel [49]. Under these conditions, we could not detect dissociation of RAD51 filaments by SYCP3 probably due to non-specific cross-linking of all proteins and ssDNA (**Fig. 4.12**).

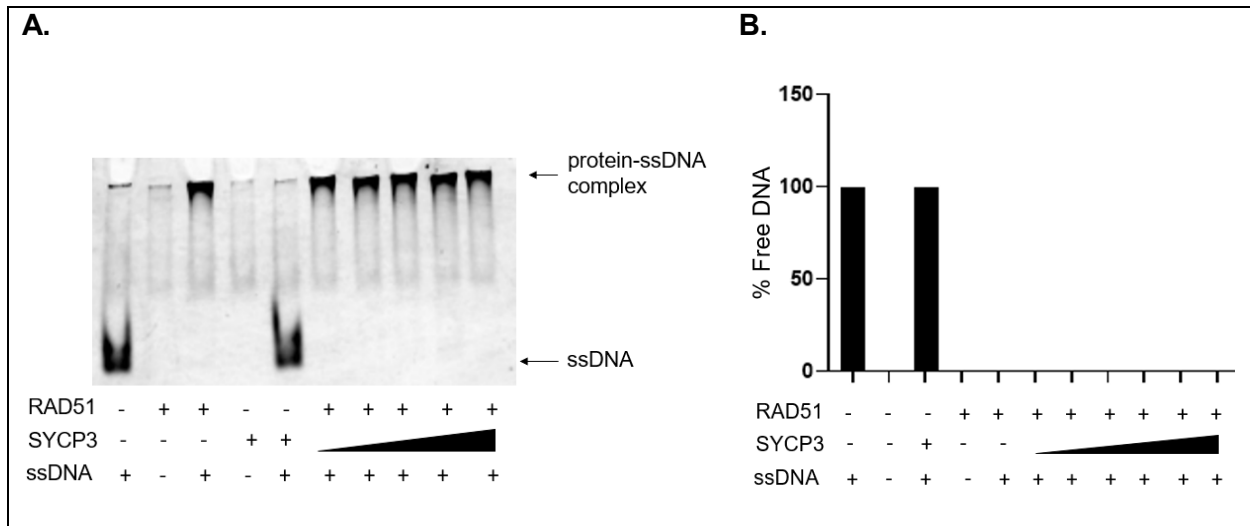


Figure 4.12: With Crosslinking no dissociation of RAD51 filaments by SYCP3. **A.** PAGE gel of EMSA assay of SYCP3 titration with RAD51 (0.2 μ M) filaments formed on ssDNA (7.5 nM molecule) with SYCP3 titration from 0.05 μ M, 0.1 μ M, 0.2 μ M, 0.8 μ M. **B.** Quantification of the results in A. n=1.

To assess if SYCP3 can affect DMC1 filament stability, we performed similar EMSA assays, titrating SYCP3 with pre-formed DMC1 filaments. DMC1 was incubated with ssDNA at a ratio of 1:3 nucleotides to form saturated filaments at 37°C for 10 minutes. Then increasing concentrations of SYCP3 were added (4-fold lower relative to DMC1 up to slightly less than a 4-fold higher concentration) for another 15 minutes before resolving the products by 6 % PAGE (**Fig. 4.13 A**). Shifted species corresponding to DMC1 filaments were observed for about 30-40% of the available DNA. With increasing concentrations of SYCP3, there was no significant change in the level of protein DNA complex 1. The Proteinase K control confirmed the absence of nuclease contamination (Lane 1 in **Figure 4.13 B**). Thus, unlike RAD51, SYCP3 did not exhibit a significant effect on DMC1 filament stability (**Fig. 4.13 B, C**).

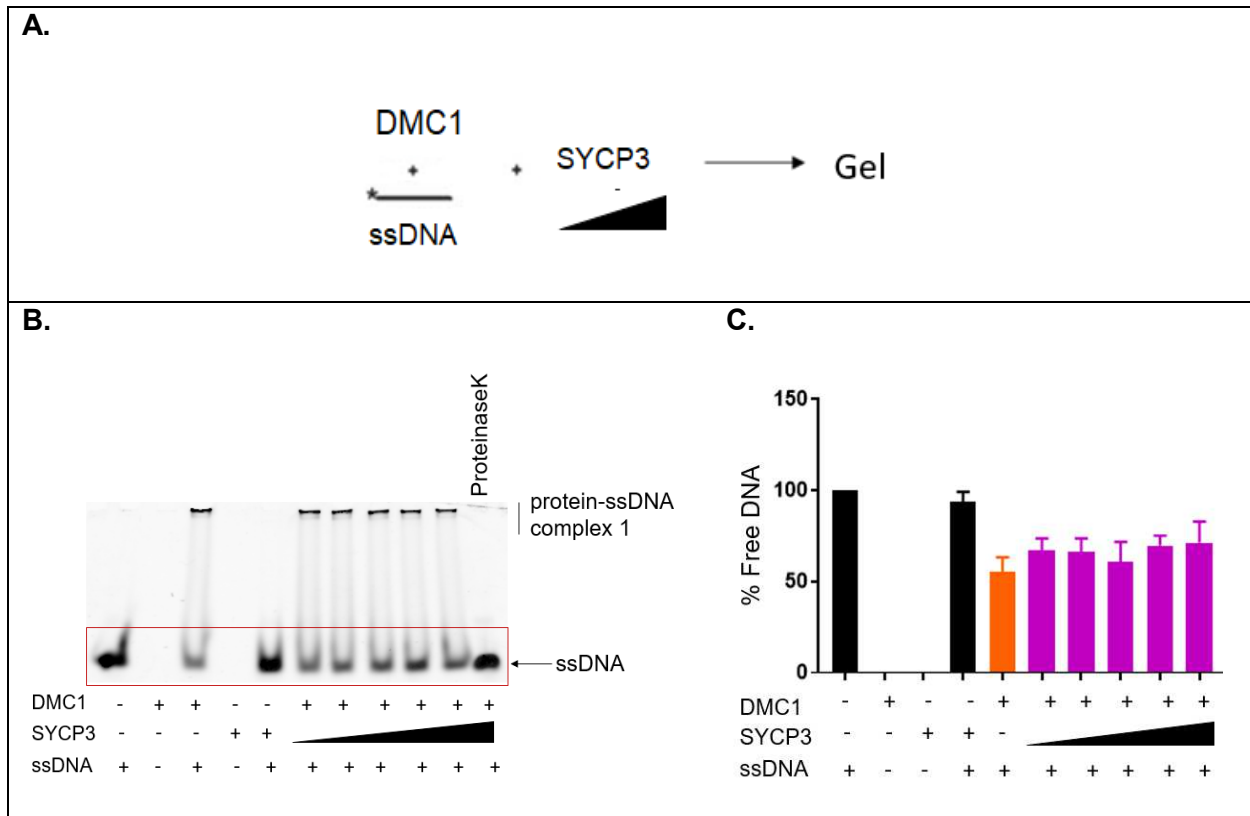


Figure 4.13. SYCP3 does not affect DMC1 filament stability. **A.** Scheme of EMSA assay. **B.** PAGE gel of EMSA assay of SYCP3 titration with DMC1 (0.4 μ M) filaments formed on ssDNA (15 nM molecule). **C.** Quantification of the results in **A.** SYCP3 titrations are 0.1 μ M, 0.2 μ M, 0.4 μ M, 0.8 μ M, 1.4 μ M. Reported are means from n=3 with standard deviations.

To determine if SYCP3 could affect DMC1 filament stability when saturated DMC1 filament formation was more efficient, EMSAs were repeated with higher concentrations of DMC1 and SYCP3 (**Fig. 4.14**). In these reactions, the efficiency of DMC1 filament was around 50 %. However, similar to the observations in **Figure 4.13**, addition of SYCP3 had no effect on the levels of protein-ssDNA complex 1 and free ssDNA. These findings confirm that SYCP3 does not appreciably affect DMC1 filament stability.

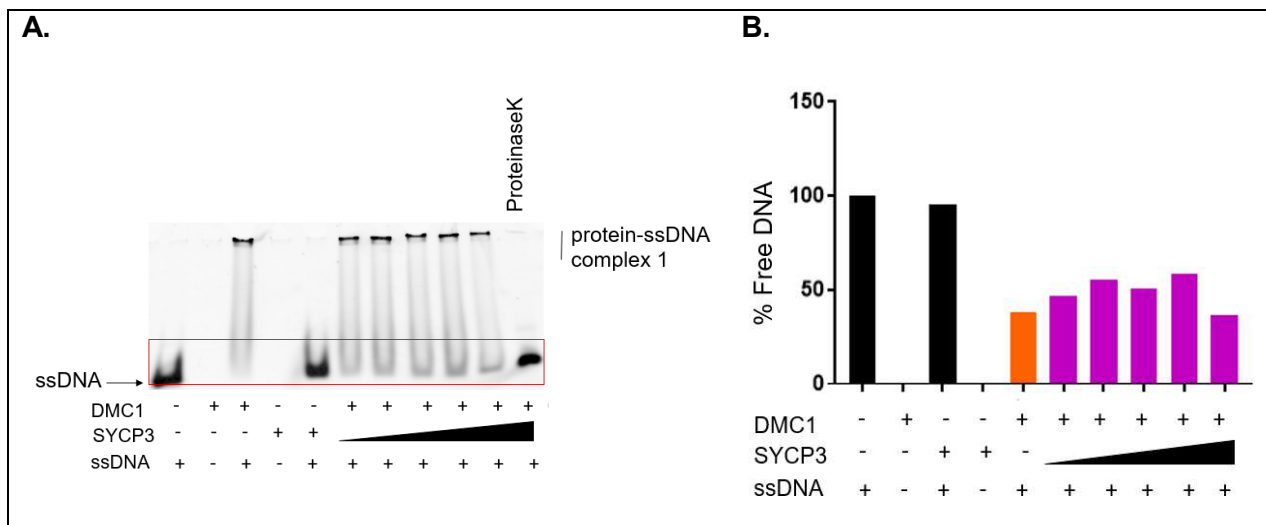


Figure 4.14. SYCP3 does not affect DMC1 filament stability when DMC1 filaments are more saturated. **A.** PAGE gel of EMSA assay of SYCP3 titration with DMC1 (0.8 μ M) filaments formed on ssDNA (15 nM molecule). **B.** Quantification of the results in A. SYCP3 titrations are 0.2 μ M, 0.4 μ M, 0.8 μ M, 1.4 μ M, 2.8 μ M. n=1.

In conclusion, SYCP3 selectively destabilizes RAD51 filaments but not DMC1 filaments. It has been shown that SYCP3 has a stronger binding affinity for RAD51 relative to DMC1 [37] and SYCP3 likely affects RAD51 filaments by directly binding to RAD51. There are two possible models that could explain how SYCP3 affects RAD51 filaments:

Model 1: SYCP3 binds to RAD51 filaments and leads to its dissociation.

Model 2: When RAD51 dissociates from DNA following ATP hydrolysis, SYCP3 binds to free RAD51 and prevents it from re-binding.

These models can be discerned by EMSAs of Rad51-ssDNA filaments in which filament dynamics are blocked by preventing ATP hydrolysis that in turn prevents RAD51 turnover from DNA. We can block ATP hydrolysis by RAD51 using either calcium or non-hydrolysable ATP analogues in the reaction buffer. Model 1 would predict that SYCP3 disrupts RAD51 filaments even when RAD51 turnover from DNA is inhibited, while Model 2 would predict that SYCP3 does not affect RAD51 filaments under non-turnover conditions.

SYCP3 inhibits RAD51 filament formation

The above results show that SYCP3 disrupts preformed RAD51 filaments, but it is not clear yet which model (described above) best describes how SYCP3 leads to RAD51 filament instability. Our hypothesis is that direct binding of SYCP3 and free RAD51 inhibits RAD51 ssDNA binding as suggested in Model 2. To test this possibility, we tested the prediction that SYCP3 should inhibit the formation of RAD51 filaments. RAD51 was preincubated with increasing concentrations of SYCP3 for 10 minutes at 37 °C before adding ssDNA for another 10 minutes. As SYCP3 concentration increased, levels of protein-ssDNA complex 1 decreased and a corresponding increase in free ssDNA and partial filaments indicated by protein-ssDNA complex 2. When SYCP3 concentration was close to 4-fold higher than RAD51, almost 100% of the input DNA was unbound or present in partial filaments (protein-ssDNA complex 2). These results support a mechanism in which direct interaction of SYCP3 with RAD51 prevents RAD51 from forming filaments on ssDNA (**Fig. 4.15**).

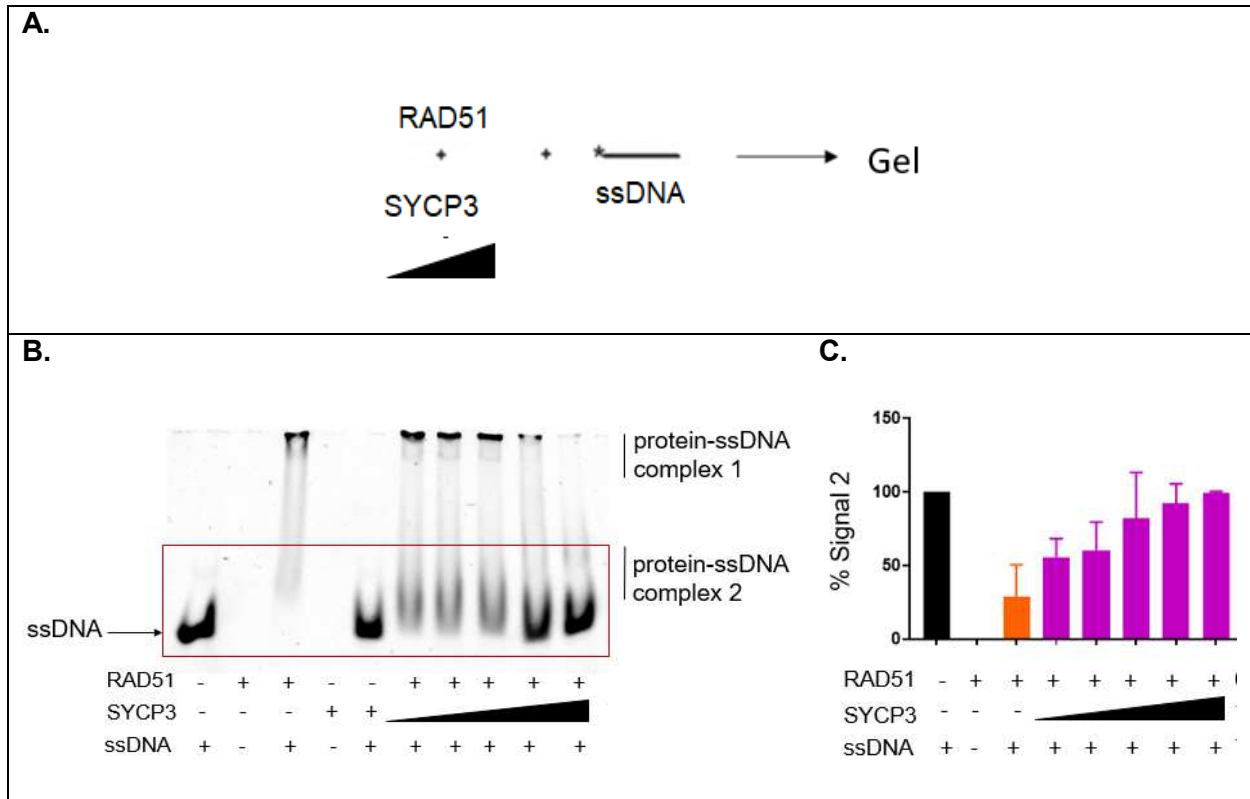


Figure 4.15: SYCP3-RAD51 binding inhibits RAD51 filament formation on ssDNA. **A.** Scheme of EMSA assay. **B.** PAGE gel of EMSA assay of SYCP3 pre-incubation with RAD51(0.4 μ M) before adding ssDNA (15 nM molecule) with SYCP3 titration from 0.1 μ M, 0.2 μ M, 0.4 μ M, 0.8 μ M, 1.4 μ M. **C.** Quantification of the DNA signal within the red box in **A.** Signal 2 includes % free DNA and % of DNA in protein-ssDNA complex 2. Reported are means from n=3 with standard deviation.

We conclude that SYCP3 affects the activity of RAD51 in HR by directly interacting with RAD51 and preventing RAD51 from binding to DNA. In preformed RAD51-ssDNA filaments, SYCP3 likely binds RAD51 as it dissociates from DNA following ATP hydrolysis and thereby prevents RAD51 from rebinding to the DNA. **SYCP3 does not destabilize RAD51 filaments under non-turnover conditions**

The above results show that SYCP3 inhibits RAD51 filament formation and destabilizes pre-formed RAD51 filaments. Our hypothesis is that SYCP3 binds free RAD51 and thereby inhibits RAD51 from binding DNA. Upon ATP hydrolysis by RAD51, there is an initial accumulation of ADP bound RAD51 on the DNA which has a half-life of ≈ 5 minutes followed by slow dissociation of RAD51 from DNA that takes place in bursts starting from the filament ends [50, 51]. In our reactions, RAD51 and ssDNA are incubated for 10 minutes followed by the addition of increasing concentrations of SYCP3 for another 15 minutes incubation. The reaction products are then analyzed by PAGE which takes another hour. We suspect that during this time, as when RAD51 slowly dissociates from the DNA following ATP hydrolysis, SYCP3 binds to RAD51 and prevents it from rebinding DNA. To test this idea, we analyzed the ability of SYCP3 to destabilize RAD51 filaments under non-turn over conditions that prevent RAD51 filament dynamics. Under non-turn over conditions, ATP hydrolysis is diminished or inhibited to prevent RAD51 from dissociating from DNA. Our experiments are elaborated below:

- i. Calcium reduces ATP hydrolysis by RAD51 and thereby stabilizes Rad51 filaments [52]. We used reaction buffer with only calcium instead of calcium and magnesium, which is used under standard turnover conditions.
- ii. AMP-PNP is a non-hydrolysable analogue of ATP that also stabilizes RAD51-ssDNA filaments [53]. ATP was substituted with AMP-PNP in the reaction buffer.

The reactions were performed under non-turnover conditions accompanied by standard turnover conditions as controls. In the first case, reactions with calcium and magnesium in the reaction buffer were compared with only calcium in the buffer. Calcium stabilizes RAD51 filaments by reducing RAD51 ATP hydrolysis and thereby decreases RAD51 dissociation from DNA. In both conditions, RAD51 was incubated with ssDNA at a ratio of 1:3 nucleotides to form saturated filaments. SYCP3 was titrated as before. In the calcium-only condition, as SYCP3 concentration was increased, a small decrease in protein-ssDNA complex 1 was observed accompanied by a

corresponding increase in protein-ssDNA complex 2 indicating much lower RAD51 dissociation than observed under standard turn over conditions. Under turn over conditions, when SYCP3 concentration was close to 4-fold higher than the RAD51, there was almost no protein-ssDNA complex 1 remaining in the well; while under non-turn over conditions, about 30 % of DNA was present in the well as protein-ssDNA complex 1 (Fig. 4.16).

When ATP was substituted with the non-hydrolysable analog AMP-PNP, SYCP3 did not cause any dissociation of RAD51 filaments (Fig. 4.17). There was no reduction in protein-ssDNA complex 1 and almost no protein-ssDNA complex 2 was detected. Calcium reduces ATP hydrolysis by RAD51 [52], while AMP-PNP is not hydrolysed, which explains why AMP-PNP stabilized RAD51 filaments more robustly than calcium. These results corroborate our hypothesis that SYCP3 binds RAD51 following ATP hydrolysis as it dissociates from the DNA and prevents it from rebinding to DNA.

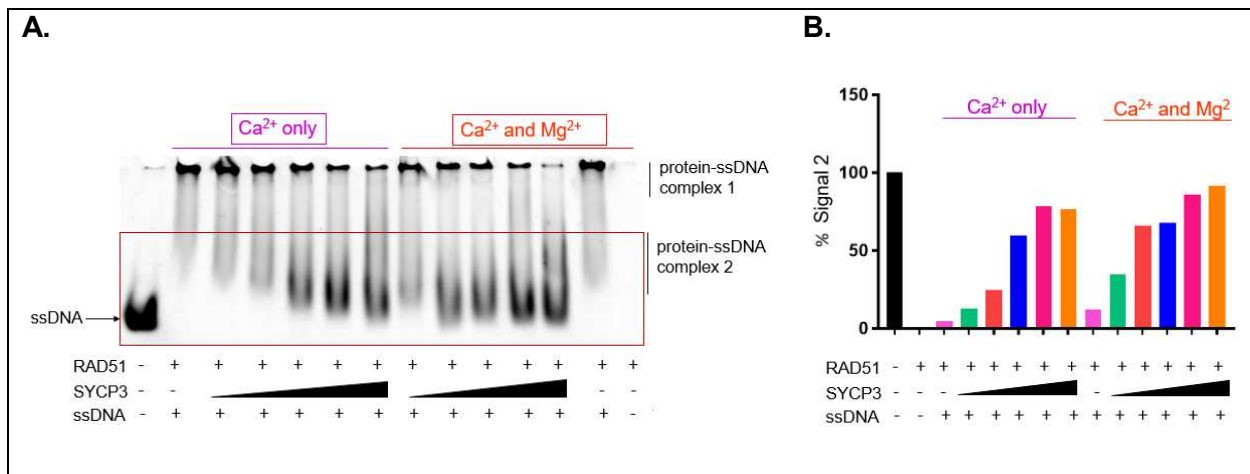


Figure 4.16: SYCP3 titration leads to lesser disruption of RAD51 Filaments under non-turnover conditions with calcium in reaction buffer. A. PAGE gel of EMSA assay of SYCP3

titration with RAD51(, 0.4 μ M) filaments formed on ssDNA (15 nM molecule) with SYCP3 titration from 0.1 μ M, 0.2 μ M, 0.4 μ M, 0.8 μ M, 1.4 μ M. **B.** Quantification of the DNA signal within the red box in **A.** Signal 2 includes % free DNA and % of DNA in protein-ssDNA complex 2. n=1.

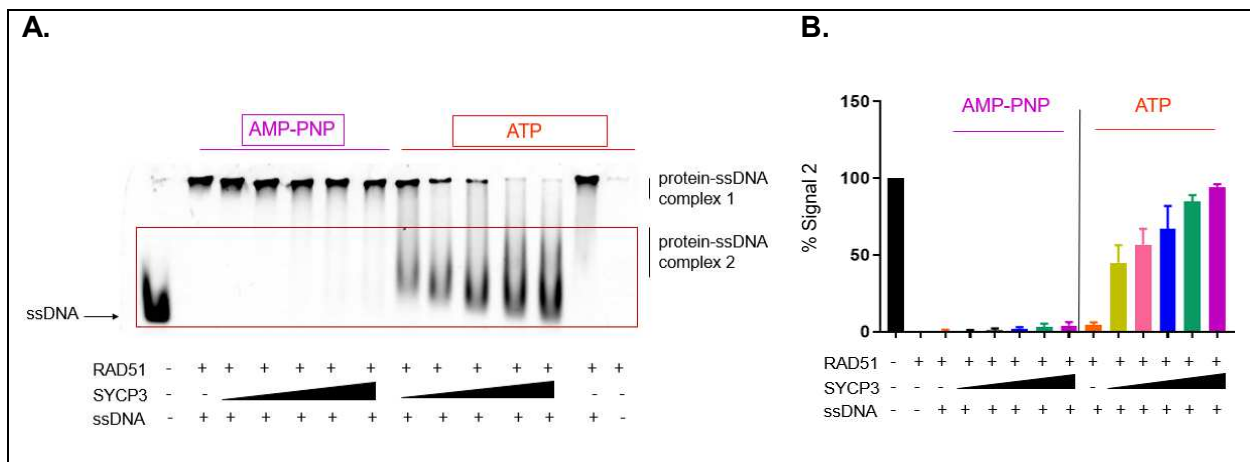


Figure 4.17: SYCP3 does not disrupt RAD51 Filaments under non-turnover conditions with AMP-PNP in reaction buffer. **A.** PAGE gel of EMSA assay of SYCP3 titration with RAD51(, 0.4 μ M) filaments formed on ssDNA (15 nM molecule) with SYCP3 titration from 0.1 μ M, 0.2 μ M, 0.4 μ M, 0.8 μ M, 1.4 μ M. **B.** Quantification of the DNA signal within the red box in **A.** Signal 2 includes % free DNA and % of DNA in protein-ssDNA complex 2. Reported are means from n=3 with standard deviation.

The above results validate model 2, described above. Upon ATP hydrolysis, there is a slow dissociation of ADP-RAD51 from ssDNA which is bound by SYCP3 and prevented from rebinding DNA. By this mechanism, SYCP3 destabilizes pre-formed RAD51 filaments under

conditions of RAD51 turnover. We conclude that SYCP3 inhibits the DNA strand invasion activity of RAD51 in D-loops by affecting the assembly and stability of RAD51 filaments.

4.5. Conclusions

SYCP3 is a germline protein whose function in meiosis as a structural component of the synaptonemal complex is well understood [23, 54]. There is emerging evidence that SYCP3 might also play a role in meiotic HR repair regulating the DNA strand exchange proteins RAD51 and DMC1, but the mechanisms involved have not yet been elucidated [30, 37, 55]. Recent findings show that SYCP3 is mis-expressed in a variety of cancers and cancer cell lines [31, 33], and its mis-expression in somatic cells causes a decrease in HR efficiency and hence leads to HR repair defect [33]. *In vitro* experiments with purified proteins show a direct interaction of SYCP3 with RAD51 and a much weaker interaction with DMC1 [37]. This direct protein-protein interaction likely inhibits the strand invasion activity of RAD51 but not DMC1 [37]. However, the mechanism by which SYCP3 disrupts the activity of RAD51 in HR had not been established. Our findings help establish a plausible mechanism.

Previously published results established that SYCP3 inhibits the stimulation of RAD51-catalyzed D-loop formation by HOP2-MND1 [37]. Our data builds on these published observations to show that SYCP3 directly inhibits the D-loop forming activity of RAD51. However, this inhibition is reversed in the presence of RAD54. Our first hypothesis was that SYCP3 binds dsDNA and blocks DNA strand invasion by RAD51 filaments. RAD54, via its translocase activity, removes SYCP3 from dsDNA and thereby rescues D-loop formation. But, it has been shown that when SYCP3 is preincubated with dsDNA, it does not affect the ability of RAD51 to form D-loops [37]. Also, we discovered that our SYCP3 protein was defective in DNA binding, ruling out our first hypothesis.

This predicts that rescue of the D-loop reaction in the presence of SYCP3 should be independent of RAD54 translocase activity. *Mazin et al.* show that RAD54 stabilizes RAD51-ssDNA filaments independently of its ATPase activity and thereby promotes its DNA strand exchange activity [42]. These observations are consistent with analysis of RAD51 foci, which likely mark RAD51-ssDNA filaments and potentially additional HR intermediates [56]. RAD54 rescues the inhibition of RAD51-mediated D-loop formation caused by SYCP3. We suggest that RAD54 out-competes SYCP3 for binding to RAD51 and forms a complex with the RAD51-ssDNA complex which stabilizes the filament and in turn stimulates RAD51 D-loop activity. Next, we performed ATPase assays to determine if SYCP3 affects the D-Loop forming activity of RAD51 by promoting its ATPase activity. Our results show that SYCP3 does not affect the ATPase activity of both RAD51 and DMC1. We conclude that the effect on SYCP3 on RAD51-mediated D-loop formation does not involve modulating the RAD51 ATPase activity.

To further determine the mechanism by which SYCP3 affects RAD51 activity but not DMC1 activity in D-Loop reactions, we performed EMSA assays. Our findings show that SYCP3 disrupts RAD51 filaments but has no effect on DMC1 filaments. Previous findings by Kobayashi *et al.* showed that SYCP3 has stronger binding affinity to RAD51 relative to DMC1 [37] and hence SYCP3 likely disrupts RAD51 filaments by direct interaction with RAD51. Next, we performed RAD51 EMSAs with SYCP3 titration under non-turnover conditions that prevent RAD51 dissociating from DNA and the results show that SYCP3 does not disrupt RAD51 filaments under these conditions. Hence, we conclude that SYCP3 binds free RAD51 and prevents its binding to DNA, thereby affecting RAD51 filament stability and its strand invasion activity in D-Loop assays.

Our model proposes that when SYCP3 is expressed in somatic cells, that lack the normal environment comprising other meiotic proteins, it binds RAD51 and inhibits it from binding to DNA (Figure 4.18). SYCP3 thereby impedes the formation and stabilization of RAD51 filaments, which are required for key steps of HR: (1) Homology search for a DNA template; and (2) DNA strand invasion. This model is supported by earlier findings in cell-based microscopy assays where SYCP3 expression in somatic cells led to a decrease in radiation induced RAD51 foci formation and reduced HR efficiency [33].

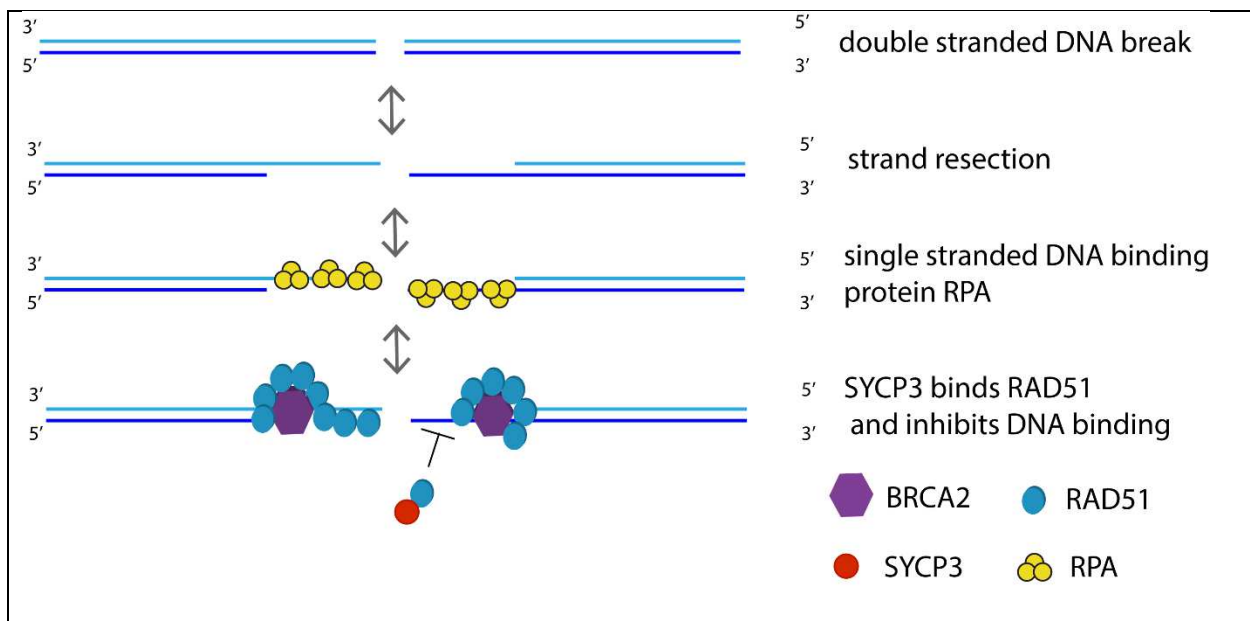


Figure 4.18: Proposed model for inhibition of RAD51 activity in HR by SYCP3. In somatic cells, when SYCP3 is mis-expressed it binds to RAD51 and inhibits RAD51-DNA binding thereby disrupting its function in HR leading to a DNA repair defect.

Previous studies [33] and unpublished work from the Heyer laboratory show that SYCP3 also binds BRCA2 and limits the interaction of BRCA2 with RAD51. This could represent a second, independent mechanism by which SYCP3 expression in somatic cells disrupts HR. In somatic

cells when SYCP3 is mis-expressed, it could bind to both RAD51 and BRCA2 independently. The SYCP3-BRCA2 interaction could limit interaction of BRCA2 with RAD51 through the BRC repeats and hence inhibit RAD51 nucleation and filament formation. In addition, SYCP3-RAD51 interaction could also inhibit RAD51 DNA binding and hence RAD51 filament formation.

4.6. Future Work

The EMSA assays showed that SYCP3 protein purified with a final Mono S column lacked DNA binding activity. Hence, the D-loop and EMSA assays should be repeated with a new SYCP3 protein preparation capable of DNA binding and lacking any ATPase contamination. The residues involved in DNA binding and RAD51 interaction in SYCP3 have been identified [23, 37]. Hence, DNA binding-deficient SYCP3 and RAD51 interaction-deficient SYCP3 mutants could be used to corroborate our model. The DNA binding-deficient SYCP3 mutant is expected to still be capable of impeding D-loop formation and destabilizing RAD51 filaments. On the other hand, because inhibition by SYCP3 is proposed to involve direct interaction with RAD51, the RAD51 interaction-deficient SYCP3 mutant is expected to be defective for inhibition of D-loop formation and destabilization of RAD51 filaments.

SYCP3 been shown to self-assemble into tetramers and interact with DNA at the tetrameric ends [23]. It is not known if SYCP3 could interact with DNA in the monomeric or dimeric forms. SYCP3 protein purified from the Mono S column could be in a monomeric or dimeric form and hence with a different conformation that is unable to bind DNA. We can assess the oligomeric state of purified SYCP3 from Mono S column by size exclusion chromatography. This will establish if SYCP3 can bind DNA only in a tetrameric form.

SYCP3 mis-expression in somatic cells leads to a decrease in radiation-induced RAD51 focus formation and reduced HR efficiency in HR reporter assays [33]. To validate our model *in vivo* (**Fig. 4.18**) analogous cell-based assays should compare wild-type SYCP3 with the RAD51 interaction-deficient SYCP3 mutant.

Our hypothesis is that RAD54 overcomes the inhibition of RAD51-mediated D-loop formation by SYCP3 independent of its ATPase activity. To test this idea, we would need to perform D-loop reactions with RAD54-K189R which is an ATPase deficient mutant of RAD54. In the D-Loop assays, the RAD54 concentration was based on the concentration of dsDNA and hence higher than RAD51 and SYCP3 concentrations. Titration experiments of SYCP3 to determine if SYCP3 could outcompete RAD54 at higher concentrations will further clarify this situation. Also, SYCP3 and RAD54 could bind to overlapping sites of RAD51 which could be mapped with cross-linking mass spectrometry. Alternatively, we could create a RAD51 mutant deficient in its interaction with RAD54 and test if the interaction with SYCP3 is also abolished.

Our data from *in vitro* D-Loop reactions show that RAD54 can rescue the inhibitory effect of SYCP3 on RAD51 activity. In cell-based assays ectopic SYCP3 expression causes decreased IR induced RAD51 foci formation, reduced HR efficiency by HR reporter assays and hypersensitivity to DNA damaging agents like cisplatin and poly (ADP-ribose) polymerase (**PARP**) inhibitors [33]. The next step is to determine if RAD54 overexpression can rescue the HR defect cause by SYCP3 in cell-based assays. For this purpose, cell lines with ectopic SYCP3 expression and endogenous RAD54 levels vs RAD54 downregulation or RAD54 overexpression can be tested with for IR-induced RAD51 focus formation and an HR levels to determine if RAD54 overexpression recovers HR efficiency. Finally, cell-based survival experiments using cisplatin or

PARP inhibitors should be conducted to test whether RAD54 overexpression improves the survival of the cells expressing SYCP3.

In EMSAs that we subsequently performed with SYCP3 that is proficient in DNA binding, complexes of both SYCP3 bound to DNA and RAD51 bound to DNA are retained near the wells. If SYCP3 is simultaneously able to bind both RAD51 and DNA then we might not be able to discern SYCP3-dependent RAD51 filament destabilization by EMSA. This limitation can be addressed by using an SYCP3 mutant that is deficient in DNA binding. Alternatively, pull-down assays could be conducted in which DNA is immobilized on the beads and bound RAD51 is quantified.

The mechanism by which SYCP3 interacts with BRCA2 and regulates its interaction with RAD51 and DMC1 is not clear. To determine the mechanism, quantitative interaction assays are required to measure the affinity of each of the BRC repeats for SYCP3 binding and then explore how interaction between SYCP3 and individual BRC repeats affects their interaction with RAD51 and DMC1. Our preliminary results show that SYCP3 has a greater affinity to class 2 repeat BRC5 than class 1 repeat BRC3 (**Fig. 4.19**), but a complete analysis using all repeats remains outstanding. Finally, experiments using full-length BRCA2 are needed to determine how its interaction with SYCP3 affects the interactions with RAD51 and DMC1. SYCP3 also interacts with RAD51 and DMC1 which complicates this analysis. Hence, we would need to create SYCP3 mutants deficient in the interaction with RAD51 and DMC1 to use as controls in these interaction assays.

The interaction domain of SYCP3 with BRCA2 is not known. To identify the interaction site, SYCP3 was cleaved into three fragments: SYCP3 NT, SYCP3 CT and SYCP3 cc, and the preliminary data from pull-down experiments show that the cc part of SYCP3 interacts with BRC repeats (**Appendix Fig. V3**). This analysis needs to be completed to establish which domain interacts with the repeats. Based on sequence conservation with other species, targeted mutagenesis of SYCP3 followed by pull down experiments can be used to determine which residues would be sufficient to abolish interaction with the BRC repeats of BRCA2. Finally, an SYCP3 mutant deficient for interaction with BRCA2 would be valuable to determine the biological significance of this interaction in cell-based HR reporter assays.

Collectively, the findings from this research will help determine the mechanism by which SYCP3 expression in somatic cells disrupts HR and thereby increasing the risk for cancer.

4.7. Appendix

The appendix includes preliminary data from exploratory experiments with an n =1.

SYCP3 has higher affinity to Class 2 BRC repeat BRC5 than to Class 1 BRC repeat BRC3

SYCP3, BRCA2, RAD51 and DMC1 are present in germline cells where they function together in the repair of programmed meiotic DSBs. However, when SYCP3 is mis-expressed in somatic cells that do not express DMC1 there is DNA repair defect [33]. Previous published results [33] and unpublished data by Dr. Jie Liu in Heyer laboratory show that SYCP3 interacts with BRCA2 and limits its interaction with RAD51. The BRC repeats are the primary interaction sites in BRCA2 for RAD51 and DMC1. The repeats are divided into 2 classes based on their differential affinity to

RAD51 and DMC1. Class 1 BRC repeats, BRC1-4 were found to have higher affinity to free RAD51 than the class 2 BRC repeats 5-8 in a study using individual BRC repeats that lack the spacer region [14]. BRC repeats 6-8 from class 2 bind with higher affinity to DMC1 than RAD51 while BRC5 displayed a low affinity to DMC1 [15]. In meiosis, DMC1 is the primary recombinase while RAD51 acts as the accessory factor to enable DMC1 nucleation and filament formation [58, 59]. Our hypothesis is that SYCP3 could bind to the BRC5 repeat in BRCA2 and thereby increase the affinity of the other repeats to DMC1 while decreasing the affinity of the repeats for RAD51. This would facilitate normal DMC1-dependent HR in germline cells in the presence of SYCP3, while HR is disrupted by SYCP3 in somatic cells because DMC1 and accessory factors are absent. First, we tested the affinity of SYCP3 to BRC5 and a representative repeat from class I, BRC3. Since the BRC repeats have a GST tag, we performed a GST pull-down assay of BRC3 and BRC5 with SYCP3. According to Bradford assay equal amounts of BRC3 and BRC5 were used for the pull-down experiment, but the input controls in the gel (**Fig. 4.19**) indicate that more BRC3 than BRC5 was present in the experiment. Hence the concentration of the proteins will need to be recalculated. The preliminary results indicate that SYCP3 displayed higher binding affinity to BRC5 than BRC3 (**Fig. 4.19**).

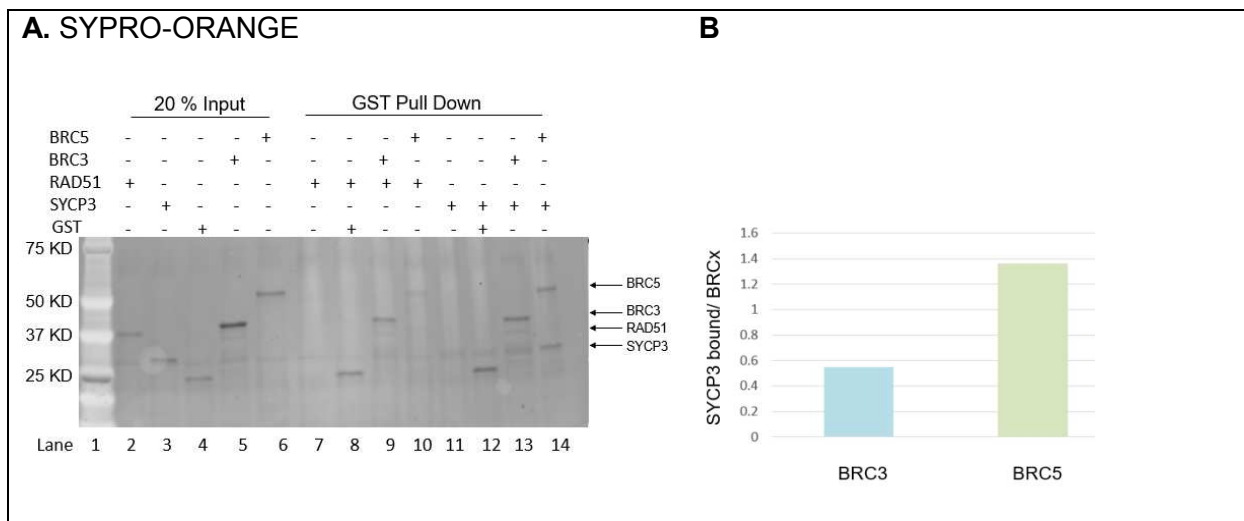


Figure 4.19: SYCP3 has higher affinity to BRC5 than BRC3. **A.** SYPRO Orange-stained gel of pull-down assays of BRC3 (0.4 μ M) and BRC5 (0.4 μ M) with SYCP3 (2.7 μ M). Lane 1: Protein ladder. Lane 2-6: 20% Input. Lane 7: Negative control of only RAD51. Lane 8: Negative control of RAD51 (2.2 μ M) pull down by GST (1.2 μ M). Lane 9: RAD51 pull down by BRC3. Lane 10: Rad51 pull down by BRC5. Lane 11: Negative control of only SYCP3. Lane 12: Negative control of SYCP3 pull down by GST. Lane 13: SYCP3 pulldown by BRC3. Lane 14: SYCP3 pulldown by BRC5. **B.** Quantification of SYCP3 pulled down by BRC5 *versus* BRC3 in A. n=1.

The data from the pull-down experiment suggest that SYCP3 could have higher affinity to BRC5 than BRC3 (**Fig VI.1**). As positive controls, we included the pull down of BRC3 and BRC5 with RAD51. BRC3 (Class I repeat) has been shown to have higher affinity to free RAD51 than BRC5 (Class II repeat) [14]. In accordance with the published data, our results showed a faint band for RAD51 pull down by BRC3 and no pull down by BRC5. In order, to obtain a better visualization of RAD51 band pulled down by BRC3 and BRC5 we need to include higher concentrations of

RAD51 titrations in the assay. The pull-down assays of SYCP3 by BRC3 and BRC5 must be repeated in independent experiments, including titrations of SYCP3 to determine the stoichiometry of the interaction before we perform similar pull-down assays to test the interaction of SYCP3 with the other BRC repeats from class 1 and class 2. Next, the BRC repeat-DMC1 interaction needs to be similarly probed. This line of enquiry was not completed as one of the repeats, BRC8, could not be purified as its expression led to low viability of the host *E. coli* cells. Hence, the purification of BRC8 requires a new approach for purification which is still being developed. Finally, the experiments need to be expanded to test how SYCP3 affects the interaction with RAD51 and DMC1 in the context of full length BRCA2.

SYCP3 interacts with BRC repeats *via* the coiled-coil region

SYCP3 has been shown to interact with BRCA2 and limit its interaction with RAD51 (unpublished data by Dr. Jie Liu in Heyer laboratory) [33]. The biological significance of the SYCP3 - BRCA2 interaction has not been established, and one strategy is to isolate a SYCP3 mutation that is specifically defective in the BRCA2 interaction and determine its biochemical, genetic, and cell biological phenotypes. As a first step towards isolating such a mutant, our goal was to determine the domain of SYCP3 that interacts with the BRC repeats. To this end, N-terminal (SYCP NT), central coiled-coil (SYCP3 cc) and a C terminal (SYCP3 CT) fragments were cloned, expressed and purified (SYCP3 NT and SYCP3 CT fragments were previously purified by Dr. Jie Liu in the Heyer laboratory); and interaction with GST-BRC5 was determined by GST pull down assays (**Fig. 4.20**).

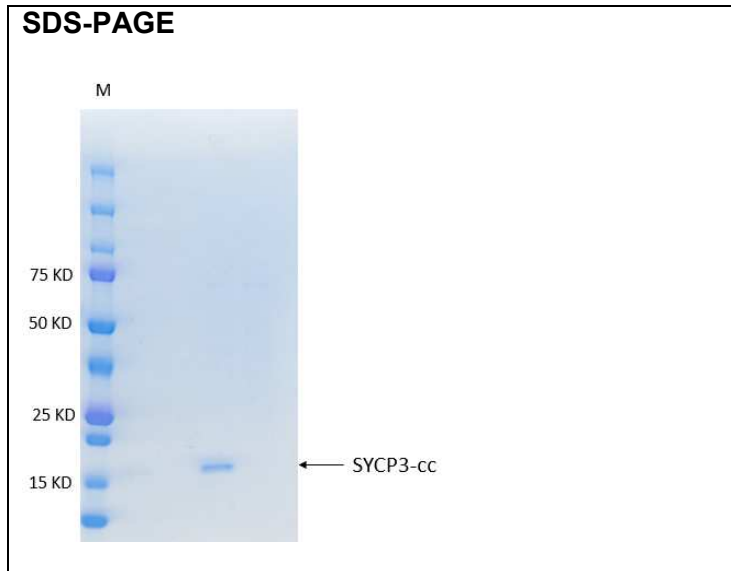
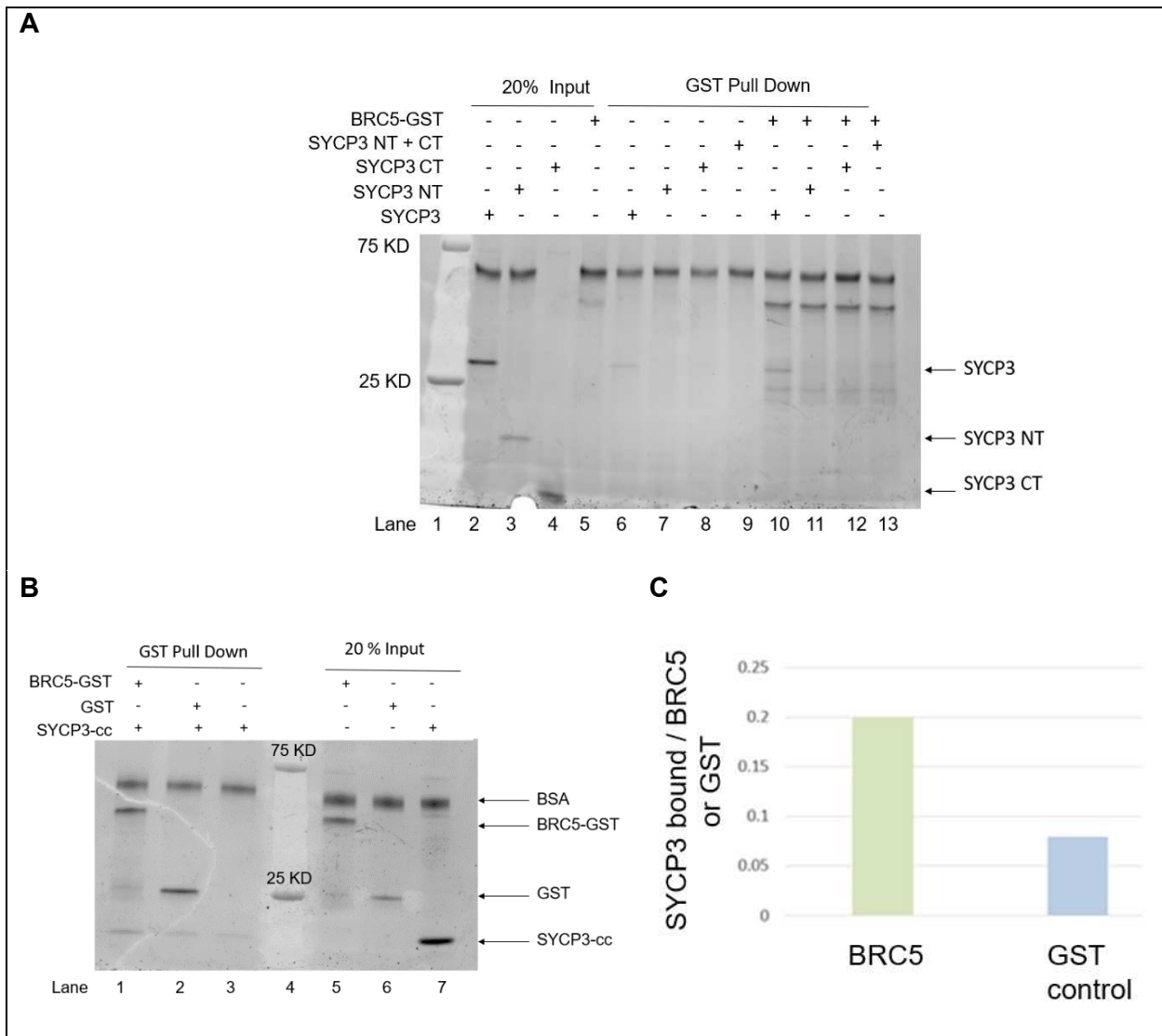


Figure 4.20: SYCP3-cc purified. SDS/PAGE gel with 0.5 µg purified SYCP3-cc stained with Denville Blue. Yield: 200 µg.

First, pull downs of equal concentrations of SYCP3 NT, SYCP3 CT and SYCP3 NT+CT were performed using GST-tagged BRC5. Full length SYCP3 served as a positive control. The preliminary results from the pull-down assay indicate that there is no interaction of SYCP3 NT, CT or combined NT+ CT fragments with the BRC5 region (**Fig. 4.21 A**). Next, we performed pull down of SYCP3 cc using GST-tagged BRC5. GST served as a negative control. The preliminary results suggest that the SYCP3 can interact with BRC5 via its cc region (**Fig. 4.21 B**).



*

Figure 4.21: SYCP3 interacts with BRC5 through its coiled-coil region. A. SYPRO Orange-stained gel of pull-down assay of SYCP3 NT (4 μ M) and SYCP3 CT (4 μ M) by BRC5 (1 μ M). Lane 1: Protein ladder; Lane 2-5: 20% Input. Lane 6: Negative control of SYCP3 pulled down by glutathione agarose resin; Lane 7: Negative control of SYCP3 NT pulled down by glutathione agarose resin; Lane 8: Negative control of SYCP3 CT pulled down by glutathione agarose resin; Lane 9: Negative control of SYCP3 NT + CT pulled down by glutathione agarose resin; Lane 10: Pull down of SYCP3 by BRC5; Lane 11: Pull down of SYCP3 NT by BRC5; Lane 12: Pull down of SYCP3 CT by BRC5; Lane 13: Pulldown of SYCP3 NT+CT by BRC5. **B.** SYPRO

Orange stained gel of pull-down assay of SYCP3 cc (4 μ M) with BRC5. Lane 1: SY*CP3 cc pull down by BRC5 (1 μ M); Lane 2: Negative control of SYCP3 cc pull down by GST (1 μ M); Lane 3: Negative control of SYCP3 cc pulled down by glutathione agarose resin; Lane 4: Protein ladder; Lane 5-7: 20% Input. **C.** Quantification of results in B. n= 1.

The data from the pull-down assays suggest that the region of SYCP3 that interacts with BRC repeats likely resides in the cc region. These assays will need to be repeated with titrations of SYCP3 fragments and quantified for $n \geq 3$. Pull-down assays of full length BRCA2 with SYCP3 NT, CT and cc fragments will serve to confirm the interaction region of SYCP3 with BRCA2. The planned experiments were completed as the yield of the purified proteins (SYCP3 cc, SYCP3 NT and SYCP3 CT) was not insufficient to complete them. Therefore, preparations will be scaled up to obtain a bigger yield. Once the region of SYCP3 that interacts with the BRC repeats and BRCA2 is confirmed, targeted mutagenesis of this region using alanine scanning guided by sequence conservation with other species will generate a mutation with low complexity, ideally with only one to a few alanine substitutions, that retains structural integrity and functions other than interaction with BRCA2. Pull down experiments with BRC repeats and BRCA2 will be used to confirm the expected interaction defect. Finally, the BRCA2-interaction defective SYCP3 mutant will be used in cell-based assays to determine the biological significance of the SYCP3-BRCA2 interaction.

No additional effect on the stimulation of RAD51 D-Loop reaction when both BRC4 and SYCP3 are present together

BRC repeats 1-4 have been shown to stimulate the D-loop activity of RAD51 specifically when RAD51 is present in excess of the concentration needed to saturate ssDNA, but not when RAD51 concentration was optimal relative to ssDNA. Excess RAD51 binds dsDNA and blocks DNA

strand invasion by the RAD51-ssDNA filament. BRC4 binds to excess RAD51 and inhibits its binding to dsDNA thereby rescuing D-Loop formation. [14, 16]. We wished to determine whether SYCP3 could interfere with the RAD51-BRC4 interaction and thereby affecting the stimulation of RAD51 D-loop activity. The first goal was to optimize the reaction conditions and recapitulate these findings with our BRC4 construct, that includes spacer regions. To this end, increasing concentrations of BRC4 were incubated with ssDNA before introducing excess RAD51. D-loop reactions were started by adding homologous dsDNA. Reactions with increasing concentrations of RAD51 indicated that RAD51 significantly inhibited strand exchange when present at 5x the optimal RAD51 concentration (not shown here); this concentration was employed in subsequent experiments (**Fig. 4.22 A**). Recapitulating previous experiments [14, 16], in the absence of BRC4, excess RAD51 significantly suppressed D-loop formation. A BRC4 concentration $\geq 2x$ relative to RAD51 stimulated the D-Loop formation restoring the efficiency of D-loop back to that seen with optimal RAD51 concentration (**Fig. 4.22 B, C**). This is likely caused by BRC4 binding to excess RAD51 and blocking its binding to dsDNA.

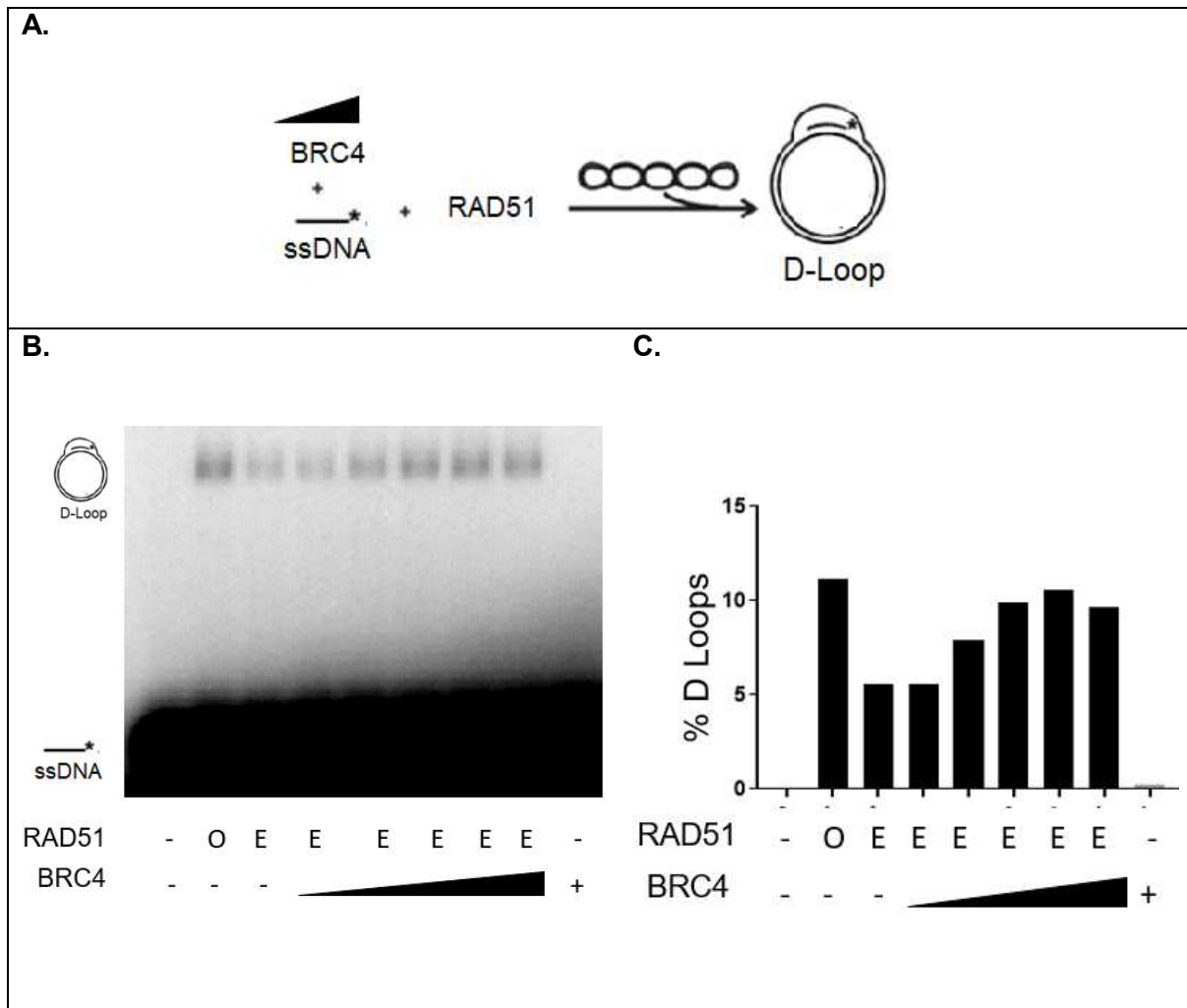


Figure 4.22. D-Loop assay when BRC4 is titrated with excess RAD51. **A.** Scheme of D-Loop assay with BRC4 titration when RAD51 is present in excess. **B.** D-Loop formation with excess RAD51 (1 μ M) while titrating in SYCP3. **C.** Quantification of D-Loop formed in **A.** Optimal RAD51 concentration: 0.2 μ M. Excess RAD51 concentration: 1 μ M. BRC4 titration: 0.5 μ M, 1 μ M, 2 μ M, 3 μ M, 4 μ M. $n = 1$. Abbreviations: O -Optimal RAD51 concentration, E - Excess RAD51 concentration.

Under these optimized conditions for RAD51 D-Loop stimulation by BRC4, SYCP3 was titrated into these optimized RAD51/BRC4 D-loop assays to determine whether SYCP3 can inhibit the

restoration of strand exchange by BRC4 (**Fig. 4.23 A**). SYCP3 inhibited RAD51 mediated D-Loop reaction when RAD51 was present at optimal concentrations as shown in (**Fig. 4.5**). However, when SYCP3 was incubated with excess RAD51, there was a stimulation of D-loop formation similar to that observed with BRC4. This result suggests that like BRC4, SYCP3 binds excess free RAD51 and thereby prevents it from binding to dsDNA. In the next set of experiments, we included both BRC4 and SYCP3 in reactions with excess concentrations of RAD51. BRC4 was present in these reactions at 3x the concentration of RAD51 and SYCP3 was titrated from 0.5x to 1.2x the concentration of RAD51. No additional effect on the efficiency of D-loop formation was seen in these experiments (**Fig. 4.23 B, C**). There are several possibilities that can explain this result:

- i. SYCP3 and BRC4 form a complex and then bind RAD51, inhibiting its binding to dsDNA
- ii. BRC4 and SYCP3 compete for binding of the same RAD51 site. BRC4 binds RAD51 and inhibits RAD51 binding to dsDNA while SYCP3 is unable to compete with BRC4-RAD51 interaction
- iii. BRC4 concentration used in the assay is in excess relative to RAD51 and SYCP3 concentrations (Fig 4.22). Hence some of the BRC4 could bind RAD51 and inhibit its from binding to dsDNA while the remaining free BRC4 could sequester SYCP3.

Another possible scenario is that SYCP3 competes with BRC4 for binding of the same RAD51 site and inhibits binding of RAD51 to dsDNA. This is unlikely as SYCP3 has been shown to inhibit RAD51 D-Loop formation at stoichiometric concentrations by destabilizing RAD51 filaments. In these reactions SYCP3 had no effect on the D-Loop formation even when it was present at 1-1.2x RAD51 concentration. It is more likely that when SYCP3 outcompetes BRC4 for interaction with RAD51, it would inhibit the D-Loop reactions especially when it is present at concentrations equal to or higher than RAD51.

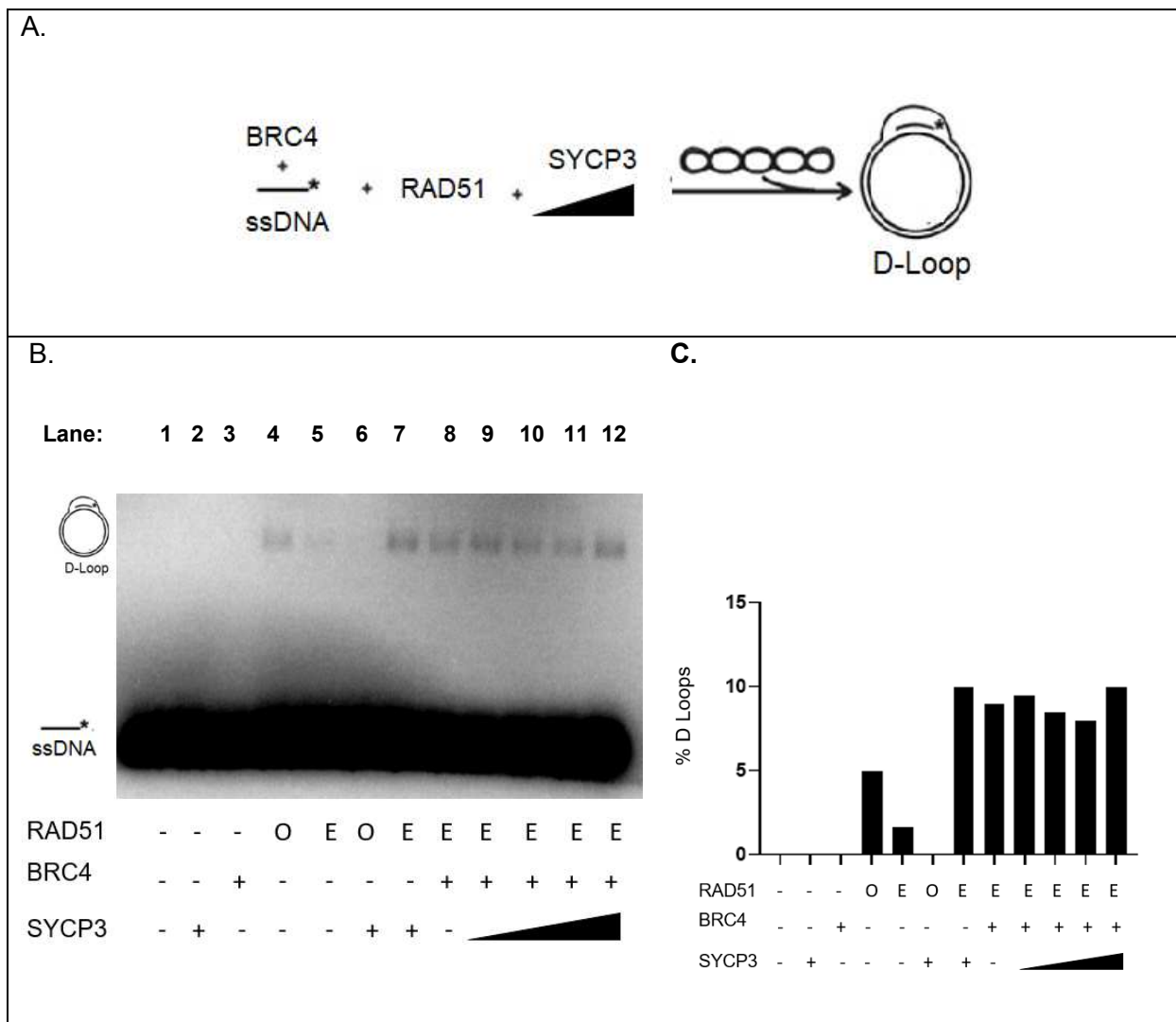


Figure 4.23: No effect on the stimulation of D-Loop reaction when both BRC4 and SYCP3 were present together in the reaction with excess RAD51. **A.** Scheme of SYCP3 titration in D-Loop assay with excess RAD51 (1 μ M) and presence of BRC4 (3 μ M). **B.** D-Loop formation with excess RAD51 and BRC4 while titrating in SYCP3. Lane 1: no protein control; Lane 2: only SYCP3; Lane 3: only BRC4; Lane 4: D-Loop with optimal RAD51 (0.2 μ M); Lane 5: D-Loop with excess RAD51(1 μ M);Lane 6: D-Loop with optimal RAD51 (0.2 μ M)

and SYCP3 (0.8 μM); Lane 7: with excess RAD51 (1 μM) and SYCP3 (0.8 μM); Lane 8: D-Loop with excess RAD51 (1 μM) and BRC4 (3 μM) ; Lane 9- 12: SYCP3 titration with excess RAD51 (1 μM) in presence of BRC4 (3 μM) . SYCP3 titrations: 0.5 μM , 0.8 μM , 1 μM , 1.2 μM . **B.** D-Loop gel. **C.** Quantification of D-Loop formed in A. n=1. Abbreviations: O -Optimal RAD51 concentration, E - Excess RAD51 concentration.

To sum up, the RAD51 D-loop reaction is inhibited in the presence of excess RAD51 as some of the RAD51 binds dsDNA and blocks strand invasion by RAD51 filaments. BRC4 and SYCP3 can both bind RAD51 [14, 16, 37]. In D-loop reactions with excess RAD51, the presence of either BRC4 or SYCP3 stimulates the reaction as they bind excess RAD51 and inhibit its from binding of RAD51 to the dsDNA target. The combined presence of both BRC4 and SYCP3 with excess RAD51 had no additional effect on the D-Loop stimulation compared to reactions with BRC4 or SYCP3 alone. We presented our hypothesis earlier as three possibilities that could explain this result. One possibility is that SYCP3 and BRC4 form a complex that together binds RAD51 and inhibits RAD51-dsDNA complex formation similar to what is observed in a reaction with BRC4 alone. The other possibility is that SYCP3 is unable to compete with BRC4-RAD51 interaction which prevents RAD51 from binding to dsDNA. The last possibility is that since BRC4 concentration is in excess of RAD51 and SYCP3 concentrations, some of the BRC4 binds RAD51 and inhibits RAD51-dsDNA binding while the rest sequesters SYCP3 and this can be assayed by titrating higher concentrations of SYCP3 in the D-Loop assay. To further determine the exact mechanism, we need to perform more quantitative pull-down experiments, first to determine the stoichiometry of interaction of BRC4 and SYCP3. Next, we could perform immunoprecipitation assays with immobilized RAD51 and then titrating in BRC4 and SYCP3. These assays will help determine if SYCP3 and BRC4 form a complex together that can then bind RAD51 or if SYCP3 is unable to compete with BRC4-RAD51 interaction.

4.8. References

1. Heyer, W.D., K.T. Ehmsen, and J. Liu, *Regulation of homologous recombination in eukaryotes*. *Annu Rev Genet*, 2010. **44**: p. 113-39.
2. Li, X. and W.D. Heyer, *Homologous recombination in DNA repair and DNA damage tolerance*. *Cell Res*, 2008. **18**(1): p. 99-113.
3. Roy, R., J. Chun, and S.N. Powell, *BRCA1 and BRCA2: important differences with common interests*. *Nature Reviews Cancer*, 2012. **12**(5).
4. Taylor, R.A., et al., *Germline BRCA2 mutations drive prostate cancers with distinct evolutionary trajectories*. *Nat Commun*, 2017. **8**: p. 13671.
5. Iqbal, J., et al., *The incidence of pancreatic cancer in BRCA1 and BRCA2 mutation carriers*. *Br J Cancer*, 2012. **107**(12): p. 2005-9.
6. Lancaster, J.M., et al., *BRCA2 mutations in primary breast and ovarian cancers*. *Nat Genet*, 1996. **13**(2): p. 238-40.
7. Levy-Lahad, E. and E. Friedman, *Cancer risks among BRCA1 and BRCA2 mutation carriers*. *British Journal of Cancer*, 2007. **96**(1): p. 11-15.
8. Wooster, R., et al., *Identification of the breast cancer susceptibility gene BRCA2*. *Nature*, 1995. **378**(6559): p. 789-92.
9. Waterworth, A., *New insights into the biological function of BRCA2 from its structural interactions*. *Breast Cancer Research*, 2003. **5**(2): p. 107-108.
10. von Nicolai, C., et al., *A second DNA binding site in human BRCA2 promotes homologous recombination*. *Nat Commun*, 2016. **7**: p. 12813.
11. Martinez, J.S., C. Baldeyron, and A. Carreira, *Molding BRCA2 function through its interacting partners*. *Cell Cycle*, 2015. **14**(21): p. 3389-95.

12. Zhao, W., et al., *The BRCA Tumor Suppressor Network in Chromosome Damage Repair by Homologous Recombination*. *Annu Rev Biochem*, 2019. **88**: p. 221-245.
13. Bork, P., N. Blomberg, and M. Nilges, *Internal repeats in the BRCA2 protein sequence*. *Nature Genetics*, 1996. **13**(1): p. 22-23.
14. Carreira, A. and S.C. Kowalczykowski, *Two classes of BRC repeats in BRCA2 promote RAD51 nucleoprotein filament function by distinct mechanisms*. *Proc Natl Acad Sci U S A*, 2011. **108**(26): p. 10448-53.
15. Martinez, J.S., et al., *BRCA2 regulates DMC1-mediated recombination through the BRC repeats*. *Proceedings of the National Academy of Sciences of the United States of America*, 2016. **113**(13): p. 3515-3520.
16. Carreira, A., et al., *The BRC Repeats of BRCA2 Modulate the DNA-Binding Selectivity of RAD51*. *Cell*, 2009. **136**(6): p. 1032-1043.
17. Ayoub, N., et al., *The carboxyl terminus of Brca2 links the disassembly of Rad51 complexes to mitotic entry*. *Curr Biol*, 2009. **19**(13): p. 1075-85.
18. Esashi, F., et al., *Stabilization of RAD51 nucleoprotein filaments by the C-terminal region of BRCA2*. *Nat Struct Mol Biol*, 2007. **14**(6): p. 468-74.
19. Davies, O.R. and L. Pellegrini, *Interaction with the BRCA2 C terminus protects RAD51-DNA filaments from disassembly by BRC repeats*. *Nat Struct Mol Biol*, 2007. **14**(6): p. 475-83.
20. Schlacher, K., et al., *Double-strand break repair-independent role for BRCA2 in blocking stalled replication fork degradation by MRE11*. *Cell*, 2011. **145**(4): p. 529-42.
21. Botelho, R.J., et al., *The genomic structure of SYCP3, a meiosis-specific gene encoding a protein of the chromosome core*. *Biochimica Et Biophysica Acta-Gene Structure and Expression*, 2001. **1518**(3): p. 294-299.

22. Heyting, C., *Synaptonemal complexes: structure and function*. Curr Opin Cell Biol, 1996. **8**(3): p. 389-96.
23. Syrjanen, J.L., L. Pellegrini, and O.R. Davies, *A molecular model for the role of SYCP3 in meiotic chromosome organisation*. Elife, 2014. **3**.
24. Syrjanen, J.L., et al., *Single-molecule observation of DNA compaction by meiotic protein SYCP3*. Elife, 2017. **6**.
25. Miyamoto, T., et al., *Male infertility and its causes in human*. Adv Urol, 2012. **2012**: p. 384520.
26. Bolor, H., et al., *Mutations of the SYCP3 Gene in Women with Recurrent Pregnancy Loss*. American Journal of Human Genetics, 2009. **84**(1): p. 14-20.
27. Yuan, L., et al., *The murine SCP3 gene is required for synaptonemal complex assembly, chromosome synapsis, and male fertility*. Molecular Cell, 2000. **5**(1): p. 73-83.
28. Yuan, L., et al., *Female germ cell aneuploidy and embryo death in mice lacking the meiosis-specific protein SCP3*. Science, 2002. **296**(5570): p. 1115-1118.
29. Wang, H. and C. Hoog, *Structural damage to meiotic chromosomes impairs DNA recombination and checkpoint control in mammalian oocytes*. Journal of Cell Biology, 2006. **173**(4): p. 485-495.
30. Li, X.C., E. Bolcun-Filas, and J.C. Schimenti, *Genetic evidence that synaptonemal complex axial elements govern recombination pathway choice in mice*. Genetics, 2011. **189**(1): p. 71-82.
31. Mobasheri, M.B., R. Shirkoohi, and M.H. Modarressi, *Synaptonemal Complex Protein 3 Transcript Analysis in Breast Cancer*. Iranian Journal of Public Health, 2016. **45**(12): p. 1618-1624.
32. Chung, J.Y., et al., *Synaptonemal complex protein 3 as a novel prognostic marker in early stage non-small cell lung cancer*. Hum Pathol, 2013. **44**(4): p. 472-9.
33. Hosoya, N., et al., *Synaptonemal complex protein SYCP3 impairs mitotic recombination by interfering with BRCA2*. EMBO Rep, 2011. **13**(1): p. 44-51.

34. Cho, H., et al., *Synaptonemal complex protein 3 is a prognostic marker in cervical cancer*. PLoS One, 2014. **9**(6): p. e98712.
35. Kitano, H., et al., *Synaptonemal complex protein 3 is associated with lymphangiogenesis in non-small cell lung cancer patients with lymph node metastasis*. J Transl Med, 2017. **15**(1): p. 138.
36. Fratta, E., et al., *The biology of cancer testis antigens: putative function, regulation and therapeutic potential*. Mol Oncol, 2011. **5**(2): p. 164-82.
37. Kobayashi, W., et al., *SYCP3 regulates strand invasion activities of RAD51 and DMC1*. Genes Cells, 2017. **22**(9): p. 799-809.
38. Chatterjee, G., et al., *Distinct binding of BRCA2 BRC repeats to RAD51 generates differential DNA damage sensitivity*. Nucleic Acids Research, 2016. **44**(11): p. 5256-5270.
39. Davies, A.A., et al., *Role of BRCA2 in control of the RAD51 recombination and DNA repair protein*. Mol Cell, 2001. **7**(2): p. 273-82.
40. Tomblin, G., et al., *Biochemical characterization of the human RAD51 protein. III. Modulation of DNA binding by adenosine nucleotides*. J Biol Chem, 2002. **277**(17): p. 14434-42.
41. Wright, W.D. and W.D. Heyer, *Rad54 functions as a heteroduplex DNA pump modulated by its DNA substrates and Rad51 during D loop formation*. Mol Cell, 2014. **53**(3): p. 420-32.
42. Mazin, A.V., A.A. Alexeev, and S.C. Kowalczykowski, *A novel function of Rad54 protein. Stabilization of the Rad51 nucleoprotein filament*. J Biol Chem, 2003. **278**(16): p. 14029-36.
43. Kiiianitsa, K., J.A. Solinger, and W.D. Heyer, *Terminal association of Rad54 protein with the Rad51-dsDNA filament*. Proc Natl Acad Sci U S A, 2006. **103**(26): p. 9767-72.
44. Solinger, J.A., K. Kiiianitsa, and W.D. Heyer, *Rad54, a Swi2/Snf2-like recombinational repair protein, disassembles Rad51:dsDNA filaments*. Mol Cell, 2002. **10**(5): p. 1175-88.
45. Gupta, R.C., et al., *Activities of human recombination protein Rad51*. Proc Natl Acad Sci U S A, 1997. **94**(2): p. 463-8.

46. Ito, K., et al., *Real-time tracking reveals catalytic roles for the two DNA binding sites of Rad51*. Nat Commun, 2020. **11**(1): p. 2950.
47. Sharma, D., et al., *Role of the conserved lysine within the Walker A motif of human DMC1*. DNA Repair (Amst), 2013. **12**(1): p. 53-62.
48. Li, Z., et al., *Recombination activities of HsDmc1 protein, the meiotic human homolog of RecA protein*. Proc Natl Acad Sci U S A, 1997. **94**(21): p. 11221-6.
49. Liu, J., et al., *Rad51 paralogues Rad55-Rad57 balance the antirecombinase Srs2 in Rad51 filament formation*. Nature, 2011. **479**(7372): p. 245-8.
50. Hilario, J., et al., *Direct imaging of human Rad51 nucleoprotein dynamics on individual DNA molecules*. Proc Natl Acad Sci U S A, 2009. **106**(2): p. 361-8.
51. van Mameren, J., et al., *Counting RAD51 proteins disassembling from nucleoprotein filaments under tension*. Nature, 2009. **457**(7230): p. 745-8.
52. Bugreev, D.V. and A.V. Mazin, *Ca²⁺ activates human homologous recombination protein Rad51 by modulating its ATPase activity*. Proc Natl Acad Sci U S A, 2004. **101**(27): p. 9988-93.
53. Spirek, M., et al., *Human RAD51 rapidly forms intrinsically dynamic nucleoprotein filaments modulated by nucleotide binding state*. Nucleic Acids Res, 2018. **46**(8): p. 3967-3980.
54. Dobson, M.J., et al., *Synaptonemal complex proteins: occurrence, epitope mapping and chromosome disjunction*. J Cell Sci, 1994. **107 (Pt 10)**: p. 2749-60.
55. Tarsounas, M., et al., *RAD51 and DMC1 form mixed complexes associated with mouse meiotic chromosome cores and synaptonemal complexes*. J Cell Biol, 1999. **147**(2): p. 207-20.
56. Agarwal, S., et al., *ATP-dependent and independent functions of Rad54 in genome maintenance*. J Cell Biol, 2011. **192**(5): p. 735-50.
57. Swagemakers, S.M., et al., *The human RAD54 recombinational DNA repair protein is a double-stranded DNA-dependent ATPase*. J Biol Chem, 1998. **273**(43): p. 28292-7.

58. Lan, W.H., et al., *Rad51 facilitates filament assembly of meiosis-specific Dmc1 recombinase*. Proc Natl Acad Sci U S A, 2020. **117**(21): p. 11257-11264.
59. Cloud, V., et al., *Rad51 is an accessory factor for Dmc1-mediated joint molecule formation during meiosis*. Science, 2012. **337**(6099): p. 1222-5.